Prepared for:

Rijkswaterstaat, RIKZ

Grain-Size and gradation effects on sediment transport under sheet-flow conditions

Part 2: Data-analysis and modelling

October 1997

TU Delft

Technische Universiteit Delft

TRIAS 2000

WL | delft hydraulics

Z2137

Grain-size and gradation effects on sediment transport under sheet-flow conditions

G. van der Hout

October 1997

Supervisors: Prof. ir. K. d'Angremond (DUT)
Dr. D.W. Dunsbergen (RIKZ)
Dr.ir. J. van de Graaff (DUT)
Ir. C.M. Janssen (DUT / WL)
Dr.ir. J.S. Ribberink (UT)

delft hydraulics

CLIENT : Rijkswaterstaat, RIKZ

TITLE : Grain-size and gradation effects on sediment transport under sheet-flow conditions
Part II: Data analysis and modelling

ABSTRACT :

This study consists of three sections:
- experiments on sand transport in oscillatory sheet flow with two sands (D_{50} = 0.21 and 0.32 mm)
- verification of three existing sediment transport models
- extension of these models to include the gradation of the sediment

The experiments are performed in the Large Oscillating Water Tunnel (see also data report: Z2137, part I). Comparison between these data and data from earlier experiments with finer sand shows the effect of the grain size and the unsteadiness on the transport rate for relatively uniform sand. Verification of three existing sediment transport models (Bailard, 1981; Ribberink, 1994; Dibajnia & Watanabe, 1992) shows that the model of Bailard largely overpredicts the measured transport rates, especially for fine sand. The model of Ribberink shows reasonably good results for all sands, except when unsteady effects become too important. In the model of Dibajnia & Watanabe unsteady effects are included. Therefore the net transport rates for fine sand are predicted well by this model, but the net transport rates for coarser sand are overpredicted. The gradation of the sediment is included into the models by using a size-fraction method. Moreover, hiding and exposure corrections are included in the model of Ribberink. Based on the results of the grain-size effect in uniform sand, a sensitivity study is performed, which shows the following results: Bailard predicts larger net transport rates than for uniform sand due to an overprediction in transport rate for the fine fractions. The transported material is finer than the bed material. For Dibajnia & Watanabe the transported material is coarser than the bed material and the net transport rate may either increase or decrease. For Ribberink the net transport rate is almost the same as for uniform sand and the transported material is hardly different from the bed material. The width of the gradation has a large effect on the difference between the net transport of uniform sand and that of a mixture with the same mean grain diameter.

REFERENCES: Contract number RKZ-369
KUST*2000 project

REV.	ORIGINATOR		DATE	REMARKS	REVIEWED BY	APPROVED BY
1	G. Van der Hout		August 1997	draft	C.M. Janssen J.S. Ribberink	T. Schilperoort
2	G. Van der Hout		October 1997	final	C.M. Janssen J.S. Ribberink	T. Schilperoort

KEYWORD(S)	CONTENTS	STATUS
sand transport sheet-flow grain size gradation	TEXT PAGES : 112 TABLES : 29 FIGURES : 72 APPENDICES : 6	☐ PRELIMINARY ☐ DRAFT ■ FINAL
	PROJECT IDENTIFICATION: Z2137	

Contents

List of Figures

List of Tables

Summary

This study is part of a research program which is aimed at improving the understanding of the sediment transport processes under combined wave-current conditions in the sheet-flow regime. The main objective of this research program is the mathematical modelling of sand transport processes. The experimental program in the Large Oscillating Water Tunnel (LOWT) at DELFT HYDRAULICS provides the necessary data for model improvement and development and a better understanding of the physical processes.

The main goals of the present study are:
- to complete a data-set for sediment transport under sinusoidal waves in combination with a net current under sheet-flow conditions
- to verify different existing transport models for uniform sediment using the experimental results
- to determine which parameters play an important role in modelling of transport rates of non-uniform sediments

For this purpose, two series of oscillating water tunnel experiments were carried out. The measured data were presented in the data report (Part I: Data report, Janssen and Van der Hout, (1997)). The present report (Part 2: Data-analysis and modelling) is divided into three sections, corresponding to the main goals of this study. The first part consists of a description of the experimental research, which is performed in order to complete a data-set on sediment transport for different grain-sizes (0.13, 0.21 and 0.32 mm). The experimental results are analysed and compared with results from previous experimental series. In the second part three transport models are verificated using the experimental results. The third part is about the modelling of transport processes for graded sediments.

Experimental research

Two series of experiments were carried out: series J (D_{50}=0.21 mm) and series I (D_{50}=0.32 mm). Net transport rates were determined for both series, while for series I also time-dependent flow velocities and sediment concentrations were measured. These experiments are performed under partly the same hydraulic conditions as previous experiments with fine sand (D_{50}=0.13 mm). In this study the data set for all grain-sizes is analysed.

The time-dependent measurements show that the time-averaged concentration profile varies significantly for the different grain-sizes. In case of a grain-size of 0.32 mm, the sediment concentration decreases very fast with increasing height above the sand bed, while the fine sediment (0.13 mm) shows a much smaller gradient. The sheet-flow layer thickness is inversely proportional to D_{50}. In case of fine sand the time-dependent concentrations show sharp peaks around flow reversal, which are dominant over the peaks during maximum velocity. For the 0.21 mm sand these peaks are much smaller and for the coarse sand they can almost be neglected. Just before the end of a positive or negative part of the wave cycle many particles are brought into suspension. These so-called suspension ejection events are an unsteady effect that significantly influences the transport process.

The transport process during a wave cycle can be considered as quasi-steady when there is a direct relation between the driving force, which is the instantaneous flow velocity or the

bed shear stress, and the sediment transport. In this case no phase lags occur between flow velocity and sediment concentration. For small grain-sizes in combination with a high oscillating velocity and a short wave period, this is no longer valid, because a phase lag effect occurs. The process of stirring up and settling down on the bed takes more time than the wave period. The particles have not enough time to settle before flow reversal. They remain partly suspended and are transported in opposite direction in the successive half of the wave cycle.

For the net transport rates, the influences of three different parameters are investigated: grain-size, flow velocity and wave period. As long as no unsteady effects occur, the net transport rate is hardly dependent on the wave period and increases for smaller grain-sizes and higher flow velocities. This is no longer valid when unsteady effects occur. Both suspension ejection events and phase lag effects result in a decreasing net transport rate for decreasing grain-sizes and wave periods and increasing oscillating velocities .

Verification of transport models for uniform sediment

Three different models are verified with the available data: Bailard (1981), Ribberink (1994) and Dibajnia and Watanabe (1992). The model of Bailard gives for the 0.32 mm sand a small overprediction of the transport rate. For the 0.21 mm sand the overprediction factor lies between 2 and 4, and for the fine sand it goes up to factor 20, with an average value around 5. The model of Ribberink gives no systematic over or underprediction for the 0.13 and 0.21 mm grains, and a small overprediction for the coarse sand. For both models, the largest overprediction occurs for conditions where unsteady effects are dominant. The model of Dibajnia and Watanabe gives good results for the fine sediment, but overpredicts for the 0.21 mm sand with a factor around 2, and for the 0.32 mm sand around 2.5. It predicts the unsteady effects in a satisfying way.

Table S-1 Approximate overprediction factors for different transport models

model	D_{50} = 0.13 mm		D_{50} = 0.21 mm		D_{50} = 0.32 mm	
	range	average	range	average	range	average
Bailard	2-20	5	1.5-4	2	1.5-1.8	1.6
Ribberink	0.4-6	1	0.8-2.2	1.2	1-1.8	1.5
Dibajnia & Watanabe	0.4-1.6	1	1.3-3	1.8	2-3	2.5

Transport of non-uniform sediment

For non-uniform sediment transport experimental results are not yet available. To take account of the effects of the variation in grain-size on the transport rate, a size-fraction method is implemented in the three transport models The predicted transport rates for a mixture characterised by several size fractions are compared to the predicted transport rate for a mixture characterised by D_{50} only. A sensitivity analysis is carried out to determine the effects of three model parameters on the prediction of transport rates: the gradation of the mixture (which is indicated by the geometric standard deviation σ_g), the mean diameter of the mixture D_{50} and the imposed condition It turned out that the magnitude of the mean diameter has not much impact on the results. An increasing oscillating velocity gives only in case of the model of Dibajnia & Watanabe much change in resulting transport rates, most likely caused by the unsteady effects. The gradation of the sediment mixture is the parameter resulting in the largest differences between predicted transport rates as sum of several size fractions and predicted transport rates for a mixture characterised by D_{50}.

From the model calculations it can be concluded that the three transport models show a very different selective behaviour. In case of Bailard, mainly fine fractions are transported, while in case of Dibajnia and Watanabe, mainly coarse fractions are transported. The model of Ribberink predicts that the transported sediment has almost the same composition as the original bed material.

In the model of Ribberink a hiding and exposure correction has been applied. Four different expressions to calculate the correction coefficients are implemented. All methods give similar results: a reduced transport rate for the small fractions, and a slightly increased transport for the coarsest fractions. A correction of the critical Shields parameter is only effective under conditions with a small flow velocity.

A future verification of the different models with experimental results must indicate which approach gives the best results.

1 Introduction

1.1 Sediment transport

Sediment transport is caused by the interaction of flowing water and a bed, consisting of gravel, sand or finer material. In coastal regions waves play an important role, causing an oscillating velocity close to the bottom, especially in shallow water.

At the coast, two types of sand transport can be distinguished: longshore transport parallel to the coast, and cross-shore transport, with an average net direction perpendicular to the shoreline. Longshore transport is mainly induced by oblique approaching waves causing a longshore current, and by tidal currents. The concerning timescale is often several years, in which for instance continuous, gradual erosion can take place. Because longshore transport can often be properly described with time-averaged sediment concentrations, modelling is relatively easy and advanced computer models have been developed. Cross-shore transport, on the other hand, generally plays on a much smaller timescale. Under storm conditions, severe dune erosion can take place within a few hours. Oscillating velocities caused by waves and offshore currents are the main factors. The small timescale of this process hampers modelling.

Under storms, high waves occur and the oscillating velocities close to the bottom are high. Due to the high shear stresses the entire top layer of the sand bed is set in motion. In these so-called sheet-flow conditions high transport rates occur due to the combination of large sediment concentrations and velocities.

Field observations show a variation in bed material composition along the coastal profile. These variations are at least partly due to selective transport processes. These selective processes however, are still highly unknown and cannot be predicted by transport models. Detailed knowledge about transport mechanisms for cross-shore transport for uniform sediment can be useful in order to understand the process of selective transport of non-uniform sediments. But also, the other way around, information about the cross-shore sorting of sediments may be useful to improve the present understanding of the physical processes of cross-shore sediment transport.

1.2 Laboratory experiments

Field experiments on sand transport in sheet-flow conditions are hard to perform. Sand transport can hardly be measured directly. Severe conditions under which sheet-flow occurs make it very expensive. Therefore most of the measurements are carried out in laboratory experiments. These experiments can be performed using different facilities: wave flumes, oscillating plates or oscillating water tunnels.

The facilities can be either small- or full-scale. The advantage of large scale facilities is that the prototype material can be used and scaling of the sediment is not necessary. This would probably result in very fine, even cohesive material with completely different behaviour.

Therefore it is possible to study and compare the different physical processes of transport of fine and coarser material under the same, more or less natural conditions.

One of the few large scale facilities for laboratory experiments on sand transport is the Large Oscillating Water Tunnel (LOWT) of DELFT HYDRAULICS. This tunnel was designed for full-scale simulation of near-bed horizontal oscillating water motion, which can be combined with a steady current. Due to the large dimensions of the tunnel, conditions within the sheet-flow regime can be realised for a period of several minutes to half an hour. The experiments for this study were carried out in this facility. An overview of previous series of experiments is given in Table 1.1.

Table 1-1 Experimental series carried out at the LOWT of Delft Hydraulics

series	waves/ current	asym./ symm.	D_{50} (mm)	T (sec)	measurements	reference
B	W	AS	0.21	5-12	$<q_s>$	Al-Salem (1993)
C	W	AS/S	0.21	6.5- 9.1	u(z,t) c(z,t)	Al-Salem (1993)
D	W	AS	0.13	6.5	$<q_s>$	Ribberink & Chen (1993)
C-I	W+C	AS	0.21	6.5	$<q_s>$	Ramadan (1994)
C-II						Ribberink (19945)
E	W+C	S	0.21	7.25	$<q_s>$ u(z,t) c(z,t)	Koelewijn (1994)
H	W+C	S	0.13	4-12	$<q_s>$ u(z,t) c(z,t)	Hassan (1996)
						V.d.Wal (1996)
I	W+C	S	0.21	4-12	$<q_s>$ u(z,t) c(z,t)	present
J	W+C	S	0.30	7.2	$<q_s>$	present

1.3 Scope and outline of this study

This study has two main objectives:

- to obtain a complete data set on sand transport in combined wave-current sheet-flow conditions, which can be used for verification and further development of transport models
- to determine which parameters play an important role in transport processes of non-uniform sediment, in order to improve modelling of sand transport by including the effects of the gradation

For the first objective, experiments were carried out which completed a data-set for three different grain-sizes (D_{50}=0.13, 0.21 and 0.32 mm). The experimental research is done in the LOWT at DELFT HYDRAULICS, from October 1996 until January 1997. Two experimental series with different grain-sizes were performed. They can be divided into three parts:

- series J (D_{50}=0.21 mm): time-averaged measurements (net transport rates)
- series I (D_{50}=0.32 mm): part 1: time-averaged measurements (net transport rates)
- part 2: time-dependent measurements (flow velocities, sediment concentrations)

The experiments were carried out mainly under the same hydraulic conditions as previous experiments with fine sand (series H: D_{50}=0.13 mm) and unsieved dune sand (series E: D_{50}=0.21 mm) (see Table 1.1).

Together, the results form a complete data set, which provides information about the transport processes of uniform sand, with emphasis on grain-size influences. This data-set is used for the verification of 3 transport models: Bailard (1981), Ribberink (1994) and Dibajnia & Watanabe (1992).

To start with the modelling of transport rates of non-uniform sediments, existing models predicting uniform sediment transport can be improved. In previous studies, a computer program is developed, which includes the models of Bailard (1981), Ribberink (1994) and Dibajnia & Watanabe (1992). A relatively simple adaptation to include the effect of the gradation of the sediment in these models is the implementation of a so-called size-fraction method. In this method, a mixture will be divided in several size-fractions. The transport rates will be calculated for each fraction, and the sum of these is supposed to give the total transport rate. A sensitivity analysis of the three models has been used to determine which parameters play an important role in transport processes of non-uniform sediment.

From April until June 1997, in the framework of TMR (Training & Mobility of Researchers) of the European Union, new experiments were carried out at Delft Hydraulics, in which transport rates of a mixture of two types of sand (D_m=0.13 mm and D_m=0.32 mm) were measured. The results of these tests will be used in a later stage for verification of the improved transport program.

The present study is part of the research program 'KUST*2000' of Rijkswaterstaat, funded by the Dutch Ministry of Transport and Public Works (Directorate General Rijkswaterstaat, National Institute for Coastal and Marine Management/RIKZ) (contract number RKZ-369). Project leader for Rijkswaterstaat is D.W. Dunsbergen.

The experimental research was carried out from October 1996 until January 1997. The tunnel was operated by H. Westhuis and G. van der Hout; the last one performed also the data processing and analysis. A detailed data report of the experiments is written by C.M. Janssen and G. van der Hout (1997). The project management was done by J.S. Ribberink and C.M. Janssen from DELFT HYDRAULICS. J. Bosboom from DELFT HYDRAULICS advised during the modelling phase. Comments on the draft version were given by C.M. Janssen, J.S. Ribberink, J. van de Graaff (Delft University of Technology), D.W. Dunsbergen and R. Spanhoff (RWS/RIKZ).

1.4 Structure of the report

In Chapter 2, the existing theories of uniform and non-uniform sediment transport are described, together with existing models to predict transport rates. Attention is also paid to the size-fraction method and different methods to calculate correction coefficients for the interaction of fine and coarse fractions.

Chapter 3 gives a brief description of the measurement facilities and instruments, the imposed and measured parameters and the test conditions for the series I and J experiments (see Table 1.1).

The experimental results are presented in Chapter 4. Net transport rates measured in series J are given in Section 4.1, net transport rates for series I in Section 4.2, and finally the time-dependent flow velocities and sediment concentrations from series I are described in Section 4.3.

In Chapter 5, the previous data sets are summarised (i.e. B, H, and E) and compared with the present experiments (series I and J). First, attention is paid to the time-dependent measurements, then time-averaged measurements are analysed and compared with the predicted transport rates of 3 theoretical models, with emphasis on grain-size influences.
The implementation of the size-fraction method in an existing computer program, which contains the 3 transport models used in Chapter 5, is described in Section 6.1. The set-up for the sensitivity analysis of the extended program can be found in Section 6.2, while the results are discussed in Section 6.3.

Finally, in Chapter 7 conclusions are drawn and recommendations about model improvement provided.

2 Theories on sediment transport

This chapter discusses the existing theories on sediment transport. In Section 2.1, the basic principles of sediment movement and the occurrence of sheet-flow conditions will be explained. The main physical processes are described in Section 2.2. The existing models to calculate and predict sand transport are given in Section 2.3. The final Section 2.4 is about the transport process of non-uniform sediment. The main principles of the size-fraction method will also be explained here.

2.1 Sheet-flow conditions

Sediment transport can only take place if the water movement is strong enough to lift or roll the grains from the bottom. The different forces acting on an individual sand particle laying on a sand bed, are sketched in Figure 2.1.

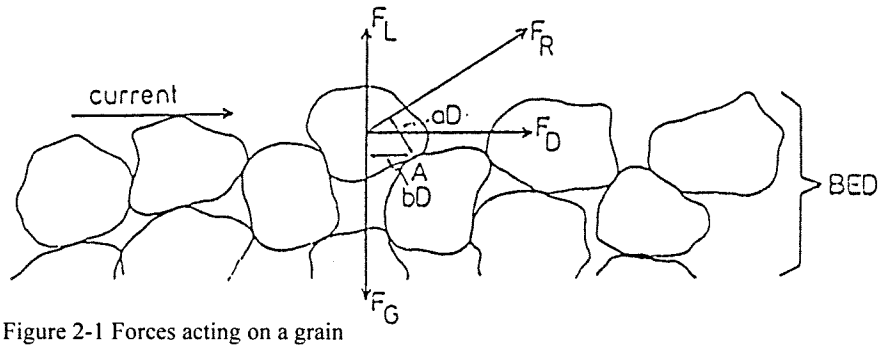

Figure 2-1 Forces acting on a grain

The forces can be divided in forces which act to move the grain, (the drag force F_D and the lift force F_L) and forces which act to keep the grain in its place (the gravity force F_G), like shown in Figure 2.1. F_L and F_D result in a resulting force F_R, which can also be expressed as a function of the shear stress. The exact interaction of these forces is not fully understood, not even for one particle. Even more complex, a sand bed is formed by many sediment particles, influencing each other. In that case, the shear stress is induced by the roughness of the bed as a whole, instead of the friction of an individual particle. Especially in case of non-uniform bed material the interaction between the grains plays an important role in the transport process. This is further explained in Section 2.4.

To express the stability of a sand particle in flowing water, the Shields parameter is normally used. It gives a relation between the shear stress τ and the submerged weight of the grain according to:

$$\theta(t) = \frac{\tau_b(t)}{(\rho_s - \rho_w) g D_{50}} \approx \frac{F_R}{F_G} \tag{2.1}$$

where: θ = Shields parameter
$\tau_b(t)$ = bottom shear stress
ρ_s = density of sediment
ρ_w = density of water
g = gravity acceleration

D_{50} is the grain-size, defined in a way that 50 % by weight of the sediment has a smaller diameter than D_{50}.

The shear stress is considered to be the driving force in the transport process. A Shields parameter below a certain threshold means no movement at all. This threshold, usually indicated θ_{cr}, is given by the critical Shields parameter; in the range between θ=0.03 to 0.06 the grains start to move and roll. For larger values of θ small ripples will occur, which will increase in size for increasing θ. This process continues until the Shields parameter is around 0.8 to 1. Then, the flow flattens the ripples out, the entire bed becomes plane again and the entire upper layer is set in motion. This layer is called the sheet-flow layer. In the sheet-flow layer high concentrations occur. Together with the fact that sheet-flow only occurs under large velocities this results in high sediment fluxes.

In case of waves, an oscillating velocity occurs at the bed. The magnitude of this velocity, and thus the occurrence of sheet-flow conditions, depends on the wave height compared to the water depth. In Figure 2.2, the amplitude of the near-bed oscillating velocity is plotted against the water depth for various waves in deep water at the North Sea. The percentages in this picture refer to the probability that the wave height is exceeded. To calculate the Shields parameter, it was assumed that the mean grain-size is 0.2 mm. A line is drawn where θ=1, which indicates when sheet-flow conditions occur. The figure shows that in the whole range of given water-depths sheet-flow can occur, depending on the magnitude of the near-bed velocity. The probability of occurrence of larger waves which induce high near-bed velocities, is low, but still these conditions are important for the sand transport. Sediment transport is often supposed to be proportional to a power of the flow velocity, with a power around order 3. The larger velocities contribute therefore relatively much to the total transport under sheet-flow conditions.

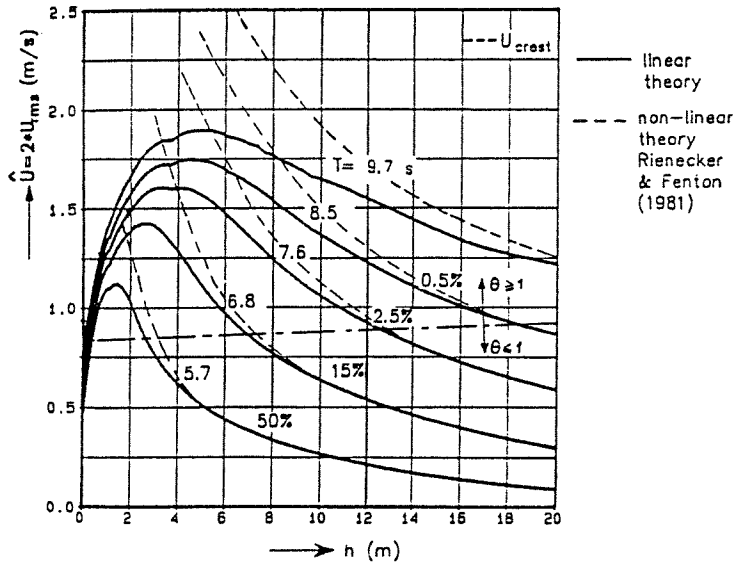

Figure 2-2 Occurrence of sheet-flow conditions ($\theta \geq 1$) [from Janssen, 1995]

2.2 Physical processes

Boundary layers

The wave boundary layer is a layer forming the transition between the bed where the velocity is zero, and the upper irrotational flow. The wave boundary layer remains thin compared to the water depth, because only during half the wave period it can grow and it has to start again as the flow reverses. In a steady current, or a tidal wave with a period of several hours, a boundary layer can fully develop and stretches over the whole water depth. Figure 2.3 shows that even if the current velocity is much larger than the wave velocity near the surface, the waves will dominate the situation at the bed.

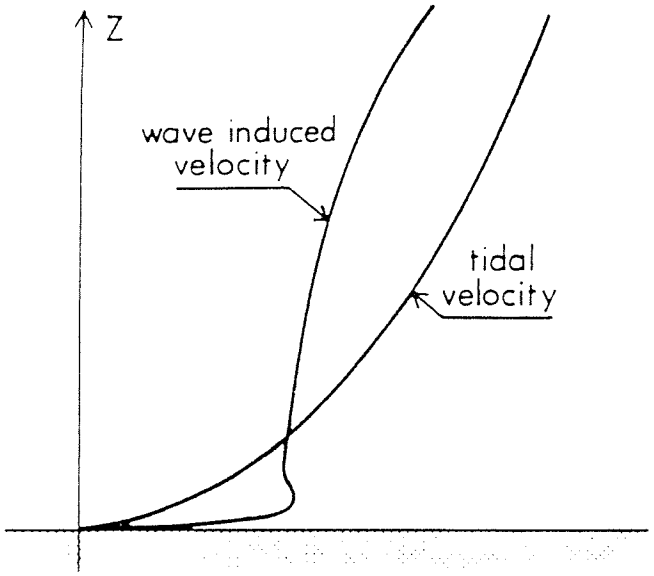

Figure 2-3 Wave and current induced boundary layers

Because the wave boundary layer is relatively thin (in most cases a few centimetres), the velocity gradients within this layer are relatively large. It is assumed that bed shear stress and turbulence intensities are proportional to the velocity gradients, which implies that the shear stress and turbulence intensity in the wave boundary layer are relatively large and important for the sediment transport processes.

Sediment concentration layers

In previous experimental series [Al Salem, 1993] [Koelewijn, 1994], time-dependent sediment concentration measurements under sheet-flow conditions revealed a three layer system. High sediment concentrations are present in the sheet-flow layer close to the bed, which can be divided into a pick-up layer and an upper sheet-flow layer. A more uniform concentration is found above these sheet-flow layers in the suspension layer. Although the behaviour of each sediment concentration layer is different from the others, they influence each other and are working as one unit. Figure 2.4 shows the time-dependent flow velocities and sediment concentrations in the three layers during a wave cycle (wave period=7.2 sec). In this picture, the 0 mm refers to the bed-level at rest.

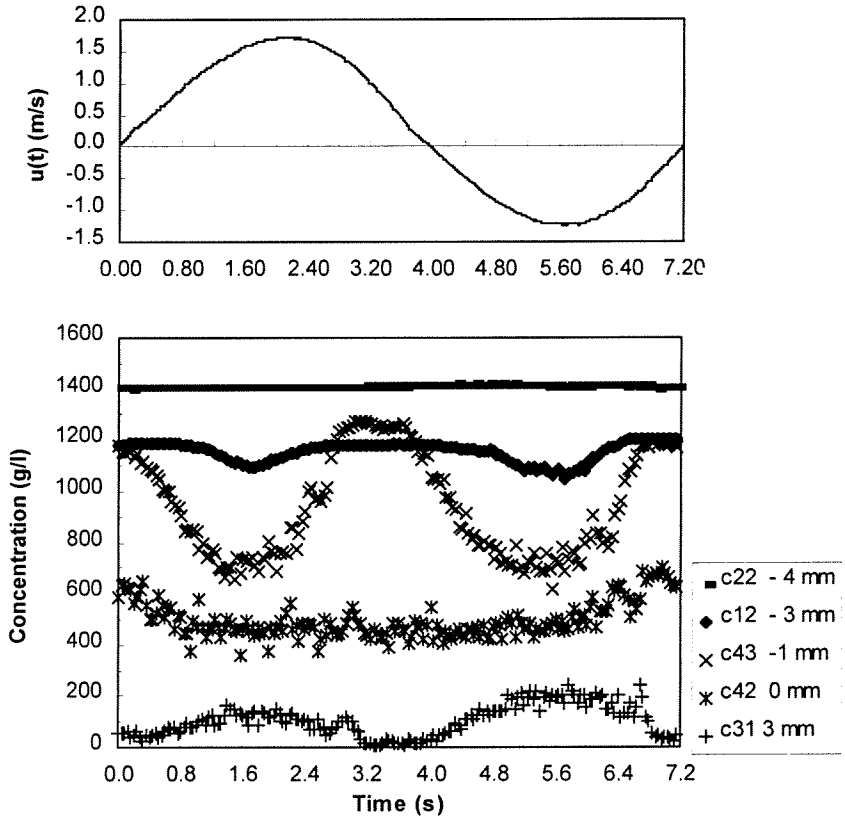

in which: **-4 mm:** **sand bed**
-3 and -1 mm: **pick-up layer**
0 mm: **transition between pick-up and upper sheet-flow layer**
3 mm: **upper sheet-flow layer**

Figure 2-4 Time-dependent flow concentrations, showing different layers

The pick-up layer lies just above the part of the sand bed which is in rest, and is the layer in which the grains are picked up and transported vertically upward to the upper sheet-flow layer. Due to the exchange of the sediment particles between these two layers, the phase behaviour is just opposite: in the pick-up layer the concentration decreases when the flow velocity increases, while at the same moment in the upper sheet-flow layer the concentrations increase; during a decrease of the flow velocity the situation is just opposite.

Figure 2.5 shows the time-averaged concentrations over the vertical and the three different layers. The thickness of the sheet-flow layer strongly depends on the flow conditions and the particle sizes. A concentration of around 1 vol%, which is 26.5 g/l, is used as value for the transition from sheet-flow to suspension layer. This was also done in previous studies [e.g. Hassan (1996)]. In the suspension layer intergranular forces are no longer important.

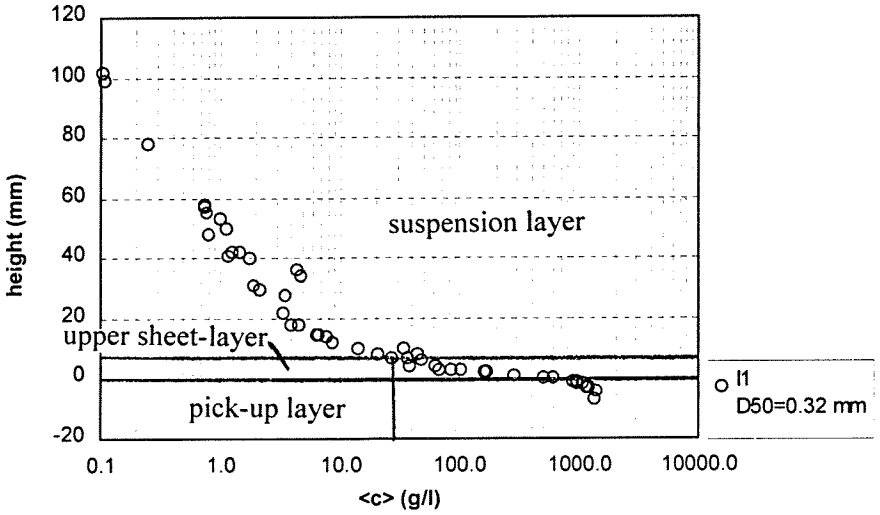

Figure 2-5 Concentration profile divided into three layers

Unsteady effects

Figure 2.6 shows the flow velocity during a wave cycle which was measured during a test, for a sinusoidal wave in combination with a steady current. The direction of the net current is called the positive direction in this study. In this direction the largest velocities occur. The wave cycle can be divided in a positive part, which is the period in which positive velocities occur (from 0 until 4 s in the figure), and a negative part, in which the direction of the flow velocity is negative (from 4 until 7.2 s in the figure). The net transport rate is the time-averaged transport over the wave-cycle.

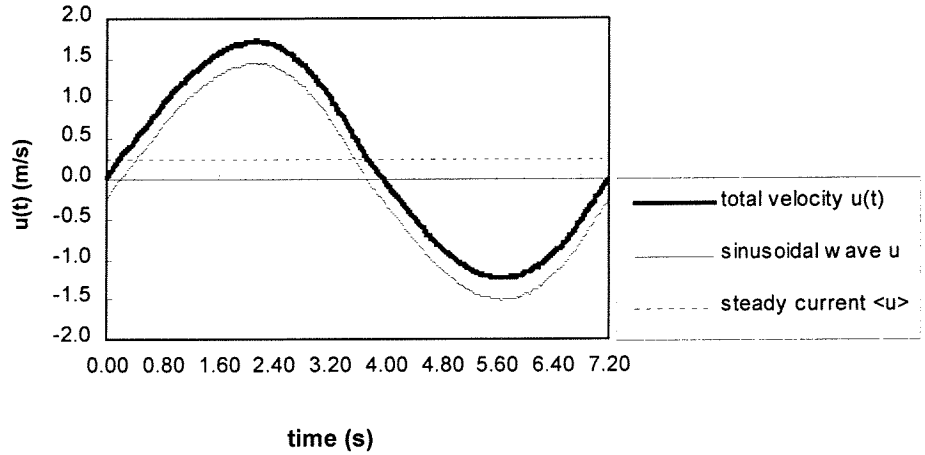

Figure 2-6 Flow velocity during wave cycle

Generally it is assumed that the time-dependent sand transport is proportional to a power of the velocity at a small distance above the bed. The power is larger than one and lies around 3. The result is a net transport rate in the direction of the net flow velocity.

Sometimes, this relation is not so clear because different unsteady effects can occur. Phase lag effects imply that sand is brought into suspension during the positive wave-cycle, but has not enough time to settle during this half wave-cycle. It remains in suspension and is thus transported in the negative direction during the succeeding negative wave-cycle. The same is valid for the following half wave cycle. Under asymmetric flow velocities these effects may be larger during the larger velocities in the positive half cycles than during the smaller negative velocities. The phase-lag effects result is a much smaller net transport rate than expected. Sometimes the net transport rate even is directed opposite to the largest velocity. Another unsteady process is the occurrence of concentration peaks around flow reversal. These concentration peaks are caused by shear instabilities in the wave boundary layer. Just before the end of a present part of the wave cycle these so-called suspension ejection effects bring lot of particles into suspension. These particles will be transported in the successive part of the wave-cycle.

These unsteady effects occur especially in case of fine sand. The small particles are easily stirred up to a high level, and due to the small fall velocities it takes long before they have reached the bed. In case of a long wave period, there is enough time for the settling process, but for a small wave period the flow reversal takes place much quicker. In addition, the flow velocity is important. A high flow velocity increases the level to which the sand is stirred up. It is the combination of grain-size, flow velocity and wave period which determines whether unsteady effects are important.

2.3 Sediment transport models

2.3.1 General background of different transport models

The basic definition of sediment transport per unit width is the product of flow velocity and sediment concentration, integrated over the water depth. The formula is given by:

$$q_s(t) = \int_0^h \varphi(z,t)dz = \int_0^h u(z,t)\cdot c(z,t)dz \qquad (2.2)$$

in which: q_s = sediment transport per unit width
h = water depth
φ = sediment flux
z = height above the sand bed
u = flow velocity
c = sediment concentration

Both flow velocity and concentration vary during a wave cycle, sometimes not in phase with each other. However, the concentration is strongly related to the flow velocity. This makes sediment transport under waves combined with a steady current a complex phenomenon.

Unsteady models

The most accurate way to resolve equation 2.2 is to calculate the unsteady flow velocity and the unsteady sediment concentration, with the correct boundary conditions. After that, the sediment transport can be averaged over the wave cycle, to calculate the net transport rate. The group of transport models based on this principle are called unsteady models, because they take into account the unsteady concentration variations. A disadvantage of these models is that they are difficult to use, because the detailed calculations require much computing time and a proper insight in the processes.

Quasi-steady models

A simplified way to predict the sediment transport is to assume a direct relation between the driving force, which is the flow velocity or the bed shear stress, and the sediment transport. No phase lags between flow velocity and concentration or acceleration effects are accounted for, and thus this type of transport model is called quasi-steady. These models can only be used in cases where the response time on the flow velocities for the sand particles is small. The process of stirring up and settling down to the bed must take place in a much shorter time than the wave period. The fall time, in which a sand particle settles on the bed, is given by:

$$t_f = z/W_s \qquad (2.3)$$

In which: t_f = the fall time of a sand particle
z = the level to which the sediment is stirred up
W_s = fall velocity of a sand particle

The fall time must be small compared to the wave period T. In quasi-steady models the velocity is the only time-dependent variable parameter, making them relatively easy in use.

Some of these models are based on experimental data, resulting in black box models, like Madsen and Grant (1976), Sleath (1978) (see also Janssen, 1995), Ribberink and Al Salem (1994) and Ribberink(1997)(see also Van Rijn et. al. 1994). The last two will be further explained in the next section.

Another group of quasi-steady models is based on a theoretical analysis of the sediment transport process. Examples are the models of Bagnold (1963) and Bailard (1981); the last one will be further worked out in Section 2.3.2.

Intermediate model

Dibajnia and Watanabe (1992) derived a model in between steady and unsteady models. Although they assume a direct relation between sediment transport rates and flow velocity, they include a time lag effect to take into account the unsteady effects (see Section 2.2).

2.3.2 Models used in this study

In this section, three transport models which are used in this study are described.

Model of Ribberink

The model of Ribberink is based on the assumption that the shear stress is the driving force for sediment transport. The shear stress is made dimensionless according to the formula of Shields, given in equation 2.1. Sediment transport occurs when the effective shear stress θ' is larger than the threshold of motion, given by the critical shear stress θ_{cr}. Under waves, the transport direction is determined by $\theta'/|\theta'|$. The general formula is:

$$\Phi(t) = \frac{q_s}{\sqrt{g\Delta D_{50}^{\ 3}}} = m\left(|\theta'(t)| - \theta_{cr}\right)^n \frac{\theta'(t)}{|\theta'(t)|} \tag{2.4}$$

in which:
- Φ = dimensionless transport
- Δ = relative density
- $\theta'(t)$ = Shields parameter
- θ_{cr} = critical Shields parameter, threshold of motion of sand particles
- m = empirical coefficient
- n = empirical coefficient

To calculate the net transport rate, the parameters in this formula must be defined.

The relative density Δ is given by:

$$\Delta = \frac{\rho_s - \rho_w}{\rho_w} \tag{2.5}$$

in which:
- ρ_s = density of sediment
- ρ_w = density of water

The critical value of the Shields parameter θ_{cr} depends on the non-dimensional grain-size:

$$\theta_{cr} = f(D_*) \text{ with } D_* = D_{50}\left[\frac{g\Delta}{\nu^2}\right]^{1/3} \tag{2.6}$$

in which: D_* = non-dimensional grain-size
ν = kinematic viscosity of water

The Shields parameter gives the relation between the bed shear stress and the under water weight of a particle, and is given by eq. 2.1. The bed shear stress, which is used in this formula, can be calculated in different ways. In the transport model of Ribberink, the model of Ribberink and Van Rijn is used. This model is based on the theory of Jonsson (1966) for waves, who assumed that the shear stress depended on the density of the sediment, the imposed velocity and a certain friction faction. This leads to the formula:

$$\tau_b(t) = \tfrac{1}{2}\rho_s f_{cw}|u(t)|u(t) \tag{2.7}$$

in which: τ_b = bed shear stress
f_{cw} = friction factor
u(t) = horizontal oscillatory flow velocity directly above the wave boundary layer

In this formula f_{cw} is a friction factor, induced by a combination of waves and a steady current. Following Madsen and Grant(1976) this friction factor is written as:

$$f_{cw} = \alpha f_c + (1-\alpha) f_w \tag{2.8}$$

in which: f_{cw} = friction factor in case of wave and a steady current
f_c = friction factor in case of currents only
f_w = friction factor in case of waves only

The parameter α gives the relation between the net current and the oscillating flow velocity, and is given by:

$$\alpha = \frac{|\langle u \rangle|}{|\langle u \rangle| + \hat{u}} \tag{2.9}$$

To estimate the wave friction factor f_w, the formula of Swart (1974) is used:

$$\begin{cases} f_w = \exp\left[-6 + 5.2\left(\dfrac{\hat{a}}{k_s}\right)^{-0.19}\right] \\ f_{w,\max} = 0.3 \end{cases} \tag{2.10}$$

in which: â = amplitude of horizontal excursion of water particles near the bottom
k_s = bed roughness height

To estimate the friction factor for currents only, the following formula was used, which is based on the logarithmic velocity distribution:

$$f_c = 2 \cdot \left[\frac{\kappa}{\ln z/z_0} \right]^2 \tag{2.11}$$

in which: κ = Von Karman coefficient = 0.4
z = height above the sand bed
$z_0 = k_s/30$

The parameter z gives the level at which the flow velocity is measured. This level must be defined before the transport rate can be calculated.

Both friction factors depend on a bed roughness height k_s. Ribberink (1997) argues that it is better to use two different values for k_s: $k_{s,c}$ for the net current flow and $k_{s,w}$ for the oscillatory flow. Possible reason is that the wave boundary layer is much thinner than the current boundary layer, and therefore the sheet-flow process interacts with a very different part of the boundary layer for waves and for currents. Generally it is assumed that the bed roughness height is related to the dimensions of the bed material. For k_s values like for example D_{50}, $2.5*D_{50}$ or D_{90} are used. In sheet-flow conditions, k_s has not a constant value, but depends on the Shields parameter. The Shields parameter varies during the wave cycle, but to simplify the model the averaged magnitude of the Shields value can be used. Nevertheless this means that the bed roughness must be calculated by an iterative process.

The coefficients m and n in equation 2.2 were found by curve fitting of experimental data. Ribberink (1997) found for a large data set of laboratory experiments m=11 and n=1.65. This results in the following formula:

$$q_s(t) = \sqrt{g\Delta D_{50}^3}\, 11 \left(|\theta'(t)| - \theta_{cr} \right)^{1.65} \frac{\theta'(t)}{|\theta'(t)|} \tag{2.12}$$

Model of Bailard

Bailard (1981) based his model on Bagnold's (1963) theoretical analysis of the energy used for sediment transport. Bailard, like Bagnold, considered the total sediment transport as the sum of the bed load and the suspended transport for waves. The power expended in transporting bed load is equal to the work done by the fluid. This is equal to the fluid shear stress times the steady mean velocity, divided by the angle of internal friction. The angle of internal friction indicates the collision between the grains. The efficiency of this process is not 100 %, and therefore Bailard used an efficiency factor ε_b. The power expended in the suspended load is derived in the same way. This process is not related to the collision of the grains but to the fall velocity W_s. The fluid must raise the particles with a velocity equal to W_s to keep them in suspension. For this process the efficiency factor ε_b is used.

Originally, the model was developed to calculate transport rates in rivers. Bailard applied it for situations in coastal areas, where in general grain-sizes are smaller than in rivers, and both waves and currents induce transport processes.

The general formula is:

$$q_s(t) = q_{s,b}(t) + q_{s,s}(t) \tag{2.13}$$

in which: $q_{s,b}$ = bed load transport
$q_{s,s}$ = suspended load transport

The bed load transport for a horizontal bed is given by:

$$q_{s,b}(t) = \frac{\frac{1}{2} f_w \varepsilon_b}{\Delta g \tan\phi} u^3(t) \tag{2.14}$$

in which: ε_b = bed load coefficient
ϕ = angle of internal friction

The suspended transport is given by:

$$q_{s,s}(t) = \frac{\frac{1}{2} f_w \varepsilon_s}{\Delta g W_s} |u^3(t)| u(t) \tag{2.15}$$

in which: ε_s = suspended load coefficient

Koelewijn (1994) used for the friction factor f_w, the following formula:

$$f_w = f_{cw} = \frac{|\tau_{b,\max}|}{\frac{1}{2}\rho u_{b,\max}^2} \tag{2.16}$$

in which $\tau_{b,\max}$ is the maximum of the bed shear stress calculated by a suitable method, for example the method given in eq. 2.7.

Model of Dibajnia and Watanabe

This sediment transport model takes into account unsteady effects that can occur under certain circumstances. If the flow velocity in e.g. the positive direction is high, the sand particles can be stirred up to such a high level that they cannot settle to the bed within the same positive part of the wave cycle. The sediment stays in suspension and will be transported in the negative direction during the successive half wave cycle. If the fall time of a sand particle is longer than the part of the wave period in which it is stirred up, it is likely that these unsteady effects occur.

Using their own experimental data, Dibajnia and Watanabe found the following equation to calculate the dimensionless total transport rate:

$$\Phi = \frac{< q_s >}{W_s D_{50}} = 0.001 |\Gamma|^{0.55} \tag{2.17}$$

The parameter Γ gives the total amount of sediment which is transported during both parts of the wave cycle:

$$\Gamma = \frac{u_c T_c (\Omega_c{}^3 + \Omega_t{}^3) - u_t T_t (\Omega_t{}^3 + \Omega'_c{}^3)}{(u_c + u_t) T} \tag{2.18}$$

in which: Ω_c = amount of sand suspended and transported during the *positive* half wave cycle (subscript c refers to the positive part, the crest of the wave)
Ω'_c = amount of suspended sand remaining from the *positive* half wave cycle, to be carried by the *negative* velocity
Ω_t = amount of sand suspended and transported during the *negative* half wave cycle (subscript t refers to the negative part, the through of the wave)
Ω'_t = amount of suspended sand remaining from the *negative* half wave cycle, to be carried by the *positive* velocity
u_c = equivalent sinusoidal velocity amplitude for the positive part of the wave cycle T_{crest},, and is defined by:

$$u_c{}^2 = \frac{2}{T_c} \int_0^{T_c} u^2 dt \tag{2.19}$$

The same is valid for the equivalent velocity during the negative part of the wave cycle u_t. These parameters describe the unsteady effects. For the *positi*ve part of the wave cycle, they are given by:

$$\omega_c \le 1 \quad (t_f \le T_c) \qquad \begin{cases} \Omega_c = 2\omega_c \dfrac{W_s T_c}{D_{50}} \\ \Omega'_c = 0 \end{cases} \tag{2.20}$$

$$\omega_c > 1 \quad (t_f > T_c) \qquad \begin{cases} \Omega_c = 2\dfrac{W_s T_c}{D_{50}} \\ \Omega'_c = 2(\omega_c - 1)\dfrac{W_s T_c}{D_{50}} \end{cases} \tag{2.21}$$

in which:

$$\omega_c = \frac{t_{fall}}{T_c} \tag{2.22}$$

The parameter ω_c indicates the occurrence of unsteady effects, and is equal to the ratio of the fall time of a sand particle and the positive part of the wave period. When the parameter ω_c is larger than one, it is likely that strong unsteady effects occur. The fall time during the positive part of the wave cycle depends on the level to which the particles are stirred up and the fall velocity of these particles. This is given by:

$$t_{fall,c} = z/W_s = \frac{1}{2}\frac{u_c{}^2}{\Delta g W_s} \tag{2.23}$$

where: z = level at which sediment is stirred up
The same is valid for the negative part of the wave-cycle.

2.4 Transport of non-uniform sediments

In nature, bed material does not consist of uniform grains. It is a mixture of small and larger grains. This influences the transport process in a complex way. Large grains are imposed to stronger forces, due to a larger friction surface and a higher drag force, but they also have a larger weight. Particles with different sizes influence each other. Small particles are often sheltered by larger ones, and larger particles are generally more exposed to the current. The different transport rates for different diameters induce a selective process and thereby cause changes in the bed composition.

In this section, attention is paid to the influence of grain-sizes on the modelled transport rates. Morphological processes due to changes in transport rates go beyond the scope of this study. In order to take account of grain-size variations the so-called size fraction method can be used, which is explained in the next section.

2.4.1 Size-fraction method

In the models described in Section 2.3.2, the sediment mixture is in most cases characterised by the D_{50} only. In this way a uniform sediment can be described, but variations in grain-sizes in the bed material can not be taken into account. The variation in grain-sizes, usually called the gradation, is defined by the relation between the percentages of fine, median and coarse grains of the sand mixture. The so-called geometric standard deviation is the parameter for the gradation which is used in this study. It is given by:

$$\sigma_g = 0.5\left(\frac{D_{84}}{D_{50}} + \frac{D_{50}}{D_{16}}\right) \tag{2.24}$$

in which: σ_g = geometric standard deviation
D_{84} = diameter for which 84 % of the mixture is finer
D_{50} = diameter for which 50 % of the mixture is finer
D_{16} = diameter for which 16 % of the mixture is finer

In order to take into account the effects of the gradation, a size-fraction method is implemented in the transport models. In the size-fraction method, the bed material is divided in a number of size-fractions, each characterised by a certain diameter D_i and a volume percentage of the bed material p_i. For each fraction the transport capacity $q_{c,i}$ is calculated, which is equal to the transport rate of uniform sand with diameter D_i. The transport rate for each fraction is given by:

$$q_i = p_i \cdot q_{c,i} \tag{2.25}$$

in which: q_i = net transport rate per unit width for fraction i
p_i = volume percentage of fraction i, present in bed material
$q_{c,i}$ = transport capacity for fraction i

The total net transport rate in case of N size fractions, q_N, is given by the sum of the transport rates of all fractions:

$$q_N = \sum_{i=1}^{N} q_i \tag{2.26}$$

in which: q_N = net transport rate in case of N fractions

The contribution of fraction i to the total net transport rate can be calculated using:

$$p_{T,i} = (q_i / q_N) \cdot 100\ \% \tag{2.27}$$

in which: $p_{T,i}$ = contribution of fraction i to the total net transport rate, as volume percentage

The mean diameter of the transported material is determined by:

$$D_T = \sum_{i=1}^{N} (D_i \cdot p_{T,i}) \Big/ 100 \tag{2.28}$$

in which: D_T = mean diameter of transported material
D_i = mean diameter of fraction i

The parameter D_T/D_m is the ratio of the diameter of the transported material and the bed material. D_m is defined by:

$$D_m = \sum_{i=1}^{N} (D_i \cdot p_i) \Big/ 100 \tag{2.29}$$

in which: D_m = mean diameter of the bed material

If D_T/D_m is larger than one, the transported material is coarser than the bed material, which means that mainly coarse fractions are transported. $D_T/D_m<1$ means that mainly fine fractions are transported. Thereby the parameter D_T/D_m, and also the difference between p_i and $p_{T,i}$, indicate which selective processes are predicted by the transport model.

When N=1 there is only one size fraction and the sediment is considered to be uniform. The parameter q_N/q_1 is the ratio of the predicted transport rate of a mixture characterised by N fractions with different diameters and the predicted transport rate for a mixture characterised by D_{50}. This parameter indicates the impact of the use of the size-fraction method on the predicted transport rate.

The size fraction is implemented into three models given in Section 2.3.2: Bailard, Ribberink and Dibajnia and Watanabe.

Bailard

The model of Bailard gives in combination with the size-fraction method:

$$q_{b,i}(t) = q_{b,c,i} \cdot p_i = p_i \frac{\frac{1}{2} f_{cw} \varepsilon_b}{\Delta g \tan\phi} u^3(t) \tag{2.30}$$

$$q_{s,i}(t) = q_{s,c,i} \cdot p_i = p_i \frac{\frac{1}{2} f_{cw} \varepsilon_s}{\Delta g W_{s,i}} \left|u^3(t)\right| u(t) \tag{2.31}$$

The wave- and current related friction coefficient f_{cw} is related to the bed roughness height, according to eq. 2.8 and 2.10. The bed roughness height is not determined by a single grain, but by the combination of all grains in the bed material. It is the same for all size fractions and is related to the D_{50} or D_{90} of the mixture. The total *bed* load transport is not related to the diameter of the fraction D_i. The total bed load in case of one fraction is equal to the total bed load in case of N fractions. The total *suspended* load transport depends on the diameter of the fraction D_i through the settling velocity $W_{s,i}$.

Ribberink

The formula of Ribberink, given in eq. 2.12, in combination with the size-fraction method results in:

$$q_{s,i}(t) = p_i \sqrt{g\Delta D_i^3}\, 11\left(\left|\theta_i'(t)\right| - \theta_{cr,i}\right)^{1.65} \frac{\theta_i'(t)}{\left|\theta_i'(t)\right|} \tag{2.32}$$

In this formula, the transport rate is directly related to D_i, and also via the Shields parameter. For every size-fraction, this parameter is defined by:

$$\theta'_i = \frac{\tau_{b,i}}{(\rho_s - \rho) g D_i} \tag{2.33}$$

The bed shear stress is related to the fraction factor f_{cw} (see eq. 2.7), but this parameter is the same for all size-fractions, like in case of Bailard. The value of the Shields parameter is therefore only directly influenced by D_i.

The critical shear stress can be regarded as a relation between the drag force and the under-water weight of a single grain, indicating the threshold of motion. Therefore, theoretically, this critical value of the Shields parameter is related to D_i according to:

$$\theta_{cr,i} = f(D_{*,i}) \qquad \text{with} \quad D_{*,i} = D_i \left[\frac{g\Delta}{\nu^2}\right]^{1/3} \tag{2.34}$$

In sheet-flow conditions, the effective shields parameter lies far above the critical value, so it gives not much change whether the critical value is related to D_m of the mixture or D_i of every fraction.

Dibajnia and Watanabe

Using the size-fraction method in this model results in:

$$q_{s,i} = p_i W_{s,i} D_i \cdot 0.001 \left|\Gamma\right|^{0.55} \tag{2.35}$$

and varies for the different fractions via $W_{s,i}$ and D_i. The parameter Γ (eq. 2.18) is also dependent on the fall velocity $W_{s,i}$ and the diameter D_i.

2.4.2 Splitting up a mixture into size fractions

Sometimes, the bed material is a mixture of two different sand types, which makes it easy to define the size fractions. In most cases the bed material consists of a whole range of diameters, often characterised by D_{50} only. T gradation, which is the width of the grain-size distribution is often given by the geometric standard deviation. The formula for this parameter is given in equation 2.24.

In many previous experimental series carried out in the LOWT, the gradation was more or less according to a log-normal grain-size distribution. Assuming this grain-size distribution means that D_{50} is not equal to the mean diameter D_m. D_m must be calculated using eq.2.29. Dividing a continuous grain-size distribution into a number of size fractions can be done in several ways. In Appendix A1, one method is explained, which was also used by Ribberink (1987). In this method a log-normal grain-size distribution is assumed, which is only characterised by D_{50} and D_{90}. For this distribution an upper and lower boundary are chosen, according to $P(D \geq D_u) = P(D \leq D_l) = 2.28$ %. This means that 97.72 % of the grain-size distribution lies between the two boundaries. The region between these boundaries is divided in N size-fractions in such a way that $\ln(D_{i+1})-\ln(D_i)$ is constant. This is similar to the diameters of the sieves which are normally used to measure the grain-size distribution of a sand mixture. The ratio of successive sieve diameters D_{i+1} / D_i is constant.

The number of size-fractions required depends on the gradation. A larger number of size-fractions gives a more accurate result, which means that q_N/q_1 and D_T/D_m converge to a specific value, but more size-fractions also require more computing time. A minimum number of fractions which gives satisfying results must be chosen .

2.4.3 Hiding- and exposure correction

The interaction between the different size-fractions can be explained by two phenomena:
- 'sheltering' or 'hiding' of the smaller grains in the lee of the larger grains
- an increased exposure of the larger sizes to the flow

These phenomena result in corrections on the transport formulas. Two types of corrections can be distinguished:
- correction of the effective Shields parameter θ_{eff}, thus reducing its value for the finer fractions and increasing it for the coarser fractions
- correction of the critical Shields parameter θ_{cr}, thus increasing its value for the finer fractions and reducing it for the coarser fractions

In the transport formulas used in this study and explained in Section 2.3.2, only the formula of Ribberink uses these parameters, so corrections can only be applied in this formula. In this method, the transport rate is proportional to θ_{eff}-θ_{cr}, which for both types of correction implies a reduced transport rate for the smaller sizes and an increase in transport for the larger sizes. The resulting formula is given by:

$$q_{s,i}(t) = p_i \sqrt{g\Delta D_i^3}\, 11\left(\xi_{eff} \cdot |\theta_i'(t)| - \xi_{cr} \cdot \theta_{cr,i}\right)^{1.65} \frac{\theta_i'(t)}{|\theta_i'(t)|} \qquad (2.36)$$

in which: ξ_{eff} = correction factor for the effective Shields parameter
ξ_{cr} = correction factor for the critical value of the Shields parameter

Einstein (1950) suggested that hiding- and exposure correction factors were only applied on finer size-fractions and not on coarser sizes, which results in only reducing the transport rates for the finer material.

Many different methods exist to calculate the hiding- and exposure correction factors. In the transport program the corrections according to Egiazaroff (1965), Ashida and Michiue (1973), Day (1980) (see Ribberink (1987)) and Komar and Wang (1984) are implemented and will be explained here.

It must be noted that the correction coefficients were not derived especially for sheet-flow conditions, and in most cases not even for situations with an oscillating velocity. Under sheet-flow conditions, when a small top layer of the bed is entirely set in motion, it is not likely that hiding-and exposure processes have much impact on the total net transport rate. Especially the effects of correcting the critical value of the Shields parameter are negligible under sheet-flow conditions, because this parameter plays only a minor role and is dominated by the effective Shields parameter.

Egiazaroff

Egiazaroff derives an expression for the critical bed shear stress for each fraction using a balance of forces acting of individual grains in a flat-bed situation in uniform flow. According to Egiazaroff, the larger grain-sizes, as part of a sediment mixture, experience a larger drag force than in the uniform case. This leads to the following correction factor for the critical shear stress:

$$\xi_{cr,i} = \frac{\theta_{cr,corrected}}{\theta_{cr,Shields}} = \left[\frac{\log 19}{\log\left(19 \frac{D_i}{D_m} \right)} \right]^2 \tag{2.37}$$

in which: ξ_{cr} = correction factor for critical shear stress
D_m = mean diameter of the bed material
D_i = mean diameter of fraction i

He verified his formula using experimental data of other researchers and found good results. Because only the critical shear stress is corrected, the correction factor of the effective shear stress $\xi_{eff} = 1$.

Ashida & Michiue

Ashida and Michiue used Egiazaroff's formula in combination with a transport formula, and compared this with a number of laboratory experiments. They came to an empirical correction on his formulation for values of $D_i/D_m < 0.4$, given by:

$$\xi_{cr,i} = 0.85 \frac{D_m}{D_i} \tag{2.38}$$

For values of $D_i/D_m \geq 0.4$ they used Egiazaroff's formula. Figure 2-7 shows the differences between the values of the parameter ξ_{cr} according to Egiazaroff and Ashida and Michiue.

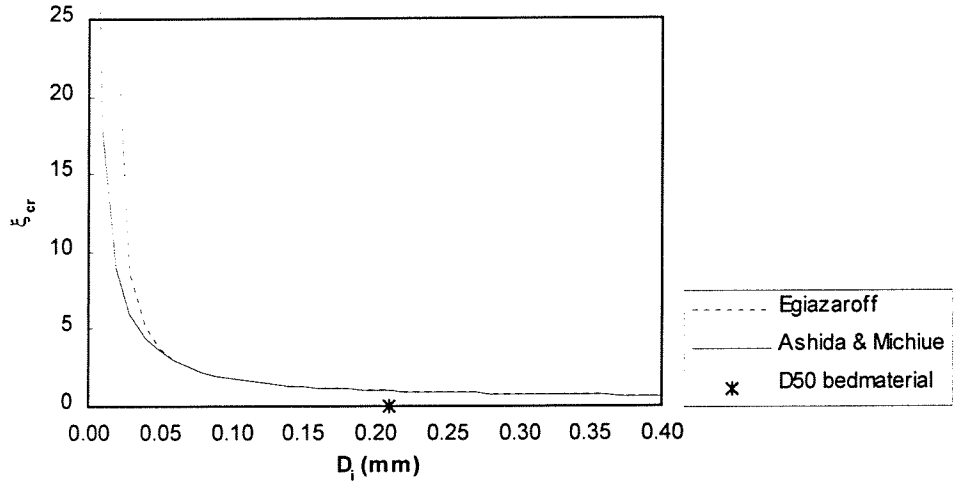

Figure 2-7 Values of ξ_{cr} according to Egiazaroff and Ashida & Michiue

Komar & Wang

Komar and Wang did not correct Shields' curve, but they found a new expression for the critical shear stress under wave conditions, given by:

$$\tau_{b,cr} = 0.00515(\rho_s - \rho)gD_m^{0.568}\tan\alpha \tag{2.39}$$

in case of grains with a diameter smaller than 1 mm.

Making this shear stress dimensionless results in:

$$\theta_{cr} = \frac{\tau_{b,cr}}{(\rho_s - \rho)gD_{50}} = 0.00515D_i^{-0.43}\tan\alpha \tag{2.40}$$

The parameter α in this formula is the angle of repose for a single particle in degrees, also called the pivoting angle, which is shown in Figure 2.8.

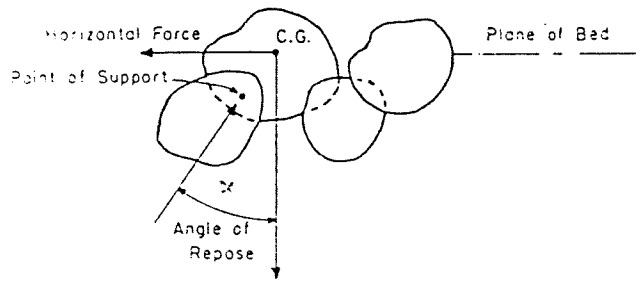

Figure 2-8 Angle of repose for a single sand particle

Miller and Byrne (1966) studied the parameter α and found the following empirical equation:

$$\alpha = a\left(\frac{D_i}{D_m}\right)^b \tag{2.41}$$

in which: a = 61.5, empirical coefficient related to the shape of the particles;
61,5 is used for intermediate sphericity and roundness
b = -0.3, empirical sorting parameter

The dimensionless shear stress according to Komar and Wang can be expressed as a correction factor ξ_{cr}. Then, this correction factor can be compared with the results of other methods, and can be implemented in the formula given in eq. 2.38.

$$\xi_{cr} = \frac{\theta_{Kom}}{\theta_{cr}} \tag{2.42}$$

in which: ξ_{cr} = the correction coefficient of the critical Shields parameter
θ_{Kom} = the dimensionless critical shear stress according to Komar and (given in eq. 2.42)
θ_{cr} = the dimensionless shear stress according to Shields

The effective shear stress is not corrected, so $\xi_{eff} = 1$.

Day

Instead of the previous corrections on the critical shear stress, Day corrected the mobility number, a kind of dimensionless bed-shear stress, using a large number of experimental laboratory data. This can be written as a sheltering coefficient for the effective shear stress, given by:

$$\xi_{eff} = \left[\frac{0.4}{\left(D_i / D_A\right)^{0.5}} + 0.6\right] \tag{2.43}$$

In this formula D_A is the grain diameter which needs no correction. D_A is not necessarily equal to D_{50} or D_m, but depends on the gradation of the mixture:

$$\frac{D_A}{D_{50}} = 1.6\left(\frac{D_{84}}{D_{16}}\right)^{-0.28} \tag{2.44}$$

In this case the correction factor for the critical shear stress $\xi_{cr} = 1$.

3 Experimental set-up

This chapter deals with the experimental set-up for series I and J. An introduction on the present measurements is given in Section 3.1. The laboratory facilities, in which the experiments were carried out, and the different instruments and measuring techniques which are used are briefly described in 3.2. Section 3.3 gives the test programmes. A more extensive description of the experimental set-up is given in Janssen and Van der Hout (1997).

3.1 Introduction

Two series of experiments were carried out from October 1996 until January 1997.
In series J net transport rates were obtained for 0.21 mm sand. In the series I experiments, coarser sand was used. Test measurements showed that a grain-size of 0.45 mm caused too many bed forms. As a consequence these experiments would not have been comparable to those with fine sand. Therefore sand with a grain-size of 0.32 mm was used. In the first part of this series I net transport rates were measured, while the second part consisted of time-dependent measurements of flow velocities and concentrations at different levels above the sand bed.

As explained in Chapter 1, the main goal of these experiments was to obtain more data and information about the influence of the grain-size on sediment transport rates and the transport mechanisms under sheet-flow conditions.

3.2 Measuring facilities and instruments

Large Oscillating Water Tunnel

All experiments were performed in the Large Oscillating Water Tunnel of Delft Hydraulics. A picture of this LOWT is shown in Figure 3.1.

The tunnel consist of a large U-shaped tube, with a long horizontal section and two vertical cylindrical risers. One of them is open to the air, in the other riser a piston is constructed. This piston, which is driven by a hydraulic servo-cylinder mounted on top of the riser, sets the water in motion. It is controlled by an electro/hydraulic valve which measures the difference between the (measured) actual piston position and the desired position (feedback system).

In the horizontal part, which is the test section, an oscillating water motion is induced, simulating the orbital motion close to the sand bed. The test section is 14 m long, 1.1 m high and 0.3 m wide. A 0.3 m thick sand bed can be brought into the tunnel, so 0.8 m height is left for the oscillating water flow. Underneath both risers two sand traps are constructed, in order to collect the sand that is removed from the test section during a tunnel run. The side walls of the test section consist of thick glass windows in a steel frame. The roof is formed by 13 steel plates which can be removed separately.

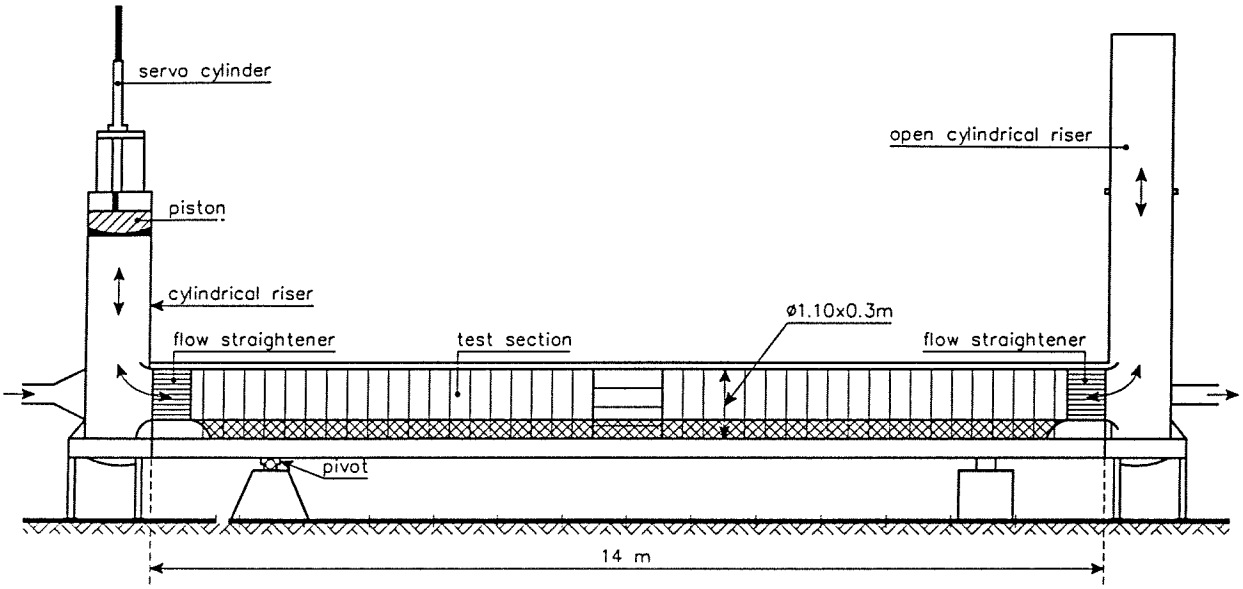

Figure 3-1 Large oscillating water tunnel

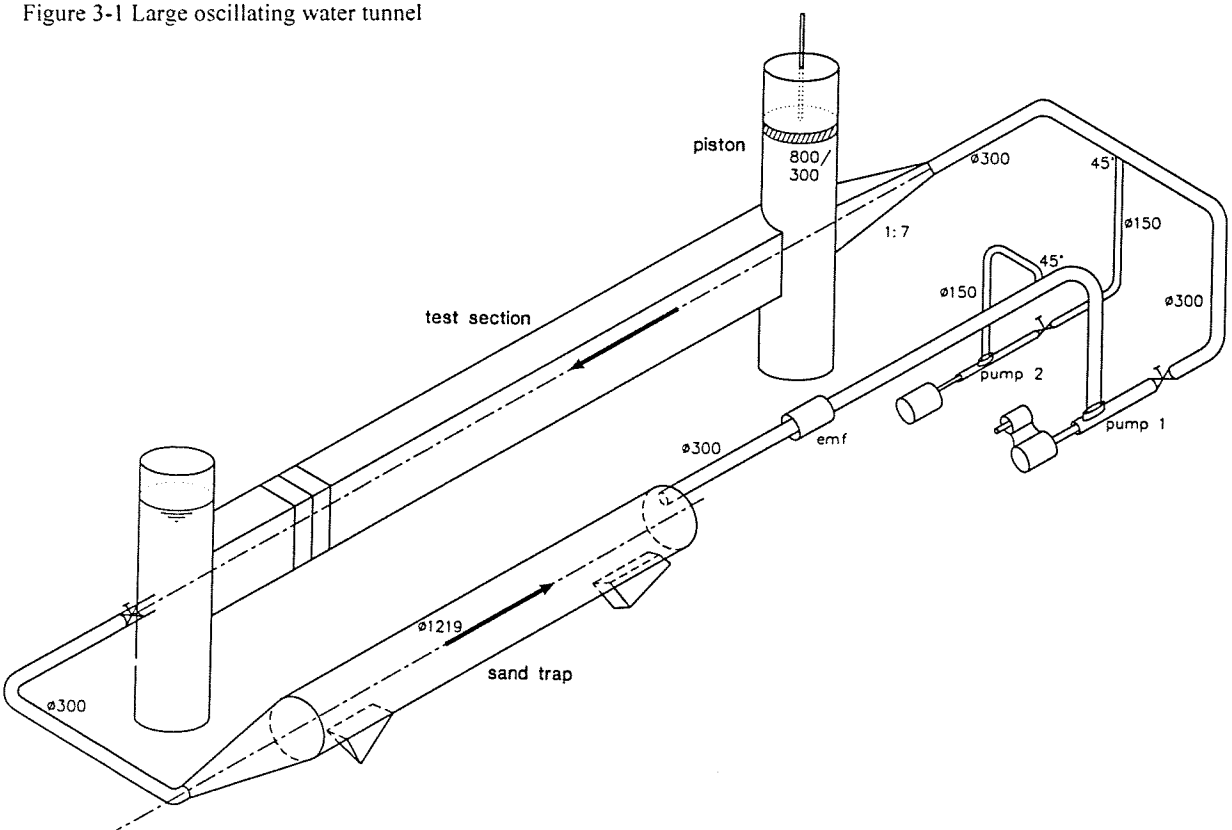

Figure 3-2 Model of the circulation system

In 1992 the tunnel was extended with a recirculating flow system, to superimpose a net current to the oscillating motion. The recirculating flow system is provided with a third sand trap consisting of a 12 m long pipe with a diameter of 1.2 m, which is connected to the downstream cylindrical riser by a pipe with a diameter of 0.3 m (see Figure 3.2).

The trap was designed for trapping 90% of the suspended sediments (min. grain-size 100 μ) at maximum flow discharge. Downstream of the trap two pumps are installed for generating a net current. The maximum capacity of the larger pump is 100 l/s and of the smaller pump 20 l/s. The maximum superimposed current velocity in the test section is about 0.45 m/s.

The maximum piston amplitude is 0.75 m, which results in a maximum semi-excursion length of the water particles in the test section of 2.45 m. The range of velocity amplitudes is 0.2-1.8 m/s and the range of oscillating periods is 4-15 seconds (see Figure 3.3). Each desired oscillatory water motion (regular/irregular, sinusoidal/asymmetric) can be realised in the test section within certain constraints for piston velocity and piston acceleration. A detailed description of the tunnel is given by Ribberink (1989).

Due to the large dimensions of the tunnel, the wave velocities close to the bed and the wave periods are equal to velocities occurring in nature, so full-scale experiments are possible. Still there are some differences between reality and the situation in the tunnel. In open water, waves propagate in a certain direction, as they change in phase along the propagation direction. Along the wave tunnel the same phase occurs at every location, which makes it impossible to indicate a positive direction of propagation. Therefore, the direction of the steady current is called the positive direction. Time-dependent horizontal pressure gradients along a horizontal line due to phase differences, as well as vertical orbital motions are not simulated in the tunnel.

Overview of other measuring instruments and techniques

Table 3-1 Overview of measuring instruments and techniques

measurements	technique/instrument	calculating/measuring
net transport rates	mass conservation technique Bed Level Sounding System (BLSS)	net transport rate bed level height
time-dependent measurements		
suspension layer	Laser Doppler Flow Meter (LDFM)	flow velocity
	OPtical CONcentration meter (OPCON)	sediment concentration
sheet-flow layer	Acoustic Doppler Velocity meter (ADV)	flow velocity
	Conductivity concentration Meter (CCM)	sediment concentration

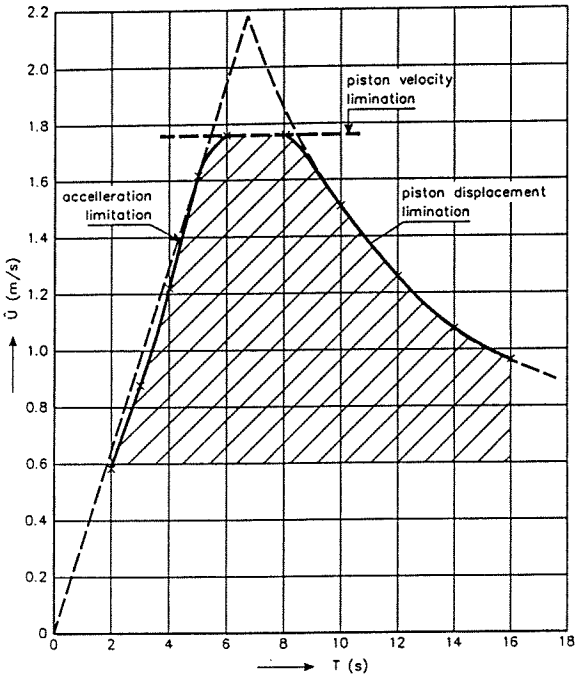

Figure 3-3 Velocity amplitude and period range

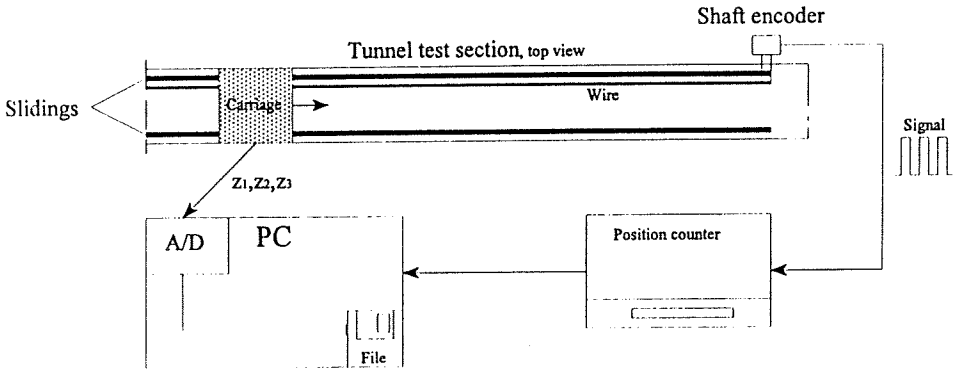

Figure 3-4 General outline of the BLSS

Mass-Conservation Technique

A mass-conservation technique has been used to estimate the time- or wave-averaged sediment transport rates in the test section. It means the volume of sand collected in the sand traps must be equal to the change of volume in the test section during the tunnel run. A sediment continuity equation is solved, starting from the left or the right sand trap. The mean value of the two computations at 2 m at the right of the middle of the test section, i.e. in the undisturbed part of the tunnel, is used as the measured result.
The volumes collected in the traps are calculated by dividing the weight under water of the collected sand by an estimated value of the porosity of the sand bed. The change of volume in the test section is estimated by measuring the bed level before and after each tunnel run. For a more detailed description this method and the formula's, see Appendix A2.

Bed Level Sounding System (BLSS)

The Bed Level Sounding System is used to measure the bed level before and after each test. The system consists of three profilers on a carriage, which can be installed on rails in the tunnel and can be moved along the test section. The measuring technique is based on conductivity. While moving along the tunnel, the conductivity in the sampling volume at the end of a profiler remains constant, which means that the probe tip is kept at a constant distance from the sand bed. At every centimetre, a computer registers the level of the profilers, together with the position along the tunnel, which gives a detailed description of the situation of the sand bed. Figure 3.4 shows the general outline of the BLSS in the tunnel.

Laser Doppler Flow Meter (LDFM)

A forward scatter laser Doppler system, developed by Delft Hydraulics, was used to measure the horizontal (in the direction along the tunnel axis) and vertical velocity components of the water particles with a 'forward scatter reference beam method'. Three laser beams, of which two are used as reference beams, are transmitted through the tunnel and received by two photo cells behind the tunnel. Part of the signal is scattered by the particles in the water. Because of the velocity of the particles the frequency of the scattered signal is different from the original, undisturbed signal. The horizontal and vertical flow velocities can be determined from this 'Doppler-shift'. A great advantage of this instrument is that it is placed outside the tunnel. The laser beams go through the glass, so nothing obstructs the flow or influences the sand bed. The height of the sensing volume is 0.2 mm. Additionally the LDFM is used to measure velocities from 100 mm down to about 20 mm above the bed. Below that level the sediment concentration is so high that the sand particles block the laser beams. In some tests the LDFM did not work correctly, caused by the clear water which did not give enough scatter. Figure 3.5 gives the configuration of the LDFM in the tunnel.

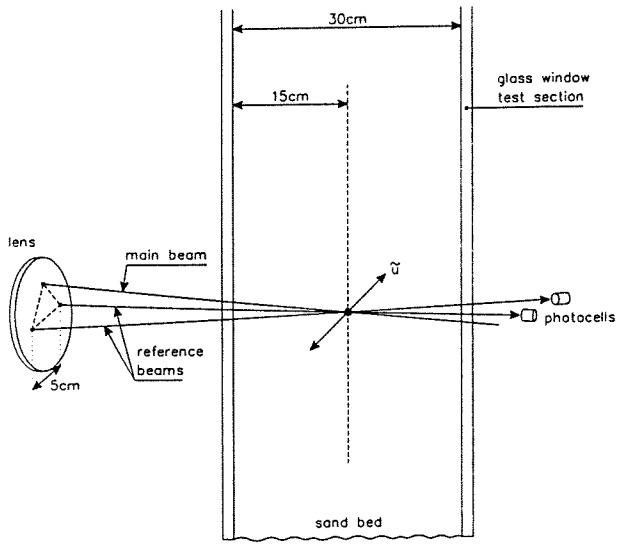

Figure 3-5 Laser-beam configuration in the tunnel

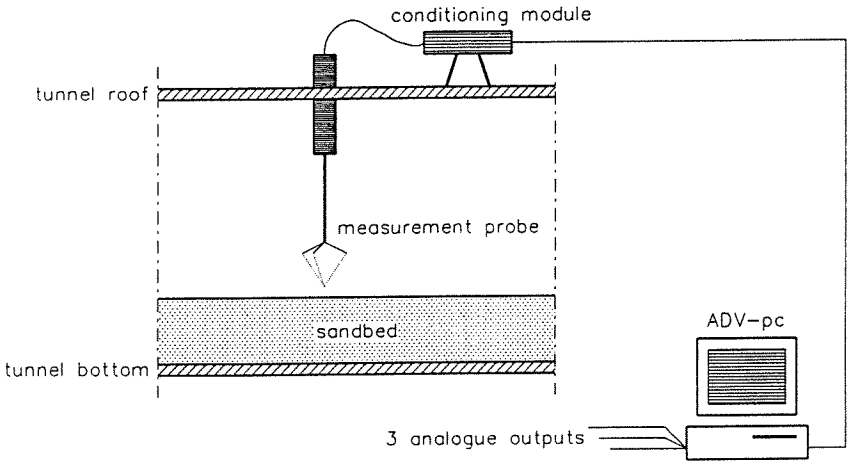

Figure 3-6 General outline of the ADV system

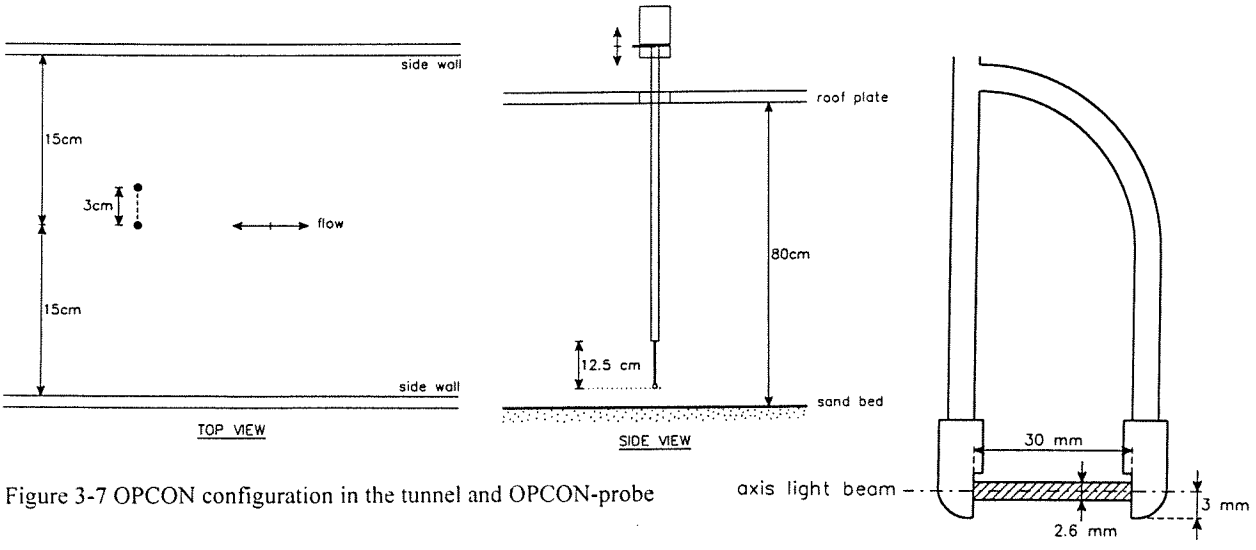

Figure 3-7 OPCON configuration in the tunnel and OPCON-probe

Acoustic Doppler Velocity meter (ADV)

An acoustic velocity meter was used for the velocity measurement closer to the sand bed. This measuring technique is based on the acoustic Doppler principle, which uses an acoustic pulse to remotely measure the three components of the water velocity at one point, at a rate of 25 Hz. The ADV sensor consists of four ultrasonic transducers, one transmit transducer in the centre of three receive transducers. The frequency of the scattered signal is shifted by the moving sand particles. The sampling volume is less than 1 cm^3. At levels very close to the bottom, around 1 cm, the ADV results give unrealistically high velocities, which might be caused by the very high concentrations of sand. The instrument is put into the water, thereby influencing the flow and causing local erosion, which makes it more difficult to measure during a certain period at a certain level above the bed. Figure 3.6 gives the general outline of the ADV system.

OPtical CONcentration meter (OPCON)

Time-dependent suspended sand concentrations were measured using an optical concentration meter. The OPCON measures volume concentration in the range of 0.1-50 g/l and is based on the extinction of the infra-red light. In Figure 3.7 the OPCON configuration in the tunnel is shown. The optical axis between light transmitter and receiver is orientated horizontal and perpendicular to the flow. The distance between transmitter and receiver is 30 mm, which is the length of the sensing volume. The height of the sensing volume is 2.6 mm.

The calibration of the OPCON strongly depends on the grain-size of the suspended material. It can be expected that the D_{50} of the suspended sediment is smaller than the D_{50} of the bed material. In previous studies, with D_{50}=0.13 and 0.21 mm, a transverse suction system was used which made it easy to take a sample of the suspended material. It showed that the $D_{50,susp}$ was about 75-80% of the $D_{50,bed}$. It is assumed to use a diameter of 75% of the $D_{50,bed}$ in this study, which could be a high estimate because of the coarse grains. This gives some uncertainties in the OPCON-results. More details about the OPCON and its calibration are given in the data-report [Janssen and Van der Hout, 1997] or in report of previous studies [e.g. Hassan, 1996].

Conductivity Concentration Meter (CCM)

Time-dependent sediment concentrations in the sheet-flow layer and in the bed were measured using a conductivity concentration meter, developed by Delft Hydraulics. The instrument measures high concentrations (100-1500 g/l) with a four point electro-resistance method. Figure 3.8 shows the CCM configuration in the tunnel. The height of the sensing volume is 1 mm. The probe is brought into the test section from below, through the tunnel bottom and the sand bed in order to minimise the flow disturbances.

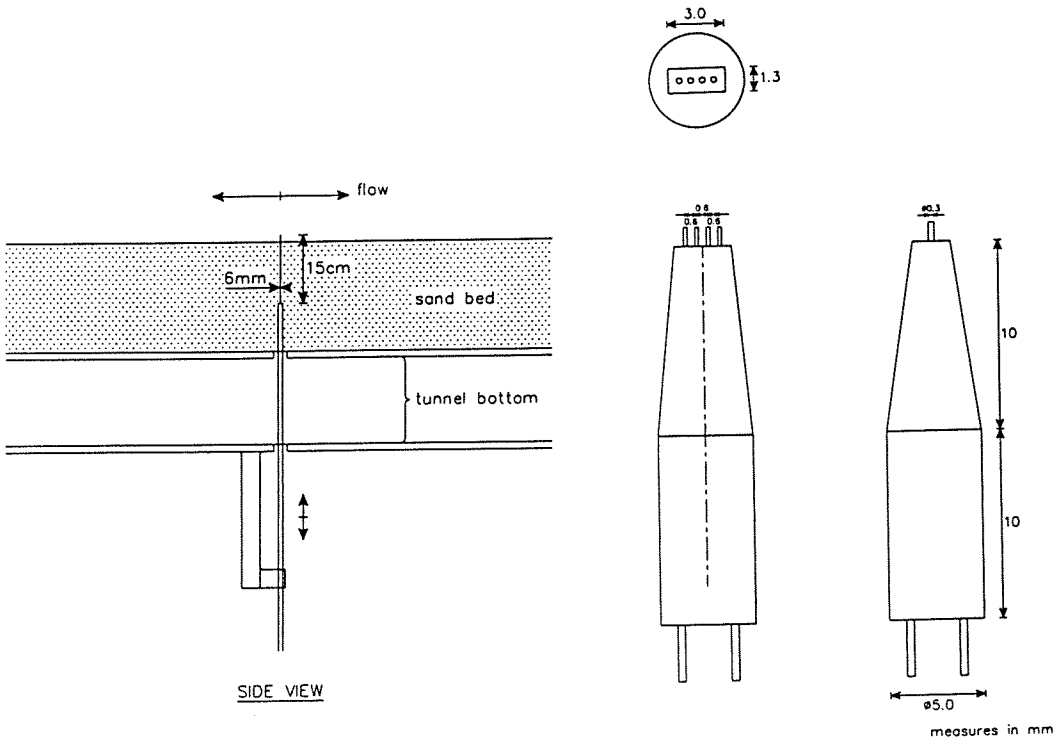

Figure 3-8 CCM configuration in the tunnel and CCM probe

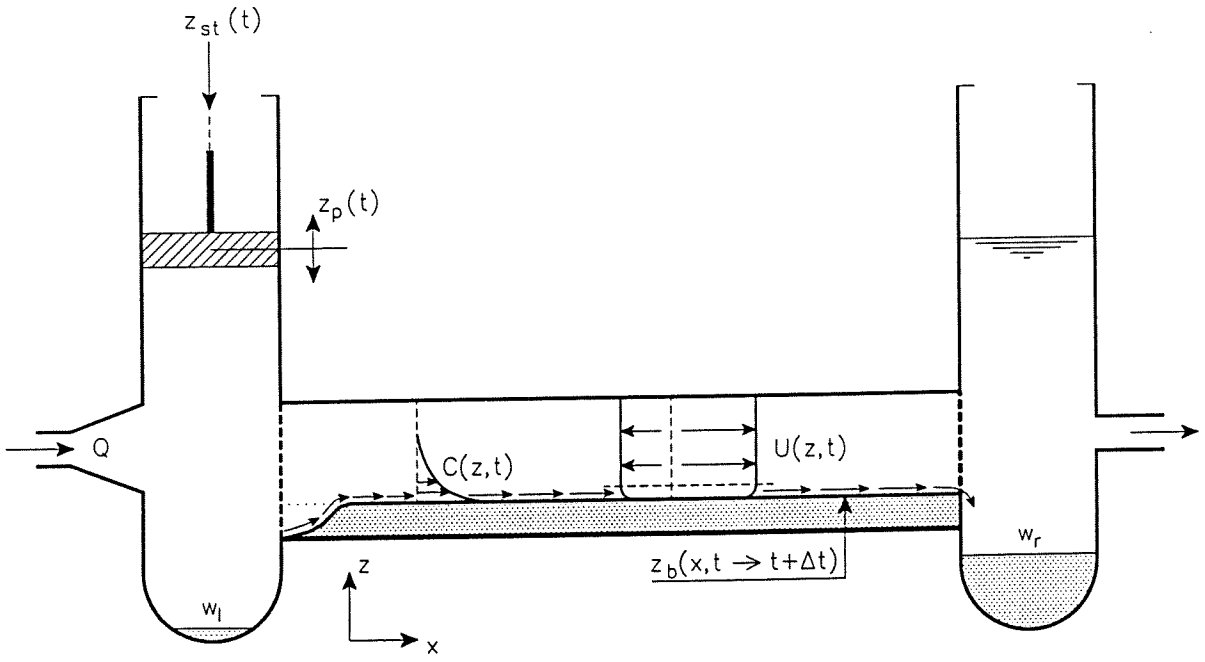

with
$z_{st}(t)$ = piston motion due to steer signal
$z_p(t)$ = measured piston motion
Q = flow discharge
U(z,t) = flow velocity
C(z,t) = sediment concentration
z_b = bed level height
w_l, w_r = weight in left and right sand traps

Figure 3-9 Imposed and measured parameters

3.3 Measurement programmes and conditions

3.3.1 Measured parameters

The test program consisted of two series of measurements. Series J concerns measurements of net transport rates with sand with a grain diameter of 0.21 mm, and series I includes, besides similar net transport measurements, also more detailed velocity and concentration measurements, with sand with a grain diameter of 0.32 mm.

The following parameters were measured (see also Figure 3.9):

Net transport rate measurements:
- bed level height (z_{bed}) and sand trap volumes for the estimation of transport rates
- flow velocities U(z,t) at 100 mm above the bed
- local change of the sand bed during the tunnel run (δz_{bed}) at the measuring point

Flow velocity and concentration profile:
- flow velocities U(z,t) and W(z.t), both in the sheet-flow and in the suspension layer
- sediment concentrations C(z,t), both in the sheet-flow and in the suspension layer
- local change of the sand bed during the tunnel run (δz_{bed}) at the measuring point

3.3.2 Test measurements

At the laboratory of Delft Hydraulics, 0.45 mm sand was easily available, so this could be used for series I. Before the actual measurements started, test measurements were carried out in order to find out if ripples would occur under the planned conditions. In order to obtain results which could be compared to results from previous experimental series, the vortex generation induced by these ripples had to be avoided. It turned out that under almost all conditions, except for the ones with the highest velocities, ripples were generated very soon after the start of a test. It could be concluded that this sand could not be used, and a better choice would be sand with a grain diameter around 0.35 mm. An order was done for new sand with this diameter, but when it was delivered, it turned out to have a D_{50} of around 0.39 mm, which was considered too large for the tests. A new order was done, for two types of sand, both with a mean grain diameter of around 0.3 mm. Sieve analysis showed that the first type had a mean grain-size of 0.275 mm and the second had a mean grain-size of 0.353 mm. A 50%-50% mixture of these two sands, of which D_{50} was 0.32 and D_{90} was 0.48 mm, was used in series I (see also Fig.3.11 Grain-size distribution series I). A complete description of the test measurements and their results is given in the data report [Janssen and Van der Hout (1997)].

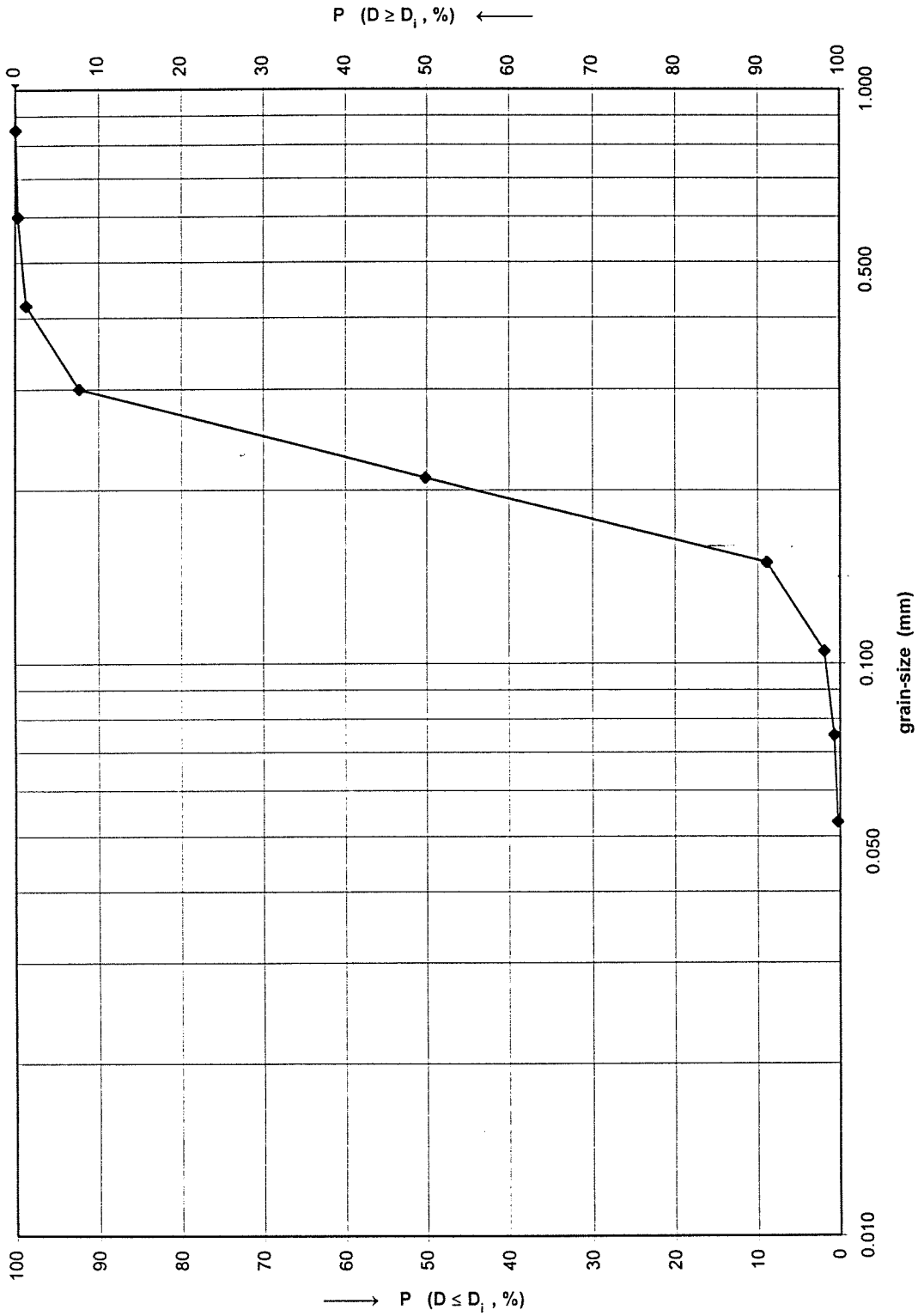

Figure 3-10 Grain-size distribution of unsieved dune sand used in series J

3.3.3 Series J

Series J was carried out first. The test program consisted of six conditions, which are similar to conditions in series H, in which net transport rates were measured for 0.13 mm sand [Hassan (1996); Van der Wal (1996)]. All conditions are a combination of regular sinusoidal waves and a steady current.

The experimental conditions can be found in Table 3.2. The net current is determined by the LDFM measurements. It is the wave-averaged velocity measured at 10 cm above the sand bed. In the table the pump discharge Q_{pump} and piston amplitude are given which are associated with the measured hydraulic condition. For the net current two velocities have been used, i.e. 0.24 and 0.41 m/s. The velocity amplitude varies between 0.46 and 1.28 m/s. The first combination of velocities is performed for three different periods, to give information about the influence of the wave period.

Table 3-2 Experimental condition series J

condition	<u> (m/s)	Q_{pump} (l/s)	û (m/s)	amplitude (%)	period (sec)
J1	0.24	45.6	1.06	49.2	7.2
J2	0.25	45.7	1.28	58.8	7.2
J3	0.41	88.2	0.46	21.1	7.2
J4	0.41	88.3	0.65	30.0	7.2
J5	0.24	45.2	1.04	43.2	4.0
J6	0.23	45.2	1.09	78.5	12.0

The sand used in series J had the following characteristics: $D_{10} = 0.15$ mm
$D_{50} = 0.21$ mm
$D_{90} = 0.32$ mm.

The measured grain-size distribution is shown in Figure 3.10.

For every condition, four tests were carried out. The experimental procedure for the net transport rates was as follows:

- the sand bed was flattened before each test
- the LDFM was positioned at the desired location along the test section, x = 2 m
- the bed level was measured every cm by BLSS
- each experiment was started by starting the computer steering/data-acquisition system
- the desired piston amplitude and net current were imposed
- the time for each tunnel run varied from 7 to 20 minutes, depending on the erosion hole generated at the upstream boundary. Tests stopped when it would influence the flow in the measuring section
- after a test the bed level was measured again
- the sand traps were emptied and the collected sand was weighed under water
- the erosion holes were refilled with the collected sand and the bed was flattened again

After all tests of this series, for all conditions video recordings were made of the bed level variation during the wave cycle.

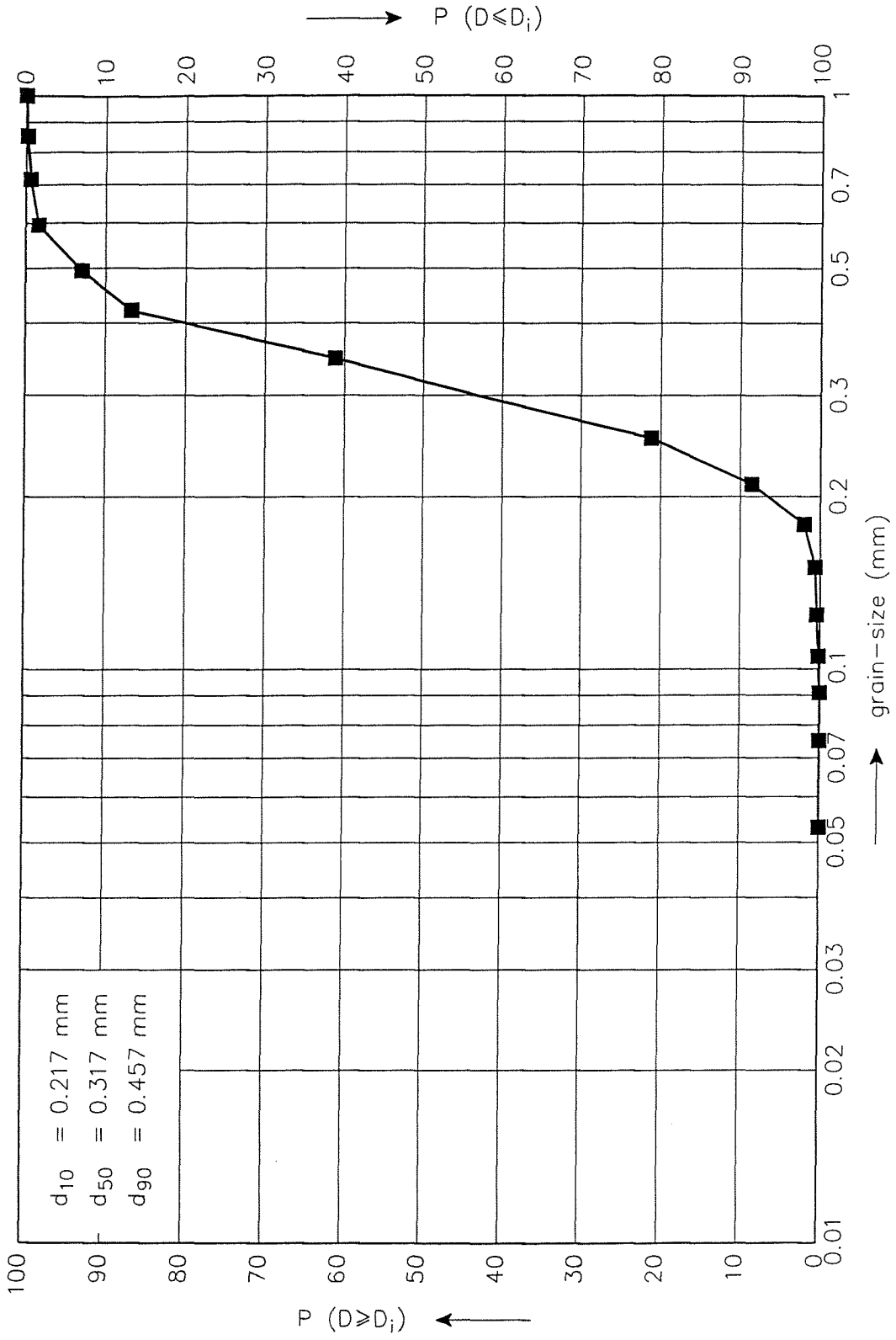

Figure 3-11 Grain-size distribution series I

3.3.4 Series I, net transport rate measurements

The test program of series I consisted of five conditions. The flow velocities are measured using the LDFM at 10 cm above the sand bed. The net current velocity was again varied between 0.24 and 0.44 m/s. The velocity amplitudes were chosen remarkably higher than at series J, to prevent the generation of ripples. The experimental conditions used in series I are given in Table 3.3.

Table 3-3 Experimental conditions series I

test	<u> (m/s)	Q_{pump} (l/s)	û (m/s)	amplitude (%)	period (sec)
I1	0.26	45.4	1.47	66.5	7.2
I2	0.25	45.4	1.70	76.9	7.2
I3	0.42	87.8	0.65	30.0	7.2
I4	0.42	87.8	0.92	42.2	7.2
I5	0.45	87.8	1.50	66.5	7.2

The sand used in series I had the following characteristics: D_{10} = 0.22 mm
D_{50} = 0.32 mm
D_{90} = 0.48 mm

The measured grain-size distribution is shown in Figure 3.11.

3.3.5 Series I, time-dependent measurements

At condition I1, comparable with condition E2 and H6 (see Table 1.1 and Appendix E) detailed velocity and concentration measurements are performed. At one location in the tunnel, x = 2 m, at different locations along the vertical, velocities and concentrations were measured.

First, velocities were measured in the suspension layer (18 to 100 mm above bed level), using the LDFM. This was done in four tests. The velocities close to the sand bed were measured in seven tests, using the ADV (6 to 39 mm above bed level).
By using the CCM, the sediment concentrations close to the bottom (-7 to +10 mm) were measured during four tests. The concentrations in the suspension layer (10 to 110 mm above bed level) were measured by using the OPCON, in six tests. The experimental procedure was slightly different from net transport rate measurements:

- the sand bed was flattened
- the instruments were positioned at the desired locations
- the data acquisition system and the tunnel were started
- the bed level variation was measured manually at the location of the instrument every 36 seconds (= 5 waves) through the glass windows. These measurements have been used to correct the different levels of each instrument.
- measurements started some minutes after starting the tunnel run, in order to avoid initial effects
- the instruments were moved to another position during the test after a period of around 20 waves
- the time of a tunnel run was around 18 minutes, so the erosion hole caused by boundary effects could not influence the flow in the measuring section
- after a test the erosion holes were refilled and the sand bed was flattened again

3.4 Measured conditions previous experimental series

The series I and J, together with the previous performed series E and H, result in a data set, of net transport rates and velocity- and concentration profiles under the same conditions using different grain-sizes. Figure 3.12 gives an overview of measured conditions of the available data sets.

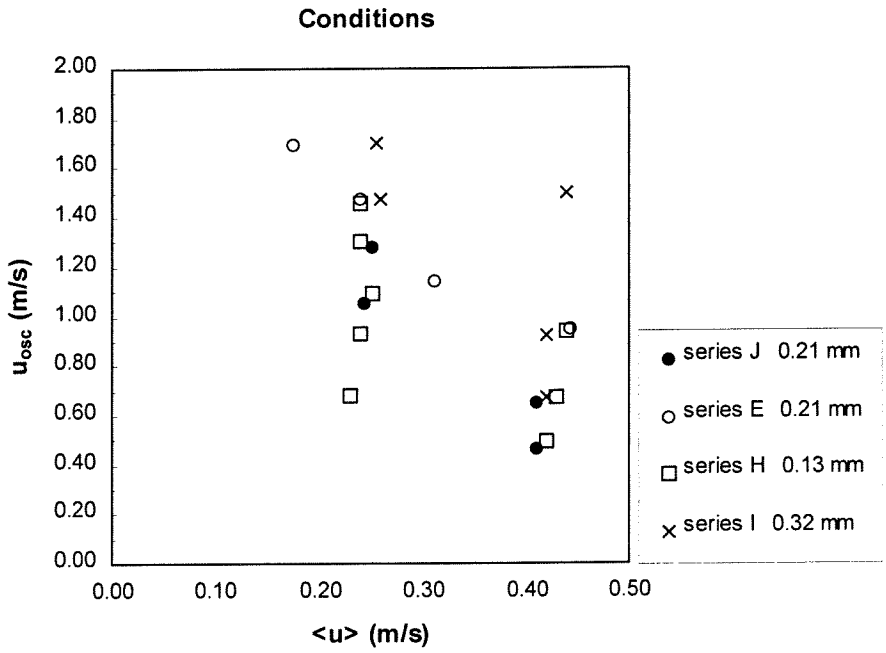

Figure 3-12 Measured conditions series E, H, I and J

4 Experimental results

In this chapter, the experimental results are described. The net transport rates from series J experiments are given in Section 4.1.1. The accuracy and reliability of these data is discussed in Section 4.1.2. In series I, first net transport rates were measured for every condition, with the results and the reliability given in Section 4.2. The time-dependent velocity and concentration profiles are presented in Section 4.3. A detailed overview of all data obtained in these experiments is given in the data report [Janssen and Van der Hout (1997)].

4.1 Net transport rates series J

4.1.1 Test results series J

In series J, experiments were carried out to measure the net transport rate. Transports are calculated using the mass-conservation technique (see Section 3.2 and Appendix A2). The assumption is made that the transport rates are uniform at the measuring location, where also the flow velocities are determined.

For every condition, four tests were performed. The results of each test individually are given in Appendix B1. One can see that the amount of sand in the sand traps strongly depends on the condition. A relative large net current velocity compared to the velocity amplitude gives no sand in the left sand trap. The change of volume during a tunnel run is the amount of sand removed from the tunnel and is determined by the difference between two bed level soundings, one before and one after the run. The loss of sand, calculated by subtracting the total volume of sand in the traps from the change of volume, is caused by real sand losses in the system, and by inaccuracies in the measurements. A positive value means that sand was 'lost'; more sand was transported out of the tunnel than was found in the sand traps. A negative value means that sand was 'produced'; a larger amount of sand was found in the traps than was carried out of the tunnel. Two estimates were done, using the mass-conservation technique, to calculate the transport rate (see Appendix A2): one starting from the left trap and one starting from the right. This results in the two transport rates q_l and q_r respectively found in Appendix A1.

The porosity during a test is calculated , using the final bed level of the test in question, the beginning bed level of the next test and the under-water weight of the amount of sand, used to refill the erosion holes. The calculated change of volume must be equal to the refilled volume of sand. The porosity of the refilled volume of sand can be determined. The average porosity is 0.38, which is used to calculate the transport rates. In series E (also 0.21 mm sand) the porosity was also determined as 0.38, and in series H (0.13 mm sand) it was 0.39.

In Table 4.1, the flow velocities and net transport rates per condition are given. The parameter <u> indicates the average velocity, measured with the LDFM at 10 cm. above the sand-bed, which is equal to the net current velocity. The parameter û indicates the oscillating velocity amplitude, and u_{rms} is the root mean square value of this horizontal oscillating velocity, given by the formula:

$$u_{rms} = \sqrt{(0.5 \cdot \hat{u}^2)} \tag{4.1}$$

Table 4-1 Average velocities and net transport rates series J

test	<u> (m/s)	û (m/s)	u_{rms} (m/s)	$<q_s>_{avg}$ (10^{-6} m^2/s)
J1	0.24	1.06	0.75	39.3
J2	0.25	1.28	0.91	63.6
J3	0.41	0.46	0.33	7.2
J4	0.41	0.65	0.46	20.6
J5	0.24	1.04	0.74	24.7
J6	0.23	1.09	0.77	41.7

Figures of the measured transport rates along the tunnel test section are given in Appendix B2. For every test two lines are plotted: one for the left estimation starting from the left trap, and one for the right estimation starting from the right trap. The small difference at the measuring location, x = 2 m, is caused by inaccuracies in the measurements and losses of sand. A horizontal line indicates a uniform net transport. The erosion hole at the incoming boundary, can be seen on these plots and also the partly generated bed forms at low-velocity conditions, like J3.

For every condition, the results of the different test were averaged, but sometimes not all four. In the plots of the net transport rates in Appendix B2, one can see that sometimes one test differs remarkably from the other three. If there was an explanation for this difference, the average is then taken over the remaining three tests.

The following tests are not accounted for:

- J1-t2: A higher velocity amplitude was imposed
- J2-t1: This is the first experiment that was performed. Settling of the sand bed caused remarkable inaccuracies in the calculated change of volume during the test
- J3-t1: This was the first run of a new condition, which also caused too much change in the sand bed
- J4-t1: A higher velocity amplitude was imposed
- J5-t1: This was the first run of a new condition, which caused too much change in the sand bed

The situation of the sand bed strictly depends on the imposed condition. This can be seen when a new condition is imposed, and the results of the first test at this condition differs from results of following test, which is caused by changes in the sand bed. However, these changes are not visible at first sight, and can not be measured. The best solution is to leave out the first test of every condition which shows a different transport rate when calculating the average results for a condition. This leads to the average values presented in Table 4.1.

To indicate the accuracy of the experimental results, the following statistical parameters were calculated, with the results given in Table 4.2.

averaged transport rate per condition $\langle q_s \rangle_{avg}$

standard deviation $$\sigma = \sqrt{\frac{1}{N}\sum_{i=1}^{n}\left(q_i - q_{avg}\right)^2}$$

relative error $r = \sigma/\langle q_s \rangle_{avg} * 100\%$

relative error of averaged transport rate (averaged over N tests) $r_{avg} = r/\sqrt{N}$

Table 4-2 Standard deviation and relative error series J

test	<u> (m/s)	û (m/s)	$\langle q_s \rangle_{avg}$ (10^{-6} m^2/s)	σ (10^{-6} m^2/s)	r (%)	r/√N (%)	averaged over
J1	0.24	1.06	39.3	2.71	6. 9	4.0	T 1,3,4
J2	0.25	1.28	63.6	2.00	3.1	1.8	T 2,3,4
J3	0.41	0.46	7.2	0.26	3.6	2.1	T 2,3,4
J4	0.41	0.65	20.6	0.43	2.1	1.2	T 2,3,4
J5	0.24	1.04	24.7	0.33	1.3	0.8	T 2,3,4
J6	0.23	1.09	41.7	0.69	1.7	0.8	T 1,2,3,4

The reliability of the net transport rates per condition is best indicated by averaged relative error $r_{avg} = r/\sqrt{N}$. Table 4.2 shows that, with relative errors varying from 0.8 to 4.0 %, the results are acceptable.

4.1.2 Accuracy and reliability of results

Van der Wal (1996) made an extensive study to the reliability of his results. In a similar way, the sources of inaccuracy will be determined in this section. The transport rates are calculated using the mass-conservation technique (see appendix A2). Inaccuracy in the parameters used in this calculations, leads to an error in the determined transport $\langle q_s \rangle$. Table 4.3 gives these parameters:

Table 4-3 Parameters concerning mass-conservation technique

parameter	indicating
ΔV	total eroded volume incl. pores [m^3]
G	total weight of sand collected in the traps [kg under water]
ε_0	porosity of sand [-]
ρ_s	density of sand [kg/m^2]
W	width of test section [m]
Δt	duration of one test [s]

The last three parameters will not cause inaccuracies, because ρ_s and W have a constant, resp. ρ_s = 2650 kg/m and W= 0.3 m, and the run time Δt is determined accurate by the data acquisition system recordings.

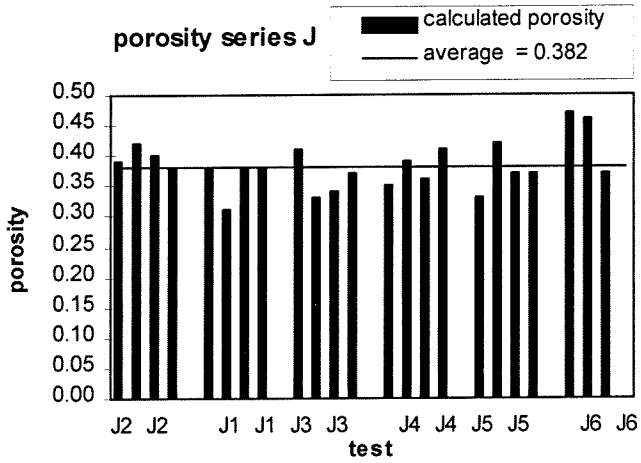

Figure 4-1 Porosity varying over all test series J

The first three parameters can be inaccurate. This might be caused by:

ΔV: inaccuracy of the BLSS
G: sand losses
inaccuracy in weighing
ε_0: variations over all tests
settlements and changes in sand bed

Van der Wal found out that the inaccuracy in weighting hardly influenced the error in the calculated transport rates, so this aspect can be neglected.
The measured velocities <u> and û can also be inaccurate, which influences the results and reliability of further study. This can be caused by inaccuracy of the measuring technique or variations in velocity across the width of the tunnel.

Sand losses

During a test, losses of sand occur in the system itself (e.g. sand staying behind in pipes), but except of some initial effects, these must be small. Other losses occur when collecting sand from the traps and weighing. Van der Wal (1996) tried to measure the loss of sand at the recirculation trap. He found a loss about 8 %. The sand used in this series had a diameter of 0.13 mm. The losses in the series J tests must be smaller, because of the diameter of 0.32 mm which makes it less likely to be washed away with the water.

Another loss of sand could be caused by the Bed Level Sounding System. The measurement carriage of this system with the three profilers cannot reach to the utmost right end of the tunnel. This means that the change of the bed level in the last part of the sand bed can not be measured. A correction can be made by estimating the volume of sand that was missing in the bed level sounding, using the change in bed level at the last measure point. This correction volume can be added to the loss of sand or to the amount of sand in the down stream sand trap. Appendix B3 gives the calculated correction volumes for every test. The loss of sand in every test is compared with the correction volume. It can be concluded that it is not right to add these two blindly. Sometimes the loss of sand is much bigger than the correction volume, but sometimes the correction volume is several times the total sand loss. During the experimental procedure this phenomenon was taken into account for as much as possible: when the traps were emptied, the last part of the sand bed was also flushed into the trap in order to lower the sand bed level to the begin level. For that reason it is not clear whether the correction volume is taken into account or not. Before and after each tunnel run, the bed level height was measured. Two measurements where done, one moving the carriage to the end of the tunnel, and one moving the carriage back to the starting point. Comparing these two measurements gives an indication of the accuracy of the bed level soundings. This is further worked out in Appendix B4.

Porosity

As was said in Section 4.2, for every test the porosity was calculated using the mass-conservation technique. This value is the porosity of the volume that is refilled after each test, and is shown in Figure 4.2. The average value of the porosity is 0.38, which is used in the calculation of the net transport rates. In these formulas, the porosity is used to calculate the weight of the total eroded volume. The porosity of the sand bed itself is not measured. It can have a lower value, especially after some tests are carried out and the sand bed has compacted. The variation in calculated porosity results in some inaccuracy in the calculated transport rate.

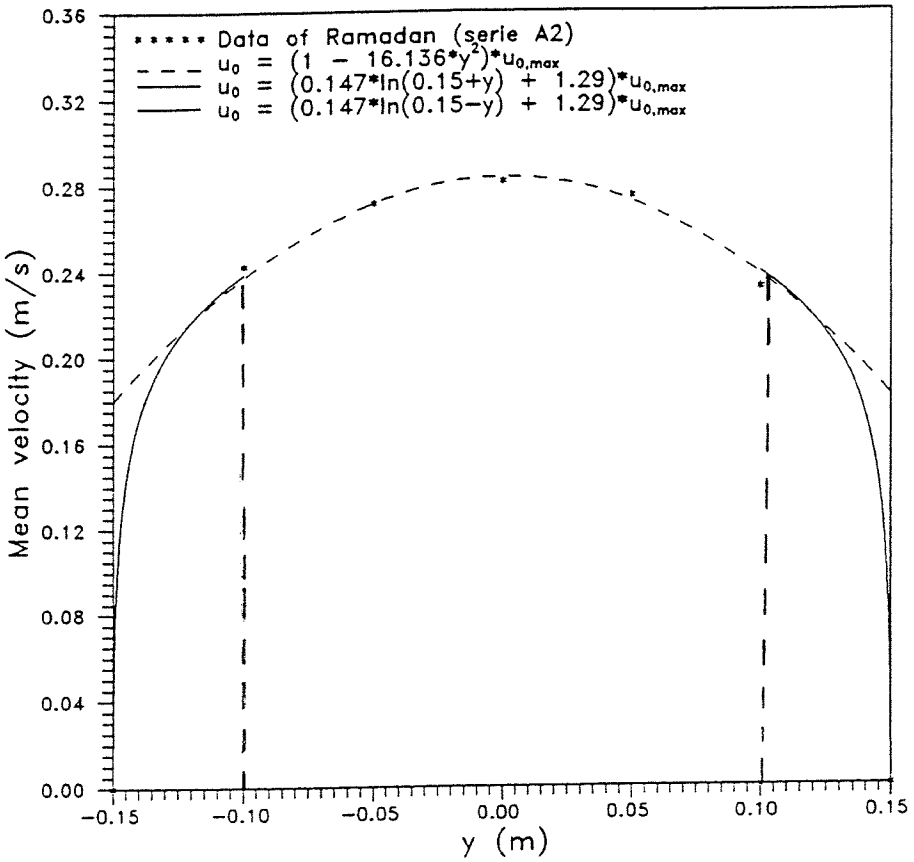

Figure 4-2 Velocity profile over cross-section

Velocity distribution over the cross-section

In all tests the flow velocity is measured at 10 cm above the sand bed, in the middle of the cross section. The net transport rates are derived from the mass balance over the complete test section and therefore correspond to the transport rate averaged over the cross section.

Ramadan (1994) measured the velocity across the width of the tunnel in order to study the influence of the side walls. One of the studied conditions consisted of sinusoidal oscillating flow combined with a net current. He found that the oscillating component was almost constant over the cross section, with a very thin boundary layer of the oscillating flow. Due to the much larger boundary layer of the net current, the mean velocity varied considerably. Koelewijn (1994) fitted the measured time-average velocity profile to an empirical curve which was a combination of a parabola and a log-profile, which can be seen in Figure 4.2. The assumption is made that in all tests the velocity is distributed over the cross-section in the same way as measured by Ramadan.

In order to find the transport rate that would have occurred when the maximum velocity would have been imposed, a correction factor is calculated according to Koelewijn, using the formula's given in Figure. 4.2. In Appendix B5 this is further explained. A new correction factor C_{new} is calculated. Using this factor corrected the net transport rates were derived. This gives for series J the following values:

Table 4-4 Correction factor for velocity distribution over cross-section

test	$\langle u_{max} \rangle$ (m/s)	$\langle u^3_{max} \rangle$ (m^3/s^3)	$\overline{\langle u^3 \rangle}$ (m^3/s^3)	C_{new} (-)	$\langle q_s \rangle_{avg}$ (10^{-6} m^2/s)	$\langle q_s \rangle_{avg}$ corrected (10^{-6} m^2/s)
J1	0.24	0.425	0.359	1.18	39.3	46.3
J2	0.25	0.625	0.533	1.17	63.6	74.4
J3	0.41	0.205	0.164	1.25	7.2	9.0
J4	0.41	0.328	0.267	1.23	20.6	25.3
J5	0.24	0.406	0.344	1.18	24.7	29.2
J6	0.23	0.415	0.351	1.18	41.7	49.2

The corrected transport rates are used in the following chapters, when comparing these series with other experimental results and models.

4.2 Net transport rates series I

4.2.1 Test results series I

The first part of series I consists of net transport measurements, carried out in the same way as series J, although under different conditions. The sand bed used in this series had a mean grain-size of 0.32 mm. The results of all tests are given in Appendix C1. First condition I2 was imposed, then I1, I5, I4 and finally I3, starting at the highest velocities. This explains the relative high losses of sand under condition I2. The last condition, I3, gave striking lower values for the porosity. This is partly due to the inaccuracies of the BLSS that occurred at the end of the measurement series, and also due to the small amount of trapped sand: small differences in the bed level measurements can result in relatively large differences between the measured volume of sand from the test section and the amount collected in the traps. In the mass-conservation calculations, the average porosity over all conditions except I3 is used, which is 0.39. The average velocities and transport rates at the measuring location are given in the following table.

Table 4-5 Average velocities and transport rates series I

test	$\langle u \rangle$ (m/s)	$\hat{u}$ (m/s)	u_{rms} (m/s)	$\langle q_{avg} \rangle$ (10^{-6} m^2/s)
I1	0.259	1.47	1.041	77.9
I2	0.254	1.70	1.202	129.1
I3	0.419	0.65	0.462	19.2
I4	0.417	0.92	0.649	44.1
I5	0.452	1.50	1.063	162.8

Plots of the net transport rates along the tunnel, giving the transport at x = 2 m, calculated both from the right and the left estimation, are given in Appendix C2. The condition with the lowest velocities, I3, shows that the transport is not completely uniform. This is caused by the presence of some bed forms. However, it was observed that these bed forms have a rather small height and large length such that the transport process was still dominated by sheet-flow over the bed forms, rather than vortex generation behind ripples.

For every condition four tests are performed, which are averaged for each condition. Some tests are left out of these calculations, because they have been carried out with slightly different conditions or have been too much influenced by initial effects, which can also be seen on the plots in Appendix C2.

The following test are not accounted for:

- I2-t2: No velocity measurements were carried out due to difficulties with the LDFM
- I3-t1: A higher velocity amplitude was imposed
- I4-t1: This was the first run with a new condition, which caused too much change in the sand bed
- I5-t1: This was the first run with a new condition, which caused too much change in the sand bed

In Table 4.6 the standard deviation and the relative error are given, for definitions see page 4-2.

Table 4-6 Standard deviation and relative error series I

test	<U> (m/s)	û (m/s)	$<q>_{avg}$ (10^{-6} m^2/s)	σ (10^{-6} m^2/s)	r (%)	r/√N (%)	averaged over
I1	0.26	1.47	79.7	2.43	3.04	1.52	T 1,2,3,4
I2	0.25	1.70	129.1	4.33	3.35	1.94	T 1,3,4
I3	0.42	0.65	19.2	1.72	9.00	5.20	T 2,3,4
I4	0.42	0.92	44.1	2.33	5.29	3.06	T,2,3,4
I5	0.45	1.50	162.8	2.47	1.52	0.88	T 2,3,4

The relative error has the highest value for condition I3. This can be explained by the non-uniform transport rate, which can be seen in the plot in Appendix C2. However, the standard deviation is still less than 10 % of the measured transport rate, which is acceptable.

4.2.2 Accuracy and reliability of results

In Section 4.1.2, the main sources of inaccuracies are given for the results of series J. The main sources were the inaccuracies of the BLSS and the uncertainties about the porosity, which will be worked out below.

Sand losses

The calculated correction volumes for the BLSS-measurements are given in Appendix C3. The same conclusion can be drawn as is done for series J in the previous section: the correction volume can not be added to the amount of sand in the right trap, but the volume missing in the bed level sounding may be one of the causes of the loss of sand during a tunnel run.

Porosity

The calculated porosity for every test is given in Figure 4.3. The average value over all tests is 0.37. The last condition I3 gave a remarkable lower result, which is probably mainly due to inaccuracies in BLSS-measurements. Therefore, the average is taken over the other conditions, which gives 0.39.

Velocity distribution over the cross-section

Also in this series the flow velocity is measured in the middle of the tunnel, while the net transport rates are calculated over the whole cross-section. To determine the transport rate corresponding to the velocities in the middle of the tunnel, the same method as in the previous section is used, which is given in Appendix B5. The results are given in Table 4.7.

Table 4-7 Correction factor C_n

test	$<u_{max}>$ (m/s)	u_{rms} (m/s)	$<u^3_{max}>$ (m^3/s^3)	$\overline{<u^3>}$ (m^3/s^3)	C_n (-)	$<q_s>_{avg}$ (10^{-6} m^2/s)	$<q_s>_{avg}$ corr. (10^{-6} m^2/s)
I1	0.259	1.04	0.859	0.725	1.18	79.7	94.0
I2	0.254	1.20	1.118	0.944	1.18	129.1	152.3
I3	0.419	0.46	0.342	0.279	1.23	19.2	23.6
I4	0.417	0.65	0.595	0.496	1.21	44.1	53.3
I5	0.452	1.06	1.625	1.362	1.19	162.8	193.7

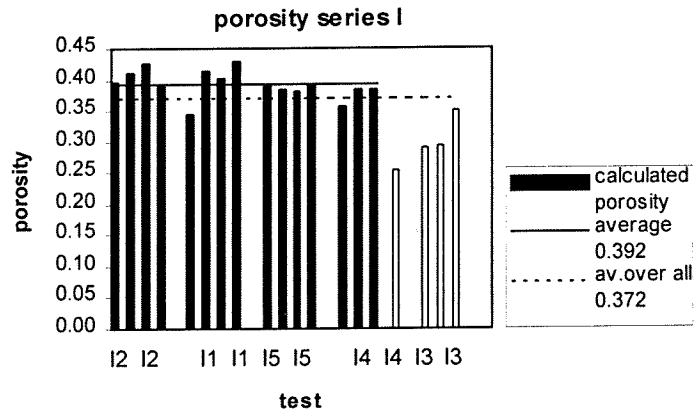

Figure 4-3 Porosity varying over all tests series I

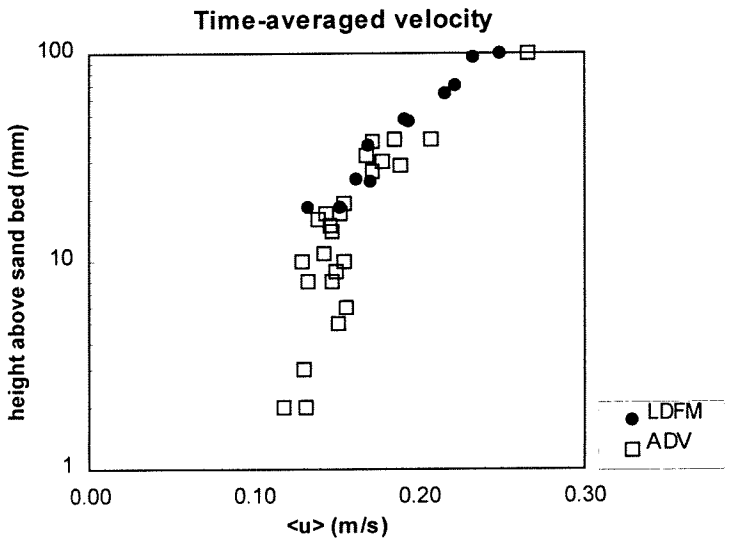

Figure 4-4 Time-averaged flow velocity

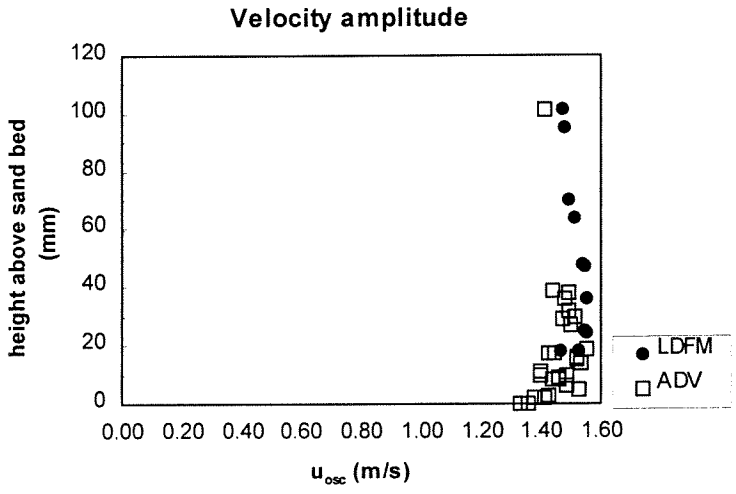

Figure 4-5 Time-average velocity amplitude

4.3 Detailed flow velocity and concentration measurements

For one condition, I1, detailed flow velocity and concentration measurements were carried out, to obtain flow velocity and concentration profiles which give more information about the physical processes that determine the sediment transport. This condition is comparable to E2 and H6, for which similar measurements in the same hydraulic condition were carried out, using sand with a grain-size of 0.21 mm and 0.13 mm, respectively.

4.3.1 Velocity profiles

The flow velocities in the suspension layer were measured using LDFM. This instrument cannot measure too close to the bed, because the high amount of sand particles block the laser beam. The range of measuring points is from 18 mm to 102 mm above bed level at rest, carried out in four tests. A great advantage of the LDFM is that there is no disturbance of the flow or the sand bed.
For measuring flow velocities close to the bed, an ADV was used. This instrument is put into the tunnel and disturbs, causing some local erosion. The bed level directly underneath the instrument was measured every 36 sec (= 5 waves) to record the bed level variations. The measured flow velocities were ensemble-averaged over 5 to 20 waves, during which the bottom was at a constant level.

Time-averaged flow velocities

- The time-averaged velocity profile is given in Figure 4.4, using both ADV and LDFM measurements.

- The time-averaged flow velocity profile shows a more or less logarithmic distribution above z = 10-20 mm. The current boundary layer stretches over the whole vertical.

- Especially at levels very close to the bed (z< 10 mm), the ADV gives velocities which are unrealistically high. It is assumed that the high concentrations have influenced the measurements.

In Figure 4.5, the vertical distribution of the time-averaged velocity amplitude (û) is given. It shows that:

- The wave boundary layer is smaller than the net current boundary layer. Above the wave boundary layer (from the figure: z≈5 mm) the oscillatory velocity is approximately constant over the vertical.

- The lower part of the wave boundary layer with reducing velocities towards the bottom is hardly visible in the measurements. The velocities at 0 mm, which is the bottom level at rest, must be smaller, but are overestimated by the ADV.

- The highest velocity amplitude occurs at about 30 mm above the bottom.

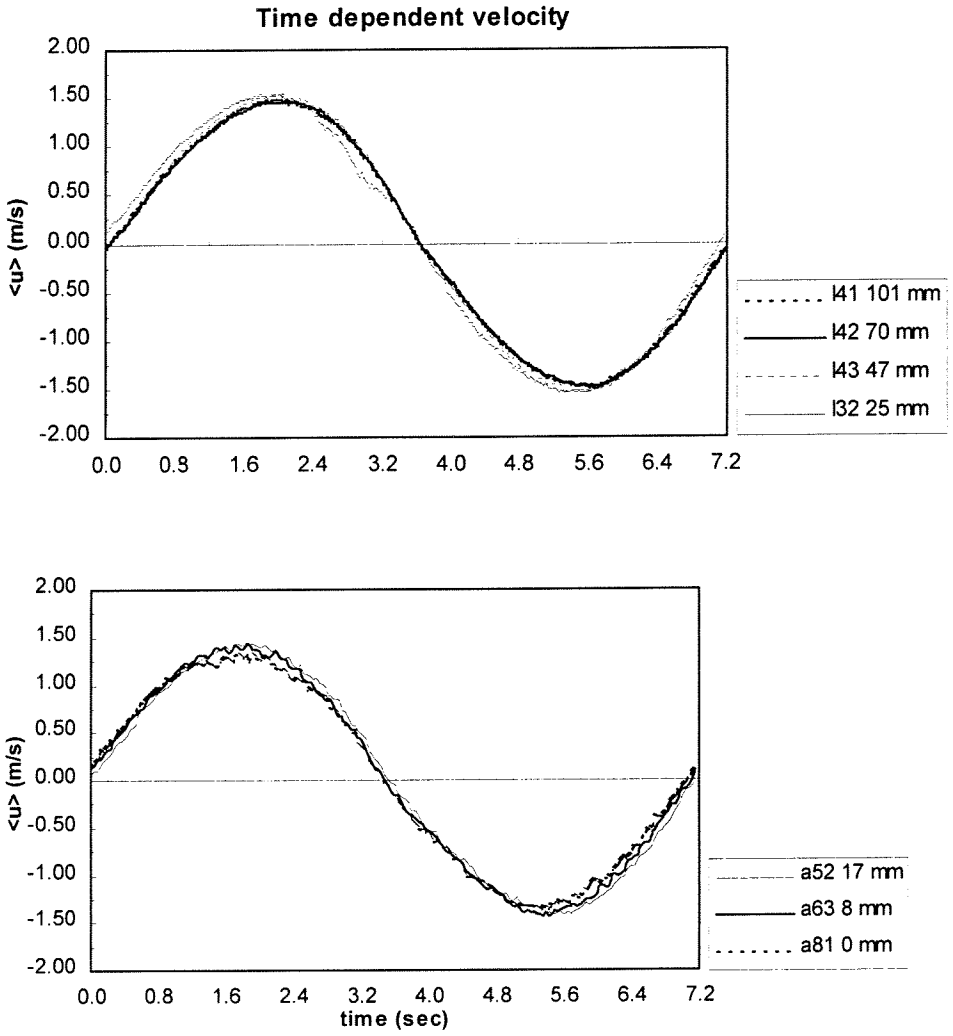

Figure 4-6 Time-dependent flow velocities measured by LDFM and ADV

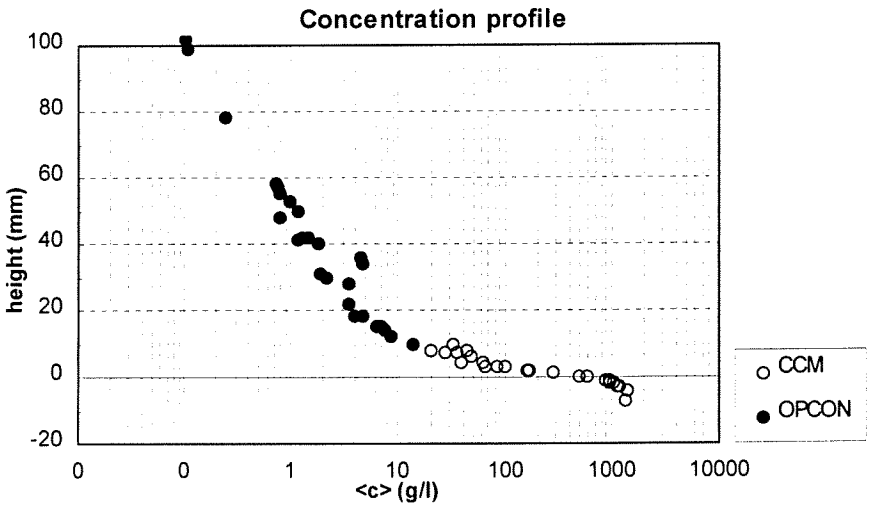

Figure 4-7 Concentration profile; time-averaged concentrations distributed over the vertical

Time-dependent flow velocities

In Figure 4.6 the time-dependent, ensemble-averaged flow velocity during one wave-cycle is shown, at different levels over the vertical. In order to study the decrease of the oscillating velocity close to the bed, and the occurring phase lag, the net current velocity is subtracted from the measured velocity. The bed level at rest lies at 0 mm, which is used as reference level. During a test, the bed level lowers, because part of the bed material is brought into suspension. At 0 mm the flow velocity could be measured.

- Going from 101 mm down to 25 mm above bed level, the velocity amplitude shows a slight increase, which is also shown in Figure 4.7.

- A small phase lag is present; closer to the bed the velocity is ahead in phase compared to the velocity further away from the bed. The peak shifts to the left. The phase difference between 101 and 8 mm is about 0.15 seconds, which is about 0.042 π.

4.3.2 Concentration profiles

For measuring the concentrations in the suspension layer, the OPCON was used, which can measure concentrations from 0.005 to 2 vol%, which is equal to 0.1 to 50 g/l. Like the ADV, the OPCON also causes local erosion. Therefore, in most cases the concentrations were ensemble-averaged over 10 waves, sometimes even less.

Concentrations in the sheet-flow layer were measured by using the CCM. The probe can be brought in from the bottom through the sand bed, and the small instrument causes no severe erosion. The measured points lie between -7 (which is in the sand bed) and 10 mm above bed level. The measuring range of the instrument lies between 100 and 1500 g/l, which is equal to 4 to 50 vol%. The ensemble-averaged value was calculated over 10 to 20 waves.

Time-averaged concentrations

In Figure 4.7 the concentrations averaged over a wave cycle are plotted on a log-linear scale. The following conclusions can be drawn:

- The time-averaged concentration profile shows a power-law distribution.

- The measuring points in the sand bed, which give the highest concentration, can clearly be distinguished. The concentration starts to decrease from -4 mm. The bed level at rest is at 0 mm, so during a tunnel run the bed level lowers.

- The transition layer between the suspension and the sheet-flow layer, for which 1 vol% (equal to 26.5 g/l) can be used as a boundary value, lies around 7 mm. This can also be seen in the Figure: in the sheet-flow layer the concentration decreases very fast, in the suspension layer the values are much smaller and are decreasing slower.

- The CCM measurements at the highest vertical levels are not very accurate and show some scatter; this is at the end of the measuring range.

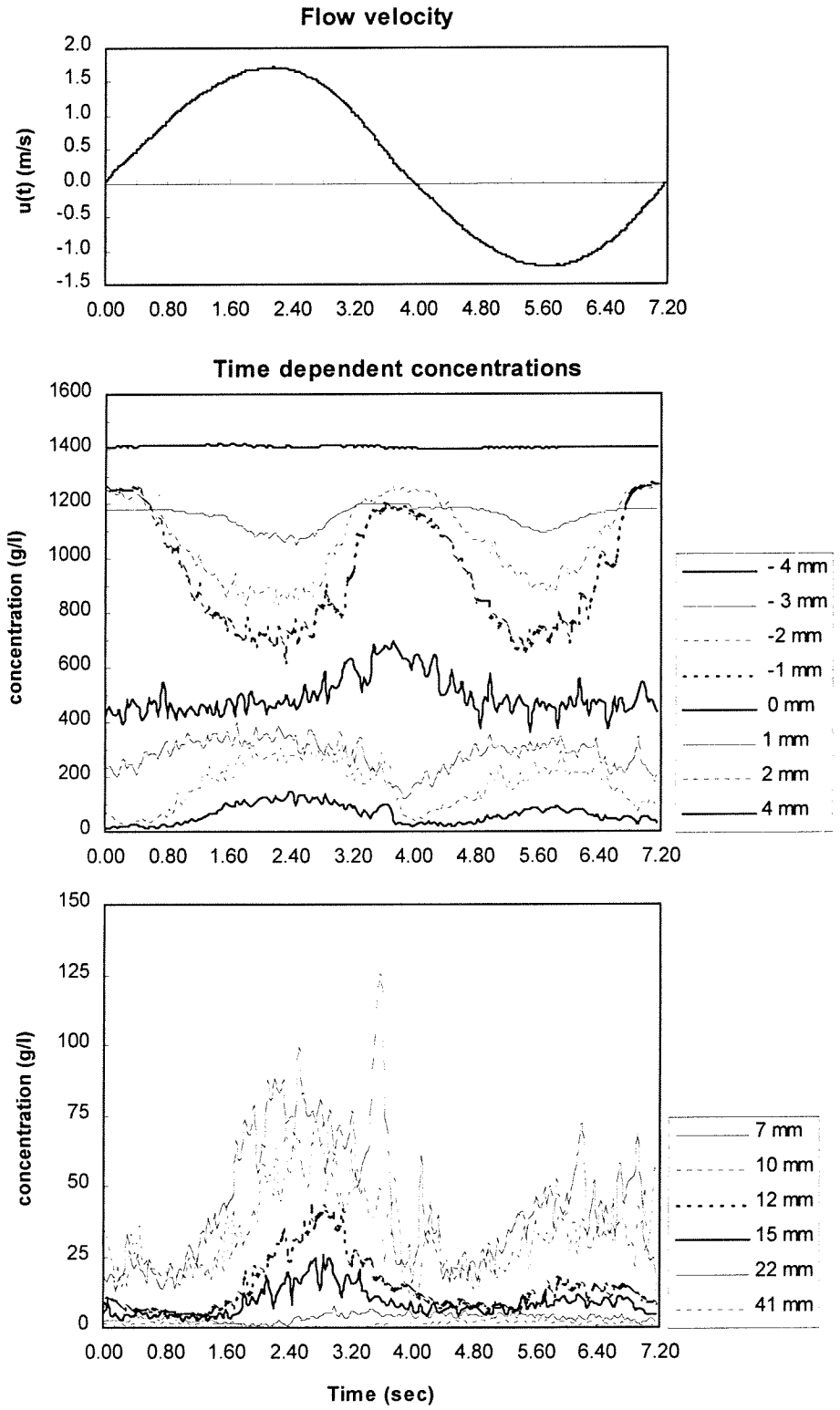

Figure 4-8 Time-dependent concentrations from CCM and OPCON measurements

Time-dependent concentrations

In Figure 4.8 the time-dependent and ensemble-averaged concentrations are given. To indicate the phase of the wave cycle the flow velocity at z = 100 mm is plotted. The first picture gives the concentration in the sheet-flow layer, measured by CCM and averaged over 20 waves. For the second picture, which shows the concentrations in the suspension layer, OPCON measurements were averaged over 10 waves. When describing Figure 4.7 it was concluded that the suspension layer starts around 7 mm above the bed level. In this Figure 4.7 some scatter is shown where the concentration is about 26.5 g/l. This explains that in Figure 4.8 the measurements at z=7 mm shows a higher concentration than the boundary value 26.5 g/l.
In Figure 4.8 one can see clearly the different behaviour of the sand in the different concentration layers:

- The measuring point at -4 mm lies in the sand bed: no changes in concentration occur there during a wave cycle. The measured concentration (1400 g/l) is smaller than expected with a porosity of the bed of 39 % (≈1600 g/l). It is likely that especially the top layer of the bed is not so densely packed and has a lower porosity.

- The pick-up layer lies between -3 and 0 mm, in which 0 mm is the initial bed level at rest. The concentration decreases when the velocity increases, due to the fact that sediment is picked up from the bed. The positive maximum flow velocity is higher than the negative maximum due to the net current, so the concentration dip is also somewhat wider. The concentration decreases very fast with increasing height from the bed.

- The upper sheet-flow layer lies between 0 and 7 mm. Here the sediment behaves completely opposite to the sand in the pick-up layer. Two peaks occur when flow velocity is maximum positive or negative; again the first peak is wider due to higher flow velocity. Small and sharp peaks occur just before flow-reversal, around t = 3.7 and t = 7.0 sec.

- At 0 mm, just at the transition layer between pick-up and upper sheet-flow layer, the concentration seems to be on a constant level around 500 g/l.

- In the suspension layer the behaviour is quite similar to the upper-sheet-flow layer. The maximum level occurs when the flow velocity is maximum negative or positive. Sharp peaks before flow reversal are quite clear at z=4 ,7 and 10 mm, around t=3.6 and 6.9 s. Another sharp peak occurs after flow reversal at the 7 and 10 mm. in the figure. Due to the different vertical axis, in this plot the asymmetry can clearly be seen: the higher positive flow velocity gives higher concentrations.

- At higher levels (>10 mm in the figure) the sharp peaks are not visible at all, but only the two major peaks occur. Going higher (22 and 41 mm in the figure) the concentration is at the highest level during the negative wave-cycle, and decreasing slowly during the positive part.

- A phase lag occurs; the peaks move to the right for higher points along the vertical. This is because the transport process starts at the bottom and goes upward through the sheet-flow and suspension layer during the wave cycle.

5 Analysis of experimental results

5.1 Previous experimental series

The experiments for this study are part of a range of other experimental series, all performed in the LOWT at Delft Hydraulics.
The experiments carried out in the LOWT, comparable with series J and I and relevant for this study, are:

Performed before 1992 in the LOWT

Series B: Measuring net transport rates under regular and irregular second order Stokes waves, D_{50}=0.21 mm [Al Salem, 1993]
Series C: Time dependent flow velocity and concentration measurements, under asymmetric and symmetric waves, D_{50}=0.21 mm [Al Salem, 1993]
Series D: Net transport rates under 2nd order Stokes waves, D_{50}=0.13 mm [Ribberink and Chen, 1993]

After 1992 in the LOWT, with a steady current velocity

Series CI: Net transport rates under asymmetric waves combined with a steady current in flow direction, D_{50}=0.21mm [Ramadan 1994]
Series CII: Net transport rates under asymmetric waves combined with a steady current opposite to flow direction, D_{50}=0.21 mm
Series E: Net transport rates and detailed flow velocity and concentration measurements under sinusoidal waves and current, D_{50}=0.21 mm [Katopodi et. al., 1994][Koelewijn, 1994]
Series H: Net transport rates and detailed flow velocity and concentration measurements under sinusoidal waves and current, D_{50}=0.13 mm [Janssen et. al., 1996][Van der Wal, 1996][Hassan, 1996]

The net transport rates of these series are given in appendix E. These transport rates are corrected for the velocity distribution over the cross-section in the tunnel.

Dibajnia, 1991

Another data set is obtained from Dr. Dibajnia from the University of Tokyo, who did a study on non-linear effects in beach processes [Dibajnia, 1991]. The main objectives in his project were to study the initiation of sheet-flow, to measure net transport rates under non-linear oscillations with a super imposed steady current, and to use the measured data to find a transport rate formula to be used in modelling of beach topography change. The resulting transport formula from Dibajnia and Watanabe is also used in this study and is described in Section 2.3.2.

His experiments were carried out in a small loop-shaped wave tunnel, which is shown in figure 5.1. The test section is 2 m long, 0.22 m high and 0.12 m wide. Sand traps are installed at both ends of the test section.

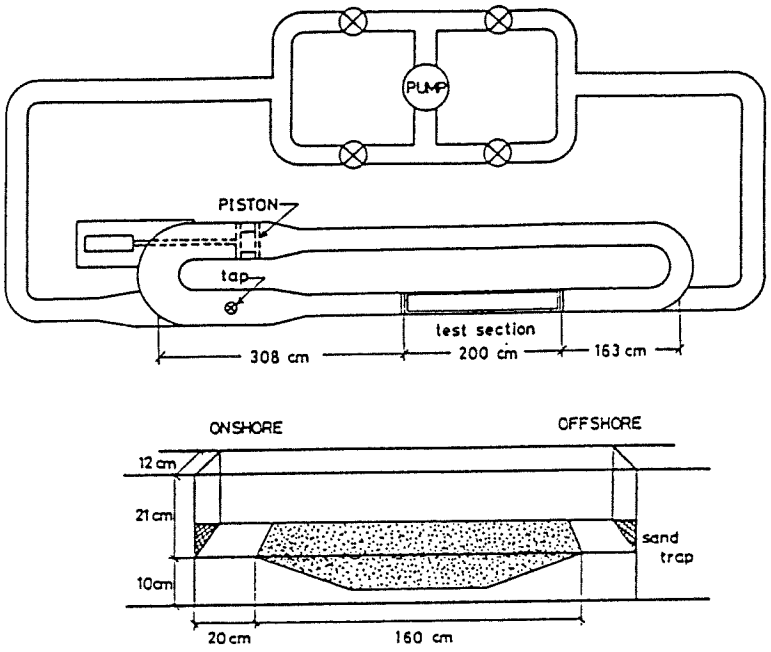

Figure 5-1 Wave tunnel used by Dibajnia

The parameters in his experiments were as follows:

- D_{50} = 0.20 mm
  W_s = 0.23 m/s.
- Flow conditions:
  net current <u> = -0.2, -0.1, 0.0, 0.1 or 0.2 m/s
  non-linearity index $u_{max}/\hat{u}$ = 0.5, 0.6, 0.7 or 0.8
  period T=1- 4 seconds
  The imposed waves are described with first order cnoidal wave theory.

It must be noted that in these series u_{max} is the maximum *oscillating* velocity, in contrary to the series in the LOWT where u_{max} is the maximum *total* velocity.
Because of the limited length of the tunnel, the periods are small. This differs from the experiments carried out in the LOWT, which makes it interesting to compare the different results and to study the wave period influence.

An overview of all experimental series is given in table 5.1.

Table 5-1 Overview of previous experimental series

series	waves/ current	asym./ symm.	D_{50} (mm)	T (sec)	measurements	reference
B	W	AS	0.21	5-12	$<q_s>$	Al-Salem (1993)
C	W	AS/S	0.21	6.5- 9.1	u(z,t) c(z,t)	Al-Salem (1993)
D	W	AS	0.13	6.5	$<q_s>$	Ribberink & Chen (1993)
C-I C-II	W+C	AS	0.21	6.5	$<q_s>$	Ramadan (1994)
E	W+C	S	0.21	7.25	$<q_s>$ u(z,t) c(z,t)	Koelewijn (1994)
H	W+C	S	0.13	4-12	$<q_s>$ u(z,t) c(z,t)	Hassan (1996) V.d.Wal (1996)
I	W+C	S	0.32	7.2	$<q_s>$ u(z,t) c(z,t)	present
J	W+C	S	0.21	4-12	$<q_s>$	present
Dibajnia	W+C	AS	0.20	1-4	$<q_s>$	Dibajnia (1991)

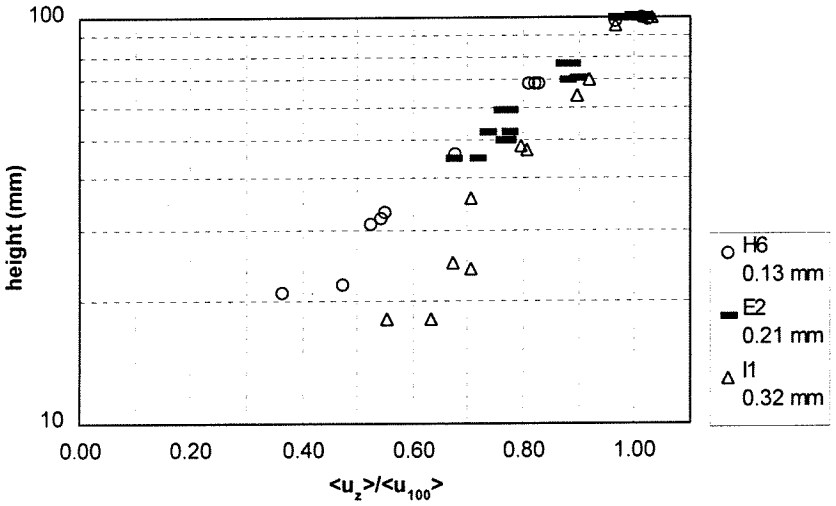

Figure 5-2 Time-averaged velocity for H6, E2 and I1, given as $\langle u_z \rangle / \langle u_{100} \rangle$

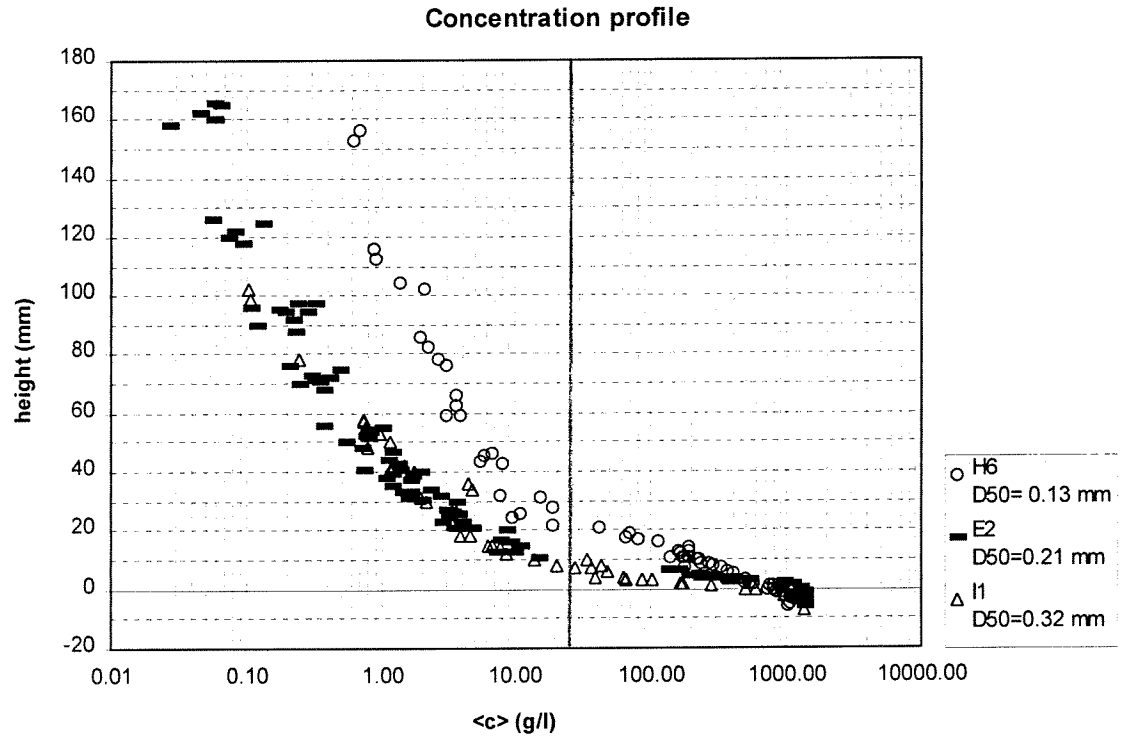

Figure 5-3 Time averaged concentration profiles in case of H6, E2 and I1

5.2 Grain-size effects in time-dependent measurements

For one flow condition with $\langle u \rangle$ = 0.24 m/s, $\hat{u}$ = 1.50 m/s (measured at 10 cm above the sand bed with LDFM) and T = 7.2 s, time-dependent flow velocity and concentration measurements were carried out for three different grain-sizes, i.e. D_{50}= 0.13 mm (in test H6), 0.21 mm (E2) and 0.32 mm (I1). These detailed measurements give more insight in the transport process, the role of unsteady effects and the influence of the particle diameter.

Time-averaged flow velocity profiles

In Figure 5.2 the averaged flow velocity, distributed over the vertical in the suspension layer, is shown for the different series. In order to show the differences in shape of the profile for the different grain-sizes, the parameter $\langle u_z \rangle / \langle u_{100} \rangle$ is plotted. The parameter $\langle u_{100} \rangle$ is defined as the average velocity at 100 mm above the sand bed and $\langle u_z \rangle$ is the average velocity at z mm above the sand bed. In case of I1, only LDFM measurements are plotted.

- In case of H6 and E2 the figure shows a straight line, which implies a logarithmic distribution over the vertical. In case of I1 the profile shows a slightly different shape below z=30 mm.

- The measuring points in case of I1 show the steepest slope, H6 the mildest slope of the straight line, and E2 lies in between. A mild slope implies a high velocity gradient over the vertical. This implies a slightly higher apparent roughness which can be explained by an increasing sheet-flow layer thickness for finer sediments.

Time-averaged concentration profiles

In Figure 5.3, the time-averaged concentration distributed over the vertical for different grain-sizes is given. It shows that for E2 there are a few measured points between $\langle c \rangle$ = 10 and 100 g/l. Figure 5.4 focuses on the concentrations in the sheet-flow layer. From these figures can be concluded:

- The fine sand in case of H6 gives higher concentrations over the whole vertical.

- The difference between E2 and I1 is small, especially in the suspension layer.

- In the sheet-flow layer there is a clear difference in slope for the different grain-sizes. The concentration in case of I1 decreases very fast with increasing height, which implies a thin sheet-flow layer. H6 has a much smaller and more uniform gradient, and does not show the abrupt change in slope like the other two. E2 lies in between.

- In previous studies, 1 vol% (=26.5 g/l) was used as boundary value for the transition layer between suspension and sheet-flow layer. The sand bed at rest is at 0 mm. This is used as a reference level. This gives the following values for the sheet-flow layer thickness δ_s :

	H6:	D_{50}=0.13 mm	$\delta_s \cong$ 22 mm	$\delta_s * D_{50}$=2.9
	E2:	D_{50}=0.21 mm	$\delta_s \cong$ 11 mm	$\delta_s * D_{50}$=2.3
	I1:	D_{50}=0.32 mm	$\delta_s \cong$ 7 mm	$\delta_s * D_{50}$=2.2

It is concluded that the thickness of the sheet-flow layer is inversely proportional to D_{50}, according to: $\delta_s = N * 1/D_{50}$ with: N= 2.2 - 2.9

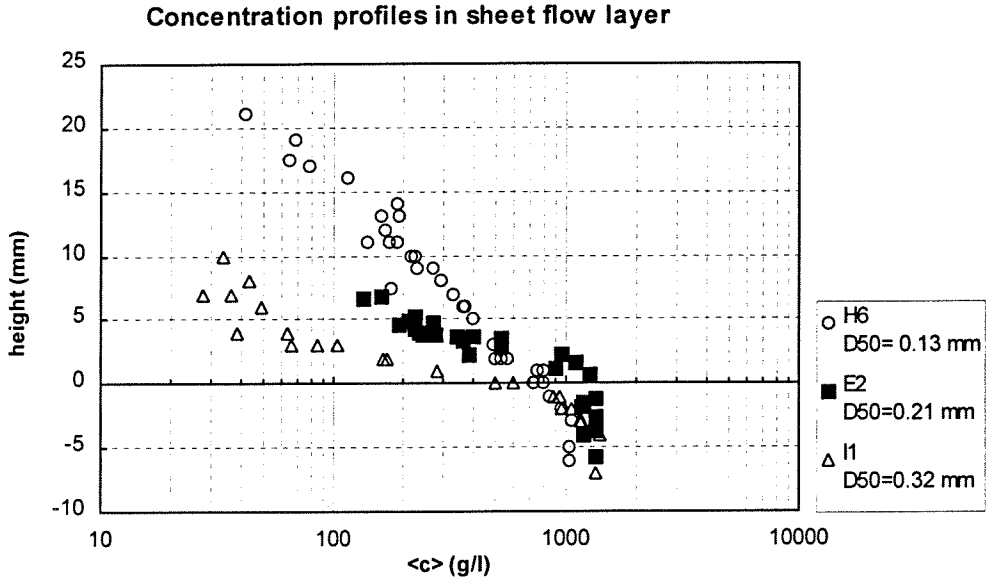

Figure 5-4 Concentration profiles in sheet-flow layer

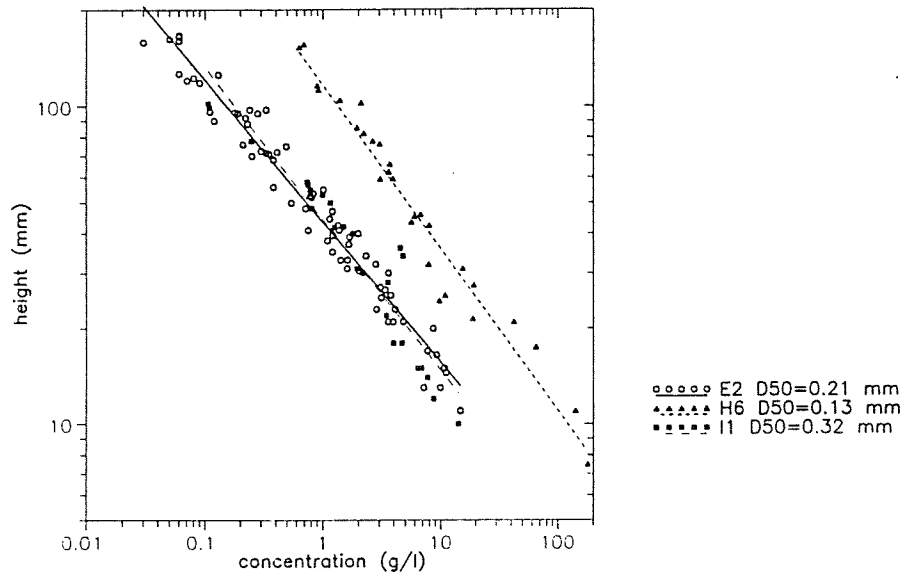

Figure 5-5 Time-averaged concentrations on log-log scale

Al Salem (1993) found that the suspended sediment has a power law distribution along the vertical. When the time-averaged concentrations in the suspension layer are plotted on a log-log scale the best fit line is linear. The decrease of the sediment concentration is indicated by the slope of this best fit line. For the series B and C (D_{50} = 0.21 mm) he found for different oscillating velocities and wave periods a similar decrease in concentration. He found for the slope of the best fit line a constant value of 2.1±0.1.

Al Salem assumed the following relation for the concentration decrease along the vertical:

$$\langle c \rangle = \langle c_a \rangle \left({}^{z_a}/_{z} \right)^{\alpha} \tag{5.1}$$

in which: c = measured concentration
z = level above bottom at which c is measured
c_a = the reference concentration at $z=z_a$
α = the concentration decay parameter = the slope of the best fit line

The concentration decay parameter is related to the level above the bottom, and the ratio of the fall velocity and a mixing coefficient. The fall velocity induces a downward movement of the sand particles, and the mixing coefficient, which indicates the turbulence intensity, results in an upward movement of the particles. This is described in the following formula:

$$\alpha = {}^{W_s z}/_{\varepsilon_s} \tag{5.2}$$

in which: W_s = fall velocity [m/s]
z = height above bed level [mm]
ε_s = time-invariant mixing coefficient [m^2/s]

A constant value of α for different conditions means that the mixing coefficient does not increase for increasing wave velocities. A higher oscillating velocity results in higher concentrations and a thicker sheet-flow layer. This results in a reduction of the turbulence intensity.

For the present measurements and series E and H, the time-averaged concentrations in the suspension layer are plotted on a log-log scale in Figure 5.5. The slope of the best-fit lines, which is equal to the value of the parameter α and the value of the fall velocity, are given in Table 5.2:

Table 5-2 Fall velocity and concentration decay parameter for H6, E2 and I1

Series	diameter D_{50}	fall velocity W_s	concentration decay parameter α
H6	0.13	11.5	1.68
E2	0.21	26	2.29
I1	0.32	42	2.05

For H6, the concentration decay parameter is reduced less than could be expected from the reduction of the fall velocity. This indicates that the turbulence intensity is reduced due to the higher concentration and a thicker sheet-flow layer. For E2, $\alpha \approx 2.1$, although the fall velocity is almost doubled compared to 0.21 mm sand. This indicates that due to a much thinner sheet-flow layer the mixing coefficient is higher.

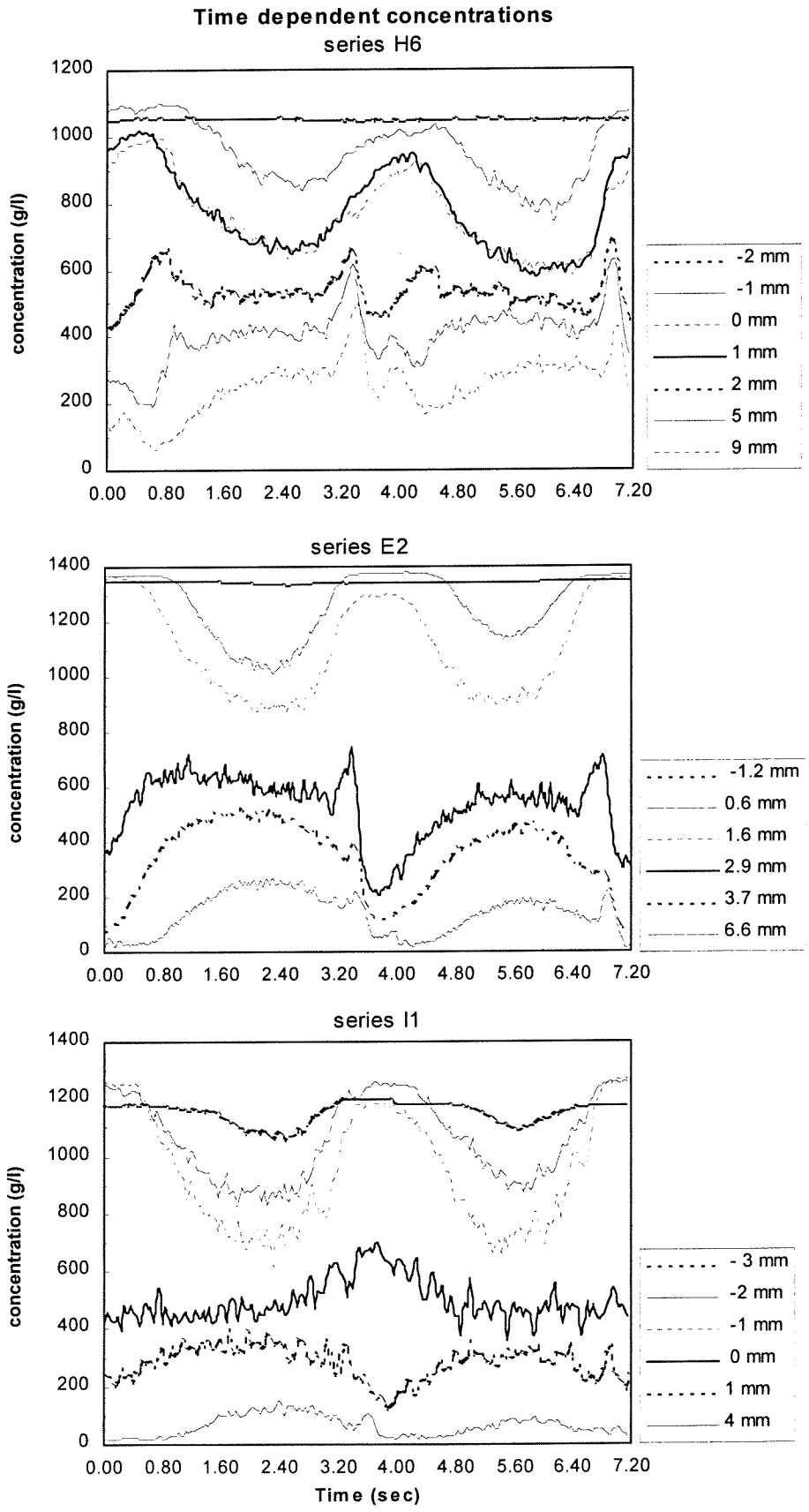

Figure 5-6 Time-dependent concentrations in case of H6, E2 and I1 in sheet-flow layer

Time-dependent concentration profiles

The time-dependent concentration profiles during the wave cycle for the three grain-sizes are shown in figure 5-6 and 5-7. Figure 5-6 shows the sheet-flow layer, close to the bed; figure 5-7 shows the suspension layer. in all cases, the reference level 0 mm is the bed level at rest. During a test the bed level is lowered. In these figures, the following is concluded:

- The concentration in the sand-bed is around 1100 g/l for H6; for E2 and I1 it lies around 1400 g/l. This can be due to the calibration of the CCM. Also, the porosity of the sand bed during series H (ε=0.39)was a little higher than during series J (ε=0.38) which was again a little higher than during series I (ε=0.37) (see appendix A2), which indicates the little grains in series H were less packed than the coarser grains in series I.

- The pick-up layer shows a minimum concentration when the flow velocity is maximum. It is expected that the positive part of the wave cycle would cause the largest reduction, because the velocity is larger due to the presence of the net current. This is true in case of E2 and I1. In H6, the maximum occurs during the negative cycle. This may be caused by unsteady effects. At the end of the positive half wave cycle not all sand, picked up under the maximum velocity, has settled on the bed. The figure shows that the maximum concentration at that time (t=4.3 s) is lower than at the end of the negative half of the wave cycle (t=0.4 s). These unsteady effects may be the reason why the decrease in concentration is larger during the negative half wave cycle, even though the velocities are slightly smaller.

- The differences between both maximum concentration levels are bigger in case of H6 than in case of series E2 and I1.

- The transition between pick-up and upper sheet-flow layer lies around 500 g/l for all grain-sizes. The level at which this occurs lies in case of

H6	D_{50}=0.13 mm	at z $\cong$ 2 mm
E2	D_{50}=0.21 mm	at z $\cong$ 2 mm
I1	D_{50}=0.32 mm	at z $\cong$ 0 mm

  The transition layer can clearly be seen in the plot of I1.

- In the upper sheet-flow layer two major peaks occur, when the flow velocity is maximum positive or negative. In cases E2 and I1 this is clearly visible. In case of H6, the grains react much slower on flow velocity changes. Due to the small fall velocity, the concentration cannot decrease as fast as it increases. This can be seen at the flow transition around t=3.9 s. In case I1 the peaks are smallest in magnitude, because coarser grain are less easily suspended than smaller grains. The differences in concentration are clear, e.g. at around 4 mm:

H6	(5 mm):	c_{max}=600 g/l	c_{avg}=400 g/l
E2	(3.7 mm):	c_{max}=500 g/l	c_{avg}=300 g/l
I1	(4 mm):	c_{max}=100 g/l	c_{avg}=50 g/l

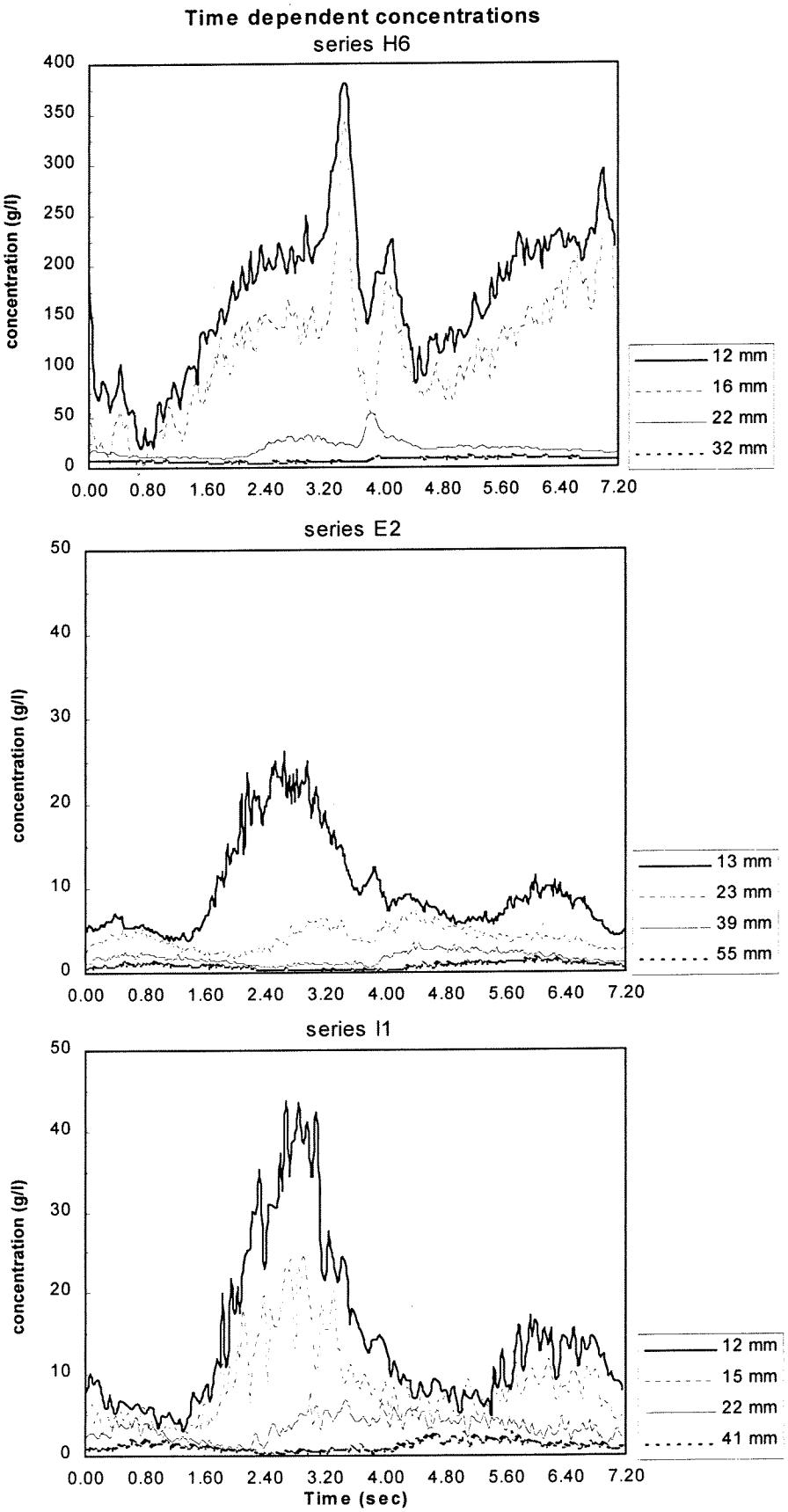

Figure 5-7 Time-dependent concentrations in the suspension layer

- In the upper sheet-flow layer little, sharp peaks occur just before flow reversal. These peaks have the largest magnitude in case of H6, in which case they are dominant over the peaks at maximum velocity, and are also visible in case of E2, but very poorly in I1. It is assumed that these concentration peaks at flow reversal are due to shear-instabilities in the wave boundary layer. Apparently, the peaks are larger in magnitude when the flow velocity goes from positive to negative direction.

- A sharp peak just after flow reversal occurs in case of fine sand at all levels, but is visible only in levels close to the bottom for E2. These peaks are hardly visible in case of the 0.32 mm sand.

- The concentrations in the suspension layer, given in Figure 5.7, are the highest in case of H6. It must be noted that the vertical axis has a different scale for H6. I1 gives slightly higher values than E2, in spite of the coarser sand. In case H6 the peaks around flow reversal play an important role, and are even dominant at levels close to the bed, like at 22 mm. In case E2 these peaks also occur, but do not seem to be dominant. In case I1 these peaks are not visible.

- In the suspension layer the asymmetry between the two major concentration peaks can clearly be seen. The first peak caused by the higher positive velocity is higher than the second concentration peak caused by the negative velocity. The asymmetry between the two major concentration peaks is not so clear in the figure of the fine sand in series H6. This is in the first place due to the larger scale of the vertical axis in this figure. It is also likely that the fine sediment is suspended very easily and stays in suspension for a long time.

- The differences between E2 and I1 are less significant than between E2 and H6. Especially the peaks, which dominate in case of H6, play a minor role in E2 and I1.

The concentration peaks before flow reversal occur especially in case of the fine sand. It is likely that these peaks have a strong impact on the unsteady effects as described before. Just before the end of a positive or negative part lots of particles are brought into suspension. These particles have not enough time to settle before the flow reversal. They remain suspended and in the successive half of the wave cycle they are transported in the opposite direction. These processes essentially influence the net transport rate.

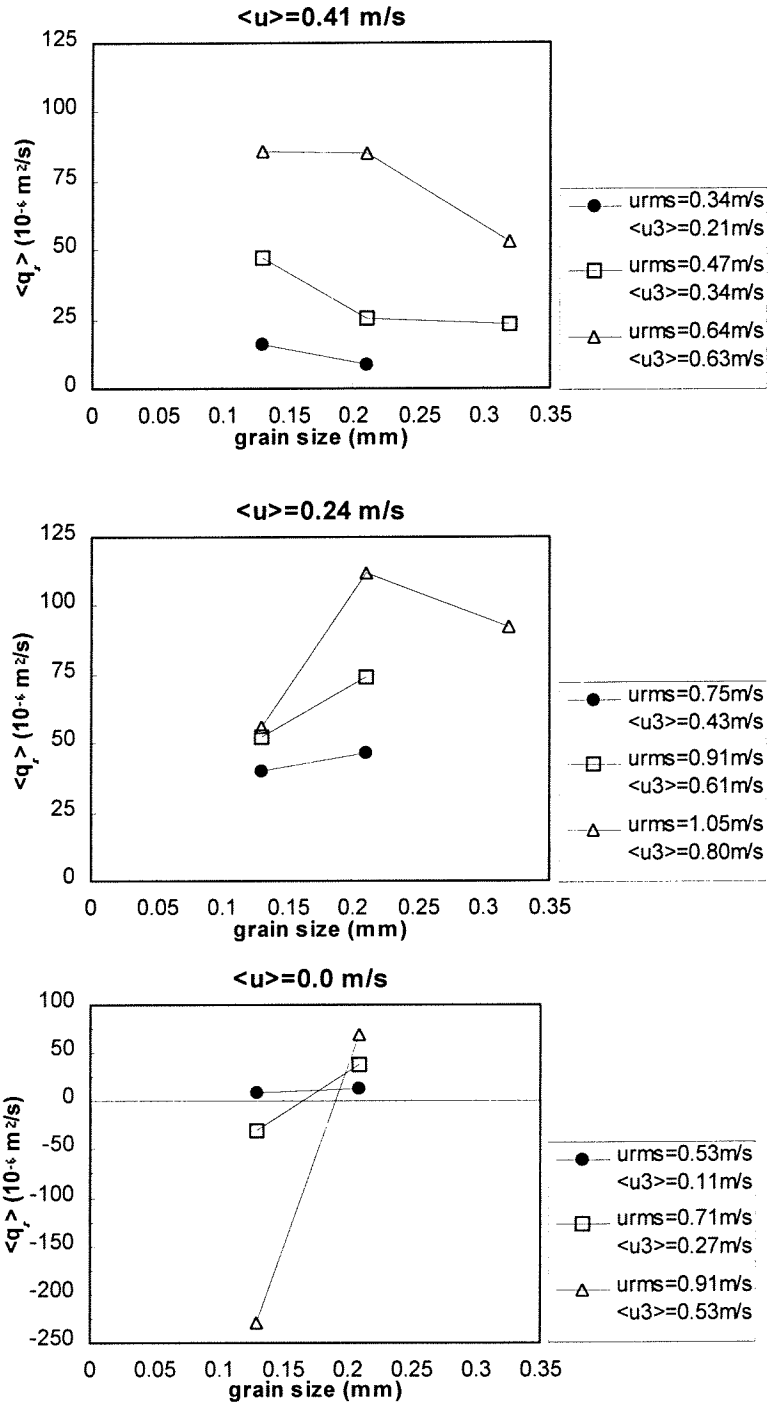

Figure 5-8 Grain-size influence on net transport rates

5.3 Comparing net transport rates

5.3.1 Grain-size influences

In Figure 5.8 the grain-size effects on the net transport rates are given. The available data is sorted using <u>, to emphasise the effects of D_{50} and not to confuse these with velocity effects. It must be noted the data with <u> = 0 m/s come from series B and D (see table 5.1 and app. E), with asymmetric waves. The other data, all derived from series E, H, I and J, consisted of conditions with a net current super-imposed on a sinusoidal oscillating flow. Sometimes, similar conditions did not have exactly the same values for û and u_{rms} in the different series. In these cases an average is taken over the three values. In the plots the u_{rms} of the *oscillating* velocity is given, not the u_{rms} of the total velocity.

In previous series it was concluded that the sediment concentration is strongly related to the third order velocity moment (see for example Al Salem (1993)). In case of sinusoidal waves in combination with a current, the third order velocity moment averaged over the wave cycle is calculated by:

$$\langle u^3 \rangle = \langle u \rangle^3 + 3\langle u \rangle \cdot u_{rms}^{\ 2} \tag{5.3}$$

in which: $\langle u^3 \rangle$ = third order velocity moment averaged over the wave-cycle
$\langle u \rangle$ = net current velocity
u_{rms} = root mean square value of the oscillating velocity

When comparing the net transport rates in the next sections, the parameter $\langle u^3 \rangle$ is used several times. It indicates the magnitude of the total velocity, as a combination of the net current and the oscillating velocity.

In the most simple transport case, when a steady current velocity is considered, the transport rate decreases when the mean grain diameter increases. A net current imposed on a sinusoidal wave will give the same grain-size effects, as long as the transport process is supposed to be quasi-steady. When unsteady effects occur, this is no longer true (see Section 2.2), and the grain-size effects become more complicated.

In the top picture of Figure 5.8, unsteady effects seem to play only a minor role because they are minimised by the steady current. The picture shows that a larger grain-size results in a decreasing transport rate. These effects are smaller for lower velocities, which can be seen by the decreasing slope of the connecting lines. Only in case of the fine sand at the highest oscillating velocity unsteady effects influence the transport process. This could explain why this point is almost equal to the 0.21 mm sand under the same condition.

With <u> = 0.24 m/s, unsteady effects seem to become more and more important. Only in case of a grain-sizes of 0.32 mm, an increase in diameter implies a reduced transport rate. For the smaller grains, the transport rate decreases with decreasing grain-size due to unsteady effects. This reduction is larger for higher velocities. Due to the steady current in positive direction no negative net transport rates occur.

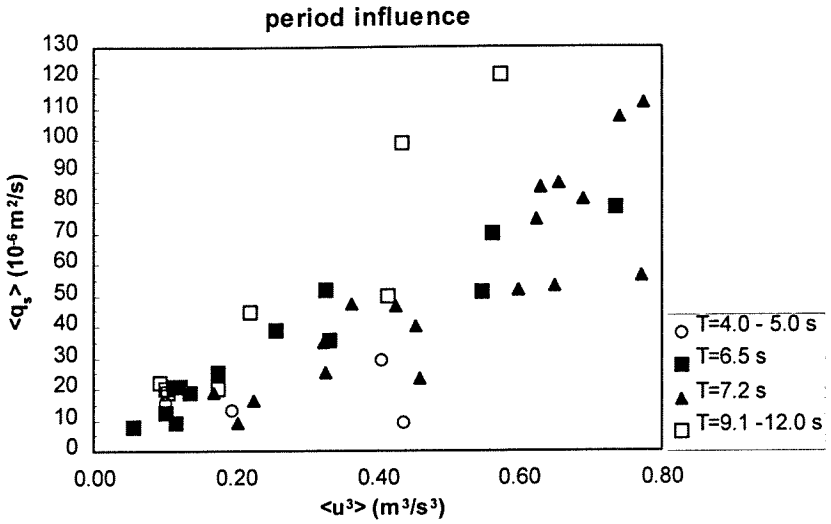

Figure 5-9 Period influence on net transport rates

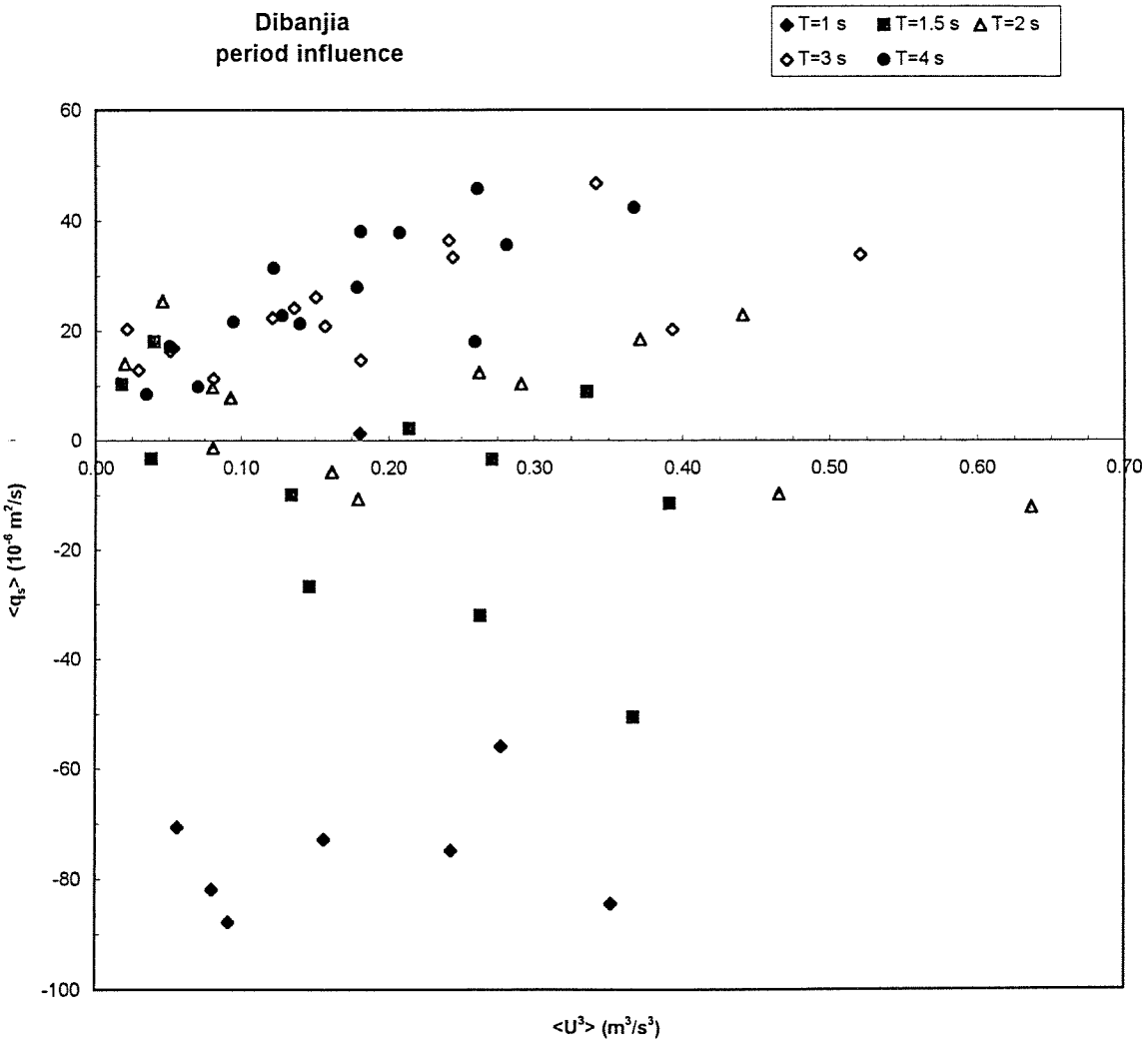

Figure 5-10 Period influence on net transport rates for data of Dibajnia

In the third picture it is clear the unsteady effects dominate the relation between grain-size and transport rate. D_{50} = 0.21 mm results in all cases in a higher transport rate than D_{50} = 0.13 mm. In case of the fine sand large negative transports occur, due to unsteady effects and the absence of a net current velocity. The grain-size effects strongly depend on the magnitude of the oscillating velocity: for u_{rms}=0.53 m/s almost no effects are visible, while u_{rms}=0.91 m/s shows a large decrease for smaller grains. There is no data available for <u> =0 m/s and D_{50}=0.32 mm.

5.3.2 Wave period influences

In Figure 5.9 and 5.10, all net transport rates are plotted against $<u^3>$, ordered by period. Figure 5.9 shows tests performed in the LOWT; Figure 5.10 shows data obtained by Dibajnia, with smaller periods, in the range of 1 to 4 seconds. It is clear that an increase in period implies a larger net transport rate. Very small periods cause large unsteady effects, because the particles have no time to settle. This results in negative net transport rates.

Figure 5.11 shows the influence of the wave period in combination with the effects of grain-size. For one flow condition, with <u> = 0.24 m/s and û = 0.75 m/s, the net transport rates are plotted for 0.13 mm sand (represented by •) and 0.21 mm sand (represented by o) for three different periods.
In case of the largest period, no strong unsteady effects are expected. The fine sand gives a doubled net transport rate compared to the 0.21 mm sand. A smaller period, 7.2 seconds, shows a large decrease for the fine sand and a much smaller decrease for the coarser sediment. This difference must be caused by unsteady effects. In case of a small period of 4 seconds, both grain-sizes show a decrease in transport rate. Now, also in case of the 0.21 mm sand unsteady effects occur. However, the effects are stronger for the fine sand resulting in a larger decrease.
The third group of points represented by triangles (Δ) represents also measurements of the 0.13 mm sand, but with a lower imposed oscillating velocity, which gives less unsteady effects. The results are quite similar to the results of the 0.21 mm sand under higher velocity: no difference between a period of 7.2 or 12 seconds, and a slight decrease in case of 4 seconds.

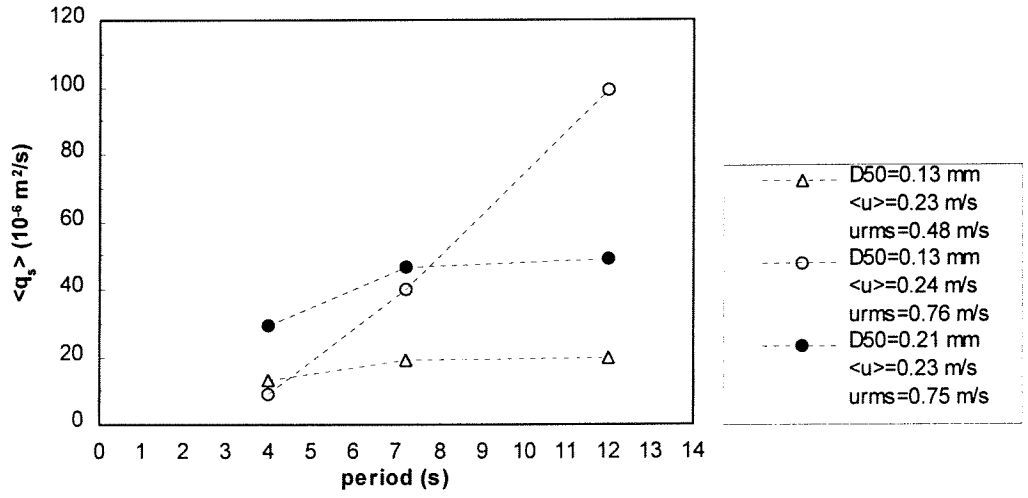

Figure 5-11 Period influence for different grain-sizes

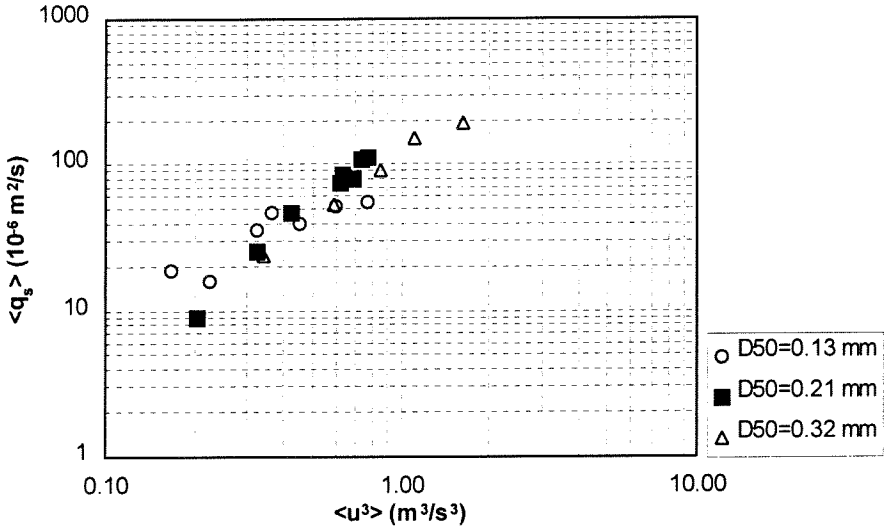

Figure 5-12 Relation between $<q_s>$ and $<u^3>$ for different grain-sizes and T=7.2 s.

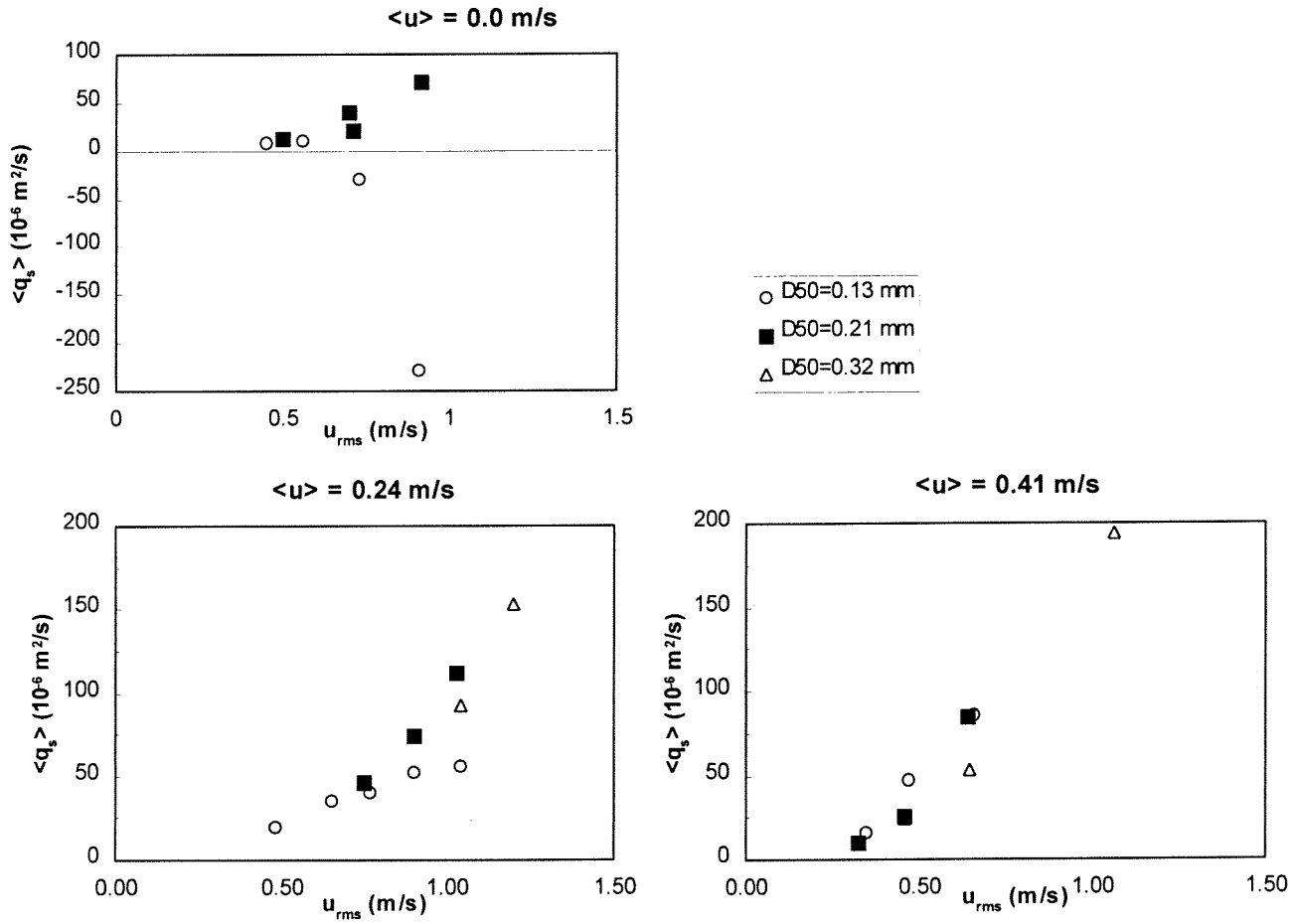

Figure 5-13 Flow velocity influence

5.3.3 Flow velocity influences

Al Salem [1993] suggested in his studies a strong relation between the third order velocity moment $<u^3>$ and the net transport rate. In figure 5.12 both parameters are plotted for series E, H, I and J. It shows the same relation between $<q_s>$ and $<u^3>$ for the different grain-sizes, although in case of the fine sand the slope seems somewhat milder.

In figure 5.13 the flow velocity influence is presented in a different way.
In the most simple case the transport only depends on the flow velocity u(t). When unsteady effects occur, like mentioned before, not only the net velocity u(t), but both $<u>$ and $\hat{u}$ become important. The unsteady effects strongly depend on the oscillating velocity $\hat{u}$, because the larger the velocity, the higher the sediment is brought into suspension. A strong current velocity $<u>$ results in a decrease of the negative transport, because the net current works in a positive direction. Also the positive part of the wave cycle T_c will increase when $\hat{u}$ remains equal and $<u>$ increases, which gives the particles more time to settle down and thus reduces the unsteady effects.

Figure 5.13 shows the net transport rate related to the u_{rms} value of the oscillating velocity for three different net current velocities. It must be noted the waves in case of $<u> = 0$ m/s are not sinusoidal, but asymmetric waves, from series B and C. In all situations the same period was imposed (T=7.2 s). The figure shows that in general a higher u_{rms} results in a higher transport rate. The gradient of this relation is stronger in case of a higher net velocity, which implies more transport for the same oscillating velocity under a stronger current. This can be explained by the fact that $<u^3>$ is larger if $\hat{u}$ is equal and $<u>$ is larger.

In a steady flow, smaller sand particles would result in larger transport rates under the same flow velocities. When no steady current is imposed, the unsteady effects in case of fine sand result in large negative transports. When there is a steady current, no negative transport rates occur. However, due to unsteady effects the fine sand gives the smallest transport rates for $<u> = 0.24$ m/s. For the largest oscillating velocity even the net transport rate of the 0.21 mm sand is smaller than of 0.32 mm sand. Apparently unsteady effects are also important here. The highest current velocity, 0.42 m/s, results in the largest transport rates. The relation for the different diameters seems to be almost similar; they show more or less the same slope. Unsteady effects do not seem to occur. They are apparently minimised by the strong current.

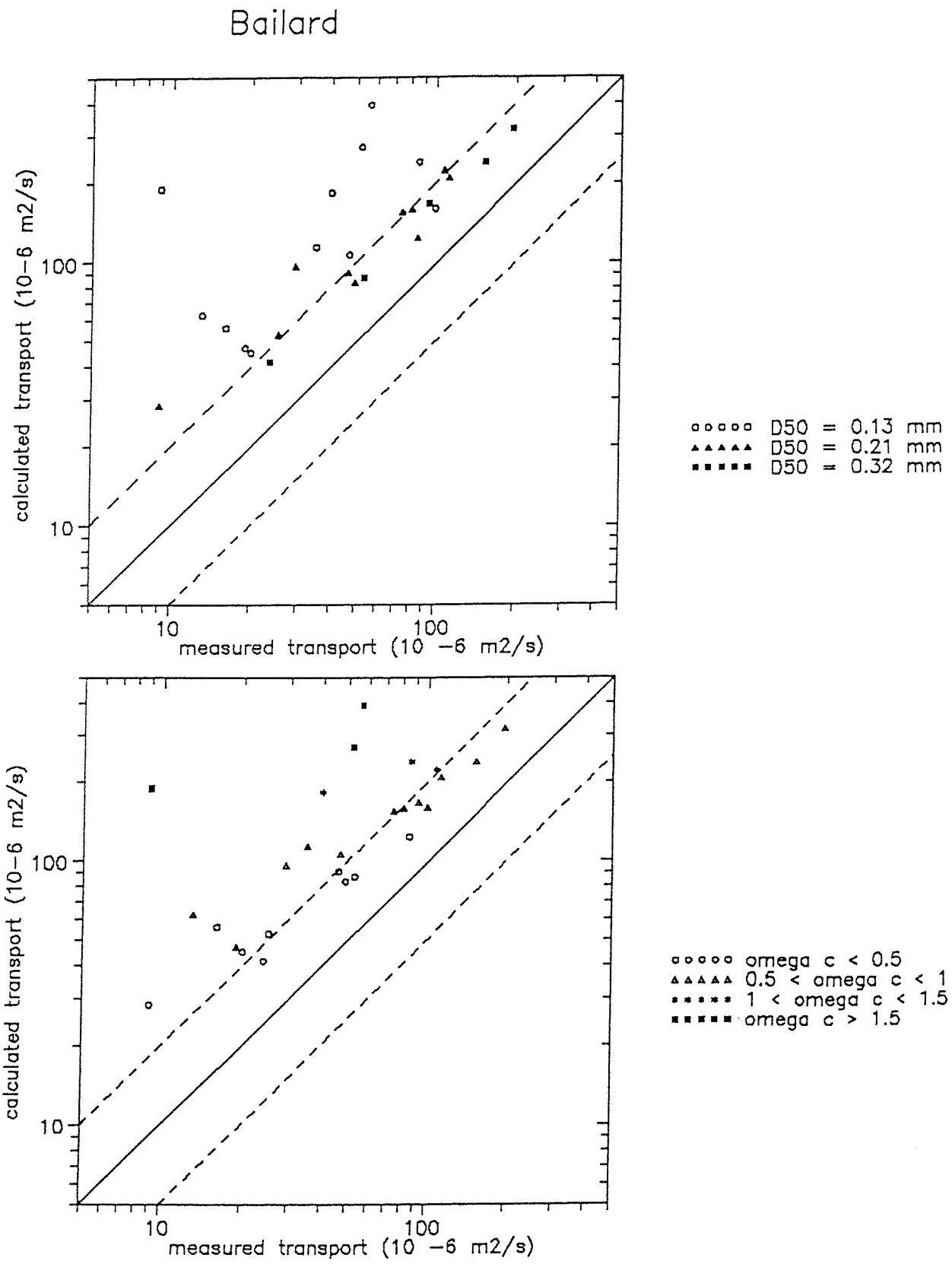

Figure 5-14 Calculation results for the model of Bailard

5.4 Verification of models

In this section the measured net transport rates from series E, H, I and J are compared with the results of three transport models, developed by Bailard, Ribberink and Dibajnia & Watanabe. The different models are briefly described here; a detailed description is given in Section 2.3.2. To calculate the transport rates the computer program written by Koelewijn and further improved by Van der Wal, is used. In order to compare the output of the models with previous verifications, the standard setting for the models is the same as used by Koelewijn (1994) and Van der Wal (1996).

For every transport model, the measured transport rates are compared to the transport rates predicted by the model. The data is ordered by grain-size, to indicate if a model can take into account the grain-size influences. From Section 5.2 and 5.3 can be concluded that unsteady effects can significantly influence the transport process. Transport models should be able to predict the influence of the unsteady effects in order to give reliable transport rates. The measured transport rates are again plotted against the calculated transport rates, but they are ordered by the occurrence of unsteady effects. A parameter which indicates the occurrence of unsteady effects is defined by Dibajnia and Watanabe (see Section 2.3.2). They use the ratio of the fall time of a sand particle and the wave period. This parameter ω_c, can easily be determined. It is given by:

$$\omega_c = \frac{t_{fall}}{T_c} = \frac{z/W_s}{T_c} = \frac{\frac{1}{2}\frac{u_c^2}{\Delta g W_s}}{T_c} \qquad (5.4)$$

in which:
- z = level to which the sediment is stirred up
- W_s = fall velocity for a sand particle with a diameter D_{50}
- T_c = positive part of the wave period
- u_c = equivalent sinusoidal velocity amplitude, according to eq. 2.20
- Δ = relative density
- g = gravity acceleration

Model of Bailard

This model is based on a theoretical approach of the energy balance. A distinction is made between bed-load and suspended transport. The total transport rate (eq 2.15) is considered as the sum of the bed load and the suspended transport, given in eq: 2.16 and 2.17.
As a standard method for calculating the bed shear stress, the formula of Ribberink/Van Rijn is used. As bed roughness height, which is used to calculate the bed shear stress, $k_{s,c}=k_{s,w}=D_{50}$ is used. Koelewijn found out this k_s gave the best results. The flow velocities are given at a level of 10 cm above the sand bed.

Figure 5.14 shows the comparison between the measured transport rates from series H (0.13 mm), I (0.32 mm) E and J (0.21 mm) and calculated results of this model. Three lines are plotted in this picture. The solid line represents the points at which the calculated and the measured values are equal. The dotted lines represent the area where the error lies within a factor 2. The figure shows that the model of Bailard gives reasonable results for the 0.21 mm and the 0.32 mm sand. Although all transport rates are overpredicted, the model gives very bad results for the fine sand.

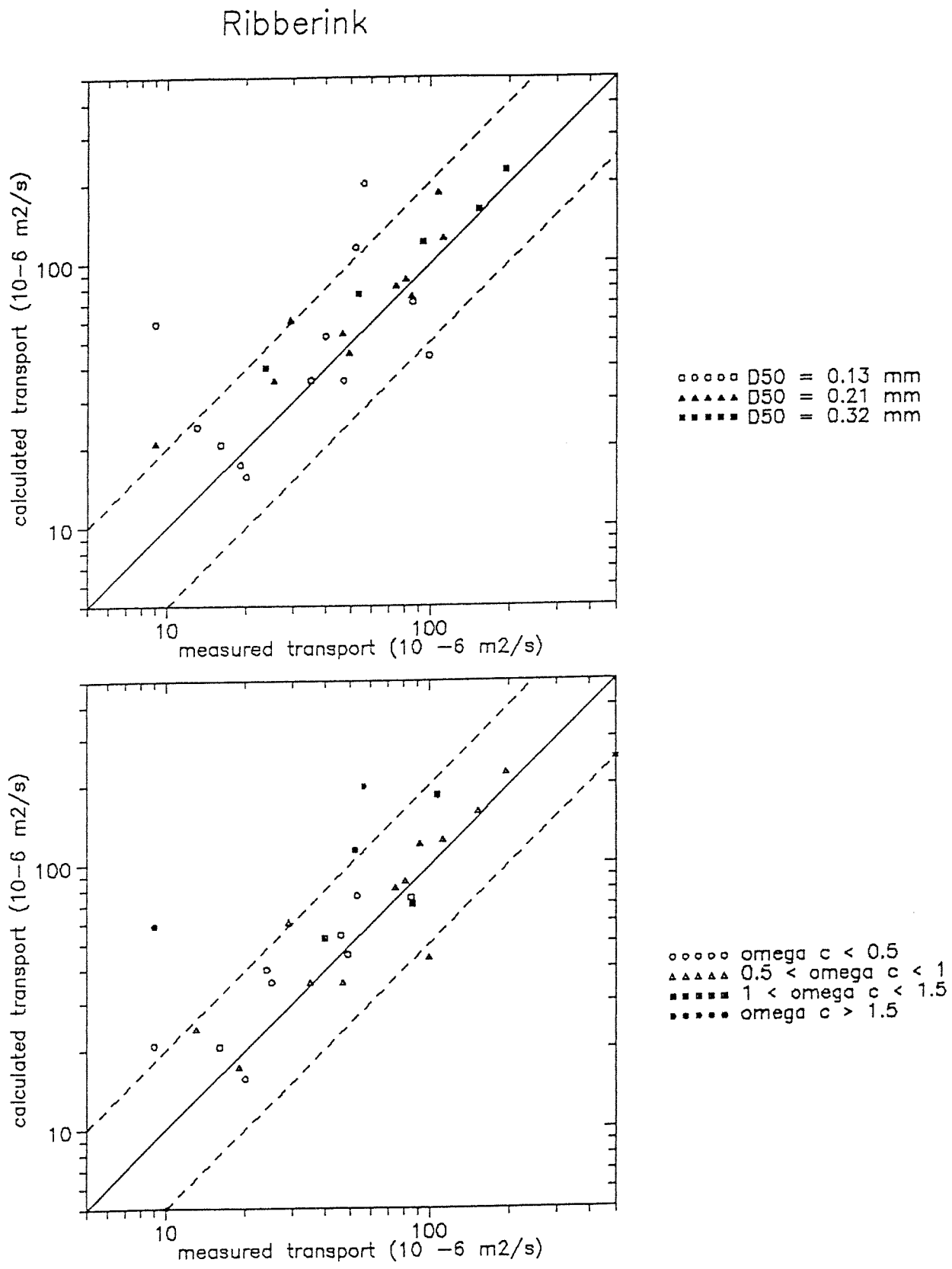

Figure 5-15 Calculation results of the model of Ribberink

Figure 5.14 makes clear the bad results for mainly the small grains can be explained by the occurrence of unsteady effects, which are not taken into account in this model.
It can also be due to the fact that the model was originally developed for situations in rivers with coarser bed material. However, Bailard adapted it to situations with finer bed material, with a D_{50} between 0.175 and 0.30 mm. There might be a strong relation between the coefficients ε_b and ε_s and the grain diameter, so the model could be improved by adapting these coefficients to the grain-size.

Model of Ribberink

This model is described in Chapter 2, with the transport formula given in eq. 2.14. The representative Shields parameter θ', which is the driving force in this model, depends on the bed shear stress, which in this case is calculated using the method of Ribberink/Van Rijn. For the bed roughness height, Ribberink found that the best results are found with:

$k_{s,w} = D_{50}(1+6(\theta-1))$
$k_{s,c}$ = the maximum of $3D_{90}$ and $D_{50}(1+6(\theta-1))$

Figure 5.15 shows the results for this model, compared with measured transport rates, sorted according to grain-size and ω_c. It is clear that this model takes better into account the grain-size influence. There is no systematically over or underprediction for grain-size of 0.21 and 0.13 mm, and only a small overprediction for the coarse sand. However, there is some scatter for the fine sand. The figure makes clear that for these points a large value for ω_c can be found, which would mean that unsteady effects are important. The model of Ribberink, like the model of Bailard, is a quasi-steady model. Unsteady effects are not taken into account.

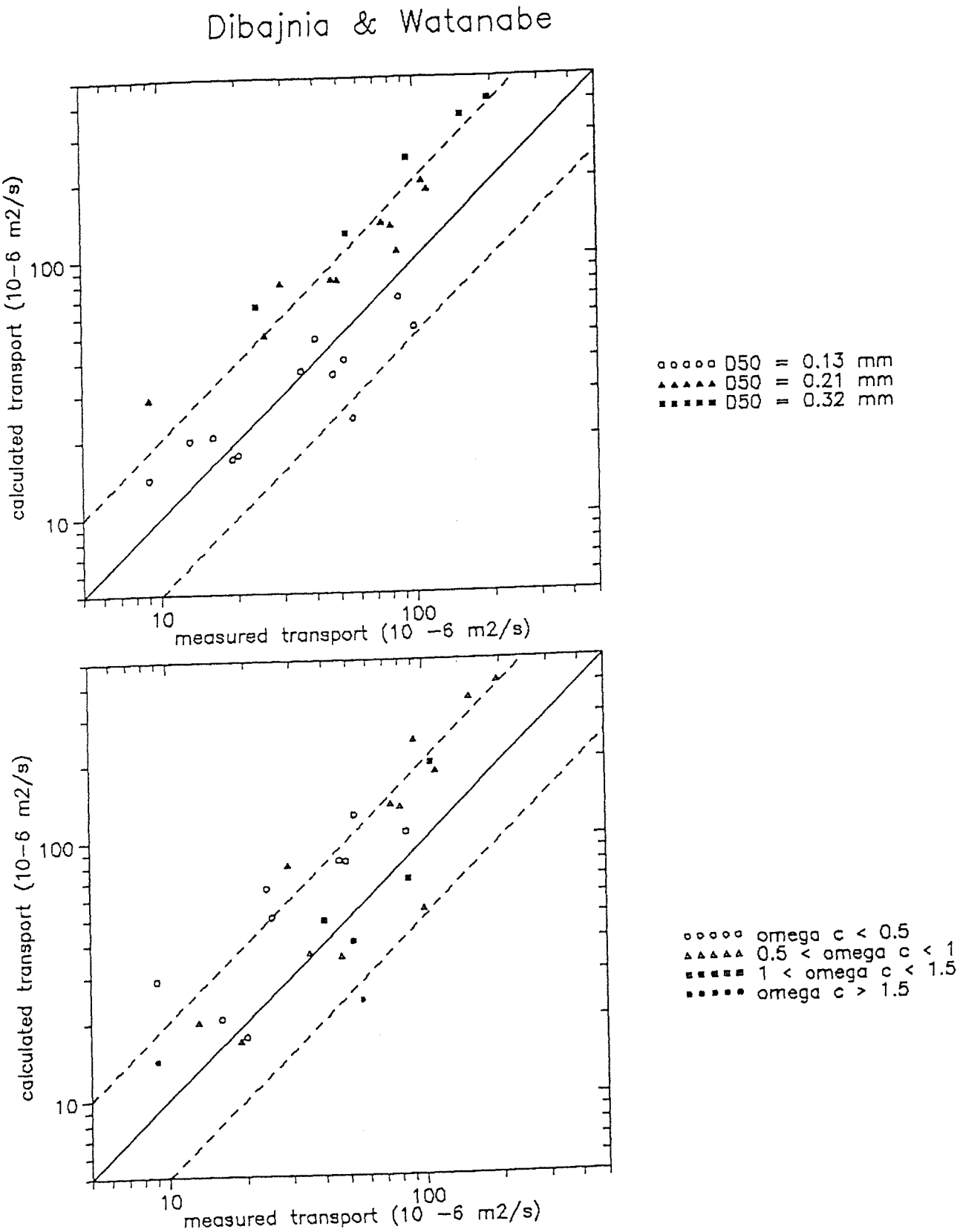

Figure 5-16 Calculation results of the model of Dibajnia & Watanabe

Model of Dibajnia and Watanabe

This model takes into account the delayed behaviour of the suspended sediment. Sediment which is brought into suspension but has no time to settle to the bed within the same half of the wave period, is transported in opposite direction during the successive part of the wave period. The transport formula is given by eq. 2.22 to 2.25.

The calculation results for this model are given in figure 5.16. It shows that this model is able to predict in a satisfying way the transport rates for the fine sand. However, this model overpredicts the results for the 0.21 mm sand and even more for the coarse sand.

The parameter ω_c plays an important role in the model of Dibajnia and Watanabe (see Section 2.3.2). It can be seen in Figure 5.16 that there is no systematic overprediction for large values of ω_c. The small values of ω_c, for which the net transport rates are overpredicted, are all related to grain-sizes of 0.32 mm or 0.21 mm.

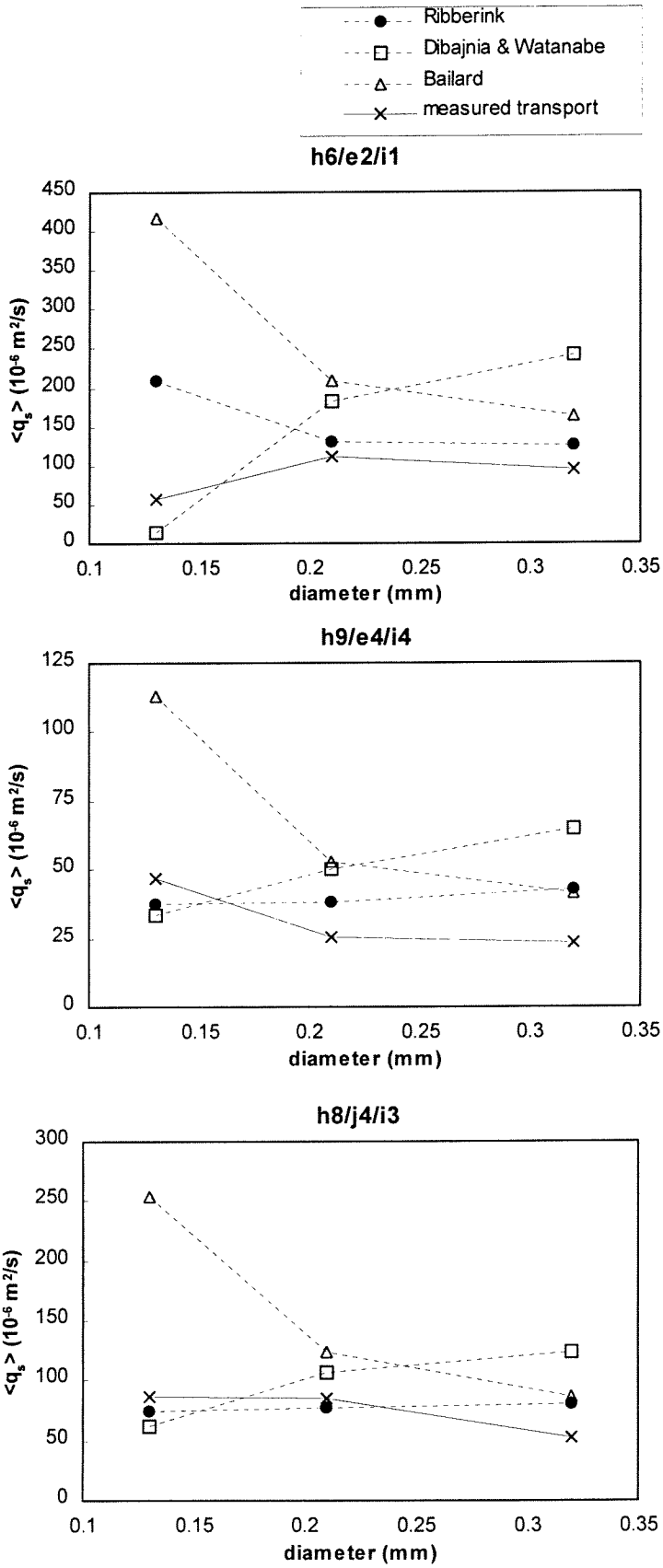

Figure 5-17 Grain-size influence on different models

Grain-size influence on different models

Figure 5.17 shows the influence of the grain-diameter on the different models. The conditions are chosen in a way that also measured values can be plotted. It should be noted that the linear scale of the vertical axis is different for every condition.

The figure shows that the model of Bailard is sensitive for the grain-diameter, especially for small diameters. A smaller grain-size gives a much larger transport rate, and thereby a large over estimation of the measured values.

The model of Ribberink is not very sensitive for changes in grain-size, which was already mentioned before. Only under the condition with the largest oscillating velocity H6/E2/I1, the smallest grains give an increased transport rate, while the measurements show that, due to unsteady effects, the measured transport rates decreases.

The model of Dibajnia and Watanabe can be very sensitive for grain-sizes under conditions with e.g. a high oscillating velocity like H6/E2/I1, but is not very sensitive under less severe conditions. The parameter ω_c, which indicates the occurrence of unsteady effects, gives for the different conditions the following values:

H6:	1.971	H9: 1.051	H8: 0.579
E2:	0.864	E4: 0.427	J4: 0.237
I1:	0.537	I4: 0.264	I3: 0.150

For values higher than 1 the unsteady effects seem to play a distinctive role and grain-size influences become important. For $\omega_c \leq 1$, the model of Ribberink gives the best results. Only in case of H6, where $\omega_c > 1$, the model of Dibajnia and Watanabe gives a better result.

6 Implementation of size-fraction method

In the existing models which predict net transport rates, the bed material is considered to be uniform, characterised in most cases by the D_{50}. In order to include the effects of the gradation of the sediment into these models a size fraction method is implemented in the three models which were used in Chapter 5: Bailard, Ribberink and Dibajnia and Watanabe. The theory about the size fraction method is explained in Section 2.4.1.

An existing computer program referred to as TRSP, which is developed to compare experimental results from the LOWT with existing theoretical transport models, is used in this study. The modified program TRSP3 gives the opportunity to compare the predicted net transport rates of a mixture, characterised by its mean grain diameter only, with the predicted net transport rates of the same mixture, characterised by a combination of several fractions with different grain diameters. An extensive sensitivity analysis is carried out with this computer program, in order to get insight in the influence of the gradation of the sediment on the predicted net transport rates in the different models and in order to study the different methods for the hiding and exposure correction in the formula of Ribberink which were implemented.

In this chapter, first the adapted version of the computer program is described. In Section 6.2 the plan for the sensitivity analysis is presented and further explained, while in Section 6.3 the results are given.

6.1 The computer program TRSP3

The computer-program TRSP, developed by Koelewijn (1994) and improved by Van der Wal (1996) is further extended in the spring of 1997, resulting in version 3. The main aim of this extension is to make it possible to calculate the transport of non-uniform sediment, which can be seen as a mixture of different size-fractions.

In the description of the program in this section the emphasis is on the extensions made in version 3. More details about the program are given by Van der Wal and Koelewijn in their reports. Some parts of the program listing of this version is given in Appendix F3.

Main program

The program is divided in five units:

unit Tools:	functions, opening- and closure screens
unit Central:	definition of all global variables and constants
unit Inout:	read, save and change input, writing output
unit Reken:	calculate transport rates, using different methods
unit Correct:	calculate hiding- and exposure coefficients when using the size-fraction method (only in case of the model of Ribberink)

Figure 6.1 shows how these different units together form the main program TRSP3.

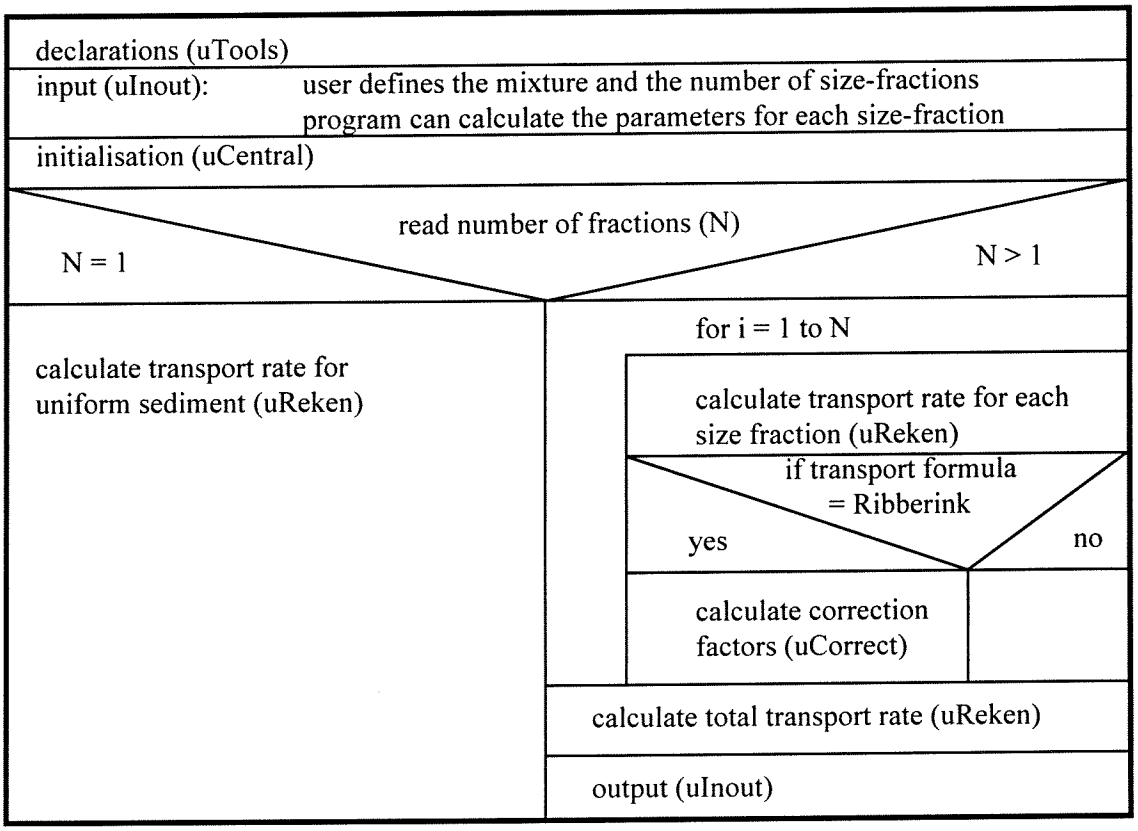

Figure 6-1 Structure of main program TRSP3

The unit Inout

The input consists of information about the water, the sediment, either concerning the mixture or concerning the different size-fractions, and about the imposed condition. All input parameters are given in Table 6.1.

Table 6-1 Input parameters

input parameters		description
water	ρ [kg/m^3]	density of the water
	ν [m^2/s]	viscosity of the water
	temperature [°C]	water temperature
sediment mixture	D_{50} [mm]	max. grain-size of 50% of the bed material
	D_{90} [mm]	max. grain-size of 90% of the bed material
	W_s [m/s]	fall velocity of particle with diameter D_{50}
	tan φ_m [-]	angle of internal friction of the mixture
	$\rho_{s,m}$ [kg/m^3]	averaged density of the sediment mixture
	N [-]	number of fractions
fractions	D_i [mm]	mean grain-size of fraction i
	Ws,i [m/s]	fall velocity of fraction i (particle with diameter D_i)
	tan φ_i [-]	angle of internal friction of fraction i
	$\rho_{s,i}$ [kg/m^3]	density of the sediment in fraction i
	p_i [%]	volume percentage of fraction i, present in bed material
condition	<u> [m/s]	averaged velocity
	u_{rms} [m/s]	root mean square value of oscillating velocity
	T [s]	wave period
	z [m]	height above bottom for input velocities
	Δt [s]	time-step for calculations

There are two options for the input:

- the user defines the parameter of both the sediment mixture and the size-fractions (see Table 6.1)
- the user defines the parameters of the sediment mixture only, the parameters of the size-fractions are determined by the computer program.

The last option is implemented in the procedure Fractions. The assumption is made that the grain-size distribution is log-normal, so this option should only be applied if this assumption agrees with reality. More details about the size-fraction method and splitting a mixture into size-fractions are given in Section 2.4 and Appendix A1.

Apart form the net transport rate per fraction and the total net transport rate, some additional parameters are given as output. All output parameters are given in Table 6.2.

Table 6-2 Output parameters of procedure Totaal

output parameters	description	formula
$q_{c,i}$ [m^2/s]	net transport capacity of fraction i, i.e. transport rate if sand was uniform with diameter D_i	result of calculation module
q_i [m^2/s]	net transport rate of fraction i	= $p_i * q_{c,i}$
q_N [m^2/s]	total net transport rate	= Σq_i
$p_{T,i}$ [vol%]	contribution of fraction i to total net transport rate	= $q_i/q_N * 100$ %
D_T [mm]	mean diameter of transported material	= $\Sigma D_i * p_{T,i}$
D_T/D_m [-]	the ratio of D_T and the mean diameter of bed material	=D_T/D_{50}

Choice of transport formula

Al Salem & Ribberink	Bailard	Ribberink	Dibajnia & & Watanabe
Choice of **bed roughness height** ksc/ksw= 1. $3\theta D_{90}$ 2. $3D_{90}$ 3. $2.5\ D_{50}$ 4. D_{50} 5. $D_{50}(1+6(\theta-1))$ 6. max 2. and 5. 7. own choice	**Choice of** **bed roughness height** ksc/ksw= 1. $3\theta D_{90}$ 2. $3D_{90}$ 3. $2.5\ D_{50}$ 4. D_{50} 5. $D_{50}(1+6(\theta-1))$ 6. max 2. and 5. 7. own choice	**Choice of** **bed roughness height** ksc/ksw= 1. $3\theta D_{90}$ 2. $3D_{90}$ 3. $2.5\ D_{50}$ 4. D_{50} 5. $D_{50}(1+6(\theta-1))$ 6. max 2. and 5. 7. own choice	
bed shear stress 1. Ribberink/Van Rijn 2. Ribb./Van Rijn adj. 3. Soulsby/Ockenden 4. Time series	**Bed shear stress** 1. Ribberink/Van Rijn 2. Ribb./Van Rijn adj. 3. Soulsby/Ockenden 4. Time series	**Bed shear stress** 1. Ribberink/Van Rijn 2. Ribb./Van Rijn adj. 3. Soulsby/Ockenden 4. Time series	
		unit Correction	
Calculate transport using Al Salem & Ribb.	Calculate transport using Bailard	Caculate transport using Ribberink	Dibajnia & Wat.

Figure 6-2 Calculation module

The unit Reken

The transport rate for each fraction separately or for a uniform sediment is generated in the procedure Reken. In case of more size-fractions, the total net transport rate q_N, which is equal to sum of the transport rates of the N different fractions, is calculated in the procedure TOTAAL.
Several choices must be made in the calculation module, about which formulas to use and what to choose for the bed roughness height, before the real calculation is done using one of the four transport models. These possibilities are presented in Figure 6.2, which gives the structure of the calculation module.

The unit Correct

The unit Correct can only be used in case of the transport formula of Ribberink. In this formula the transport rate is related to the difference between the effective and the critical value of the Shields parameter. Several methods to calculate the critical Shields parameter are implemented in the computer program. The most common method is to relate this parameter to the mean diameter of the size fraction, which results in a different critical Shields for every fraction. the critical Shields parameter can also be related to the mean diameter of the mixture D_{50}. This results in the same value for all fractions. Also a constant value can be chosen, 0.0474 or 0.035, which are used in specific formulas, or the user can give his own choice. Figure 6.3 shows the different possibilities.

Various methods to calculate the hiding- and exposure coefficient are implemented in the computer program. These methods are described in Section 2.4.3. Two correction coefficients are implemented in the formula of Ribberink: ξ_{cr} which corrects the critical Shields value, and ξ_{eff} which corrects the effective Shields value (see eq. 2.38).

The correction factors are calculated in the procedures C1-C5 (see Figure 6.3) In the different procedure different methods are used:

C1	ξ_{cr} according to Egiazaroff	$\xi_{eff} = 1$
C2	ξ_{cr} according to Ashida & Michiue	$\xi_{eff} = 1$
C3	ξ_{cr} according to Komar & Wang	$\xi_{eff} = 1$
C4	$\xi_{cr} = 1$	ξ_{eff} according to Day
C5	no hiding and exposure correction	$\xi_{cr} = \xi_{eff} = 1$

The correction coefficients can be applied for all fractions, or only for fine fractions, i.e. when $D_i < D_{50}$.

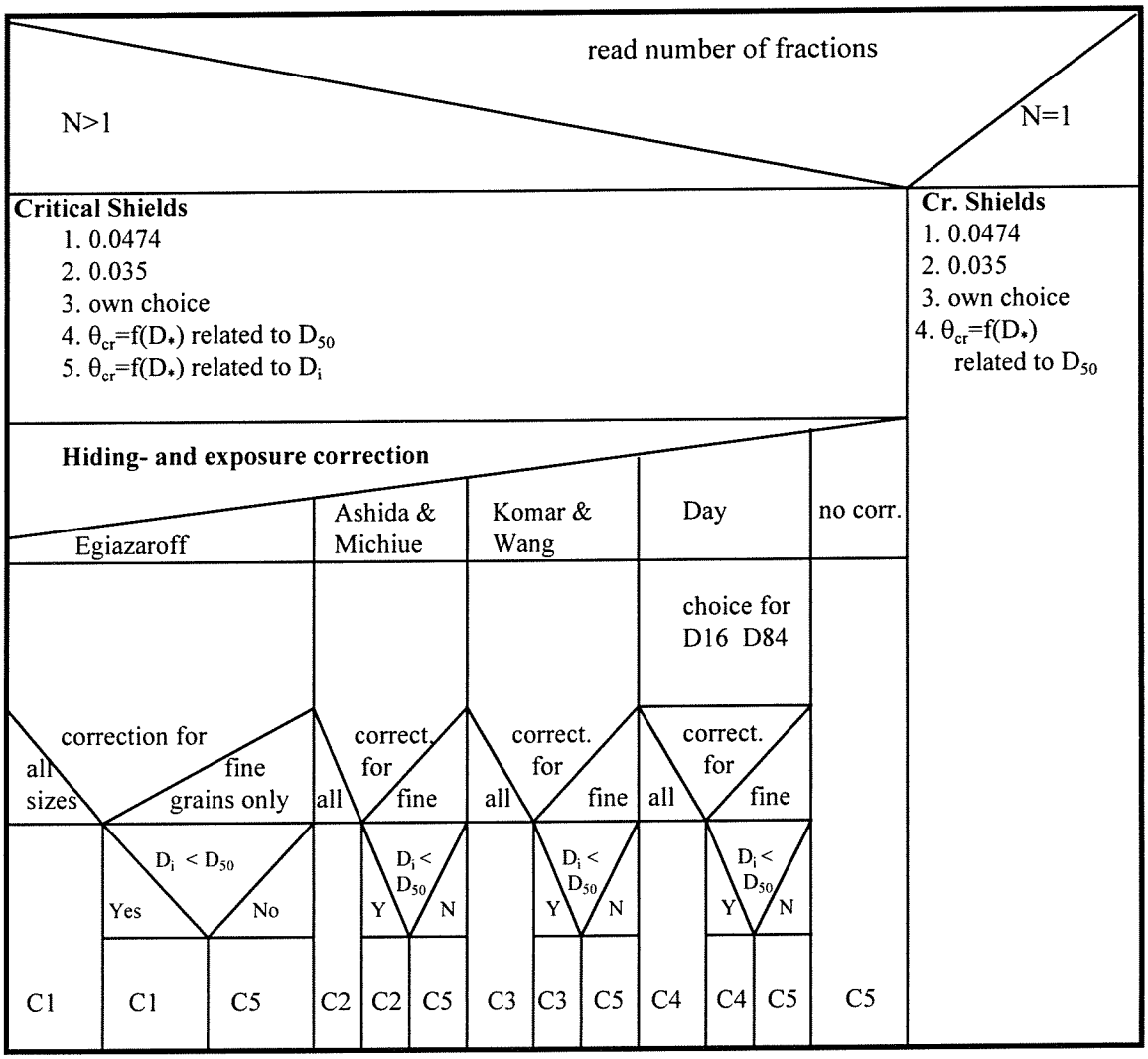

Figure 6-3 Unit Correct

The correction coefficients are implemented in the computer program in the following way:

$$\theta_{cr,corrected} = \xi_{cr} \cdot \theta_{cr} \tag{6.1}$$

For every time step:

$$\theta' = \frac{\tau_b}{(\rho_s - \rho_w) g D_{50}} \tag{6.2}$$

$$\Phi_{sum} = \Phi_t + m\left(\frac{\theta'}{\xi_{eff}} - \theta_{cr,corr}\right)^n \frac{\theta'}{|\theta'|} \tag{6.3}$$

in which: Φ_t = dimensionless transport for this time step
Φ_{sum} = sum of calculated dimensionless transport rates

The net transport rate is calculated by:

$$\Phi = \frac{\Phi_{sum}}{aantst} \tag{6.4}$$

in which: Φ = net transport rate, averaged over the wave cycle
Δt = time step used in the calculation

The equivalent value of the Shields parameter, θ_{eq}, is the value of the effective Shields parameter averaged over the wave cycle. This parameter is calculated afterwards, using:

if $\Phi > 0$: $$\theta_{eq} = \theta_{cr,corr} + \left(\frac{\Phi}{m}\right)^{\frac{1}{n}} \tag{6.5}$$

if $\Phi > 0$: $$\theta_{eq} = \theta_{cr,corr} - \left(\frac{|\Phi|}{m}\right)^{\frac{1}{n}} \tag{6.6}$$

in which: m and n: coefficients from formula of Ribberink

The essential parts of the program listing of the units Inout, Reken and Correct are given in Appendix F3.

6.2 Sensitivity analysis

The aim of the sensitivity analysis, performed with the computer program TRSP3, is to get information about the effects of gradation of the sediment on the predicted transport rates, and about the parameters which play a major roll in this transport process.

The results will be expressed by the following parameters:

- q_N/q_1 ratio of total net transport rate of a mixture characterised by N size-fractions and the net transport rate of the same mixture characterised by only D_{50} and D_{90} (i.e. one size-fraction)
- D_T/D_m ratio of the diameter of transported material and the mean diameter of bed material, in which: $D_m=\Sigma D_i * p_i$
  $D_T=\Sigma D_i * p_{T,i} p_{T,i}$ contribution of fraction i to the total net transport rate (as volume percentage)

The mixture, which is characterised by D_{50} and D_{90}, is split up into a certain number of size-fractions, which are characterised by D_i and p_i , as given by the formulas in Appendix A1.

The sensitivity analysis consists of two parts. Part A deals with the effects of the sediment parameters, like the mean diameter of the bed material and the number of fractions, under three conditions, for three transport formulas: Bailard, Ribberink and Dibajnia and Watanabe. In Ribberink's formula no correction factors will be applied here. Part B is about the effects of the hiding-and exposure correction in the transport formula of Ribberink, using different correction methods.

PART A

Flow conditions:	Condition 1	<u>=0.08 m/s	û=0.5 m/s
	Condition 2	<u>=0.16 m/s	û=1.0 m/s
	Condition 3	<u>=0.24 m/s	û=1.5 m/s

Using the standard settings for Bailard, Ribberink and Dibajnia and Watanabe, the following tests are carried out for these three conditions:

A1. Effects of the number of fractions

The standard mixture (D_{50}=0.21 mm, D_{90}=0.32 mm) will be characterised by 1,2,3,4,5,6 and 8 size fractions. The standard number of fractions which is used in the next tests depends on results of this test.

A2. Effects of the mean diameter of the mixture

standard sediment:	D_{50}=0.21 mm, D_{90}=0.32 mm
finer sediment:	D_{50}=0.13 mm, D_{90}=0.18 mm
coarser sediment:	D_{50}=0.32 mm, D_{90}=0.48 mm

A3. Effects of the width of the gradation

standard mixture:	D_{50}=0.21 mm, D_{90}=0.32 mm
wider gradation:	D_{50}=0.21 mm, D_{90}=0.51 mm
widest gradation:	D_{50}=0.21 mm, D_{90}=0.68 mm

Part B

This part is only carried out for the transport formula of Ribberink.
Calculation are performed with all combinations of the following parameters:

• wave condition:	condition 1	
	condition 3	
• critical Shields parameter:	constant value	
	related to D_i	
• hiding and exposure correction:	Egiazaroff	
	Ashida & Michiue	
	Komar & Wang	
	Day	
	none	
• correction for:	all size-fractions	
	fine sizes only	
• mean diameter of the mixture D_{50}	fine (0.13 mm)	
	standard (0.21 mm)	
	coarse (0.32 mm)	
or width of gradation:	standard	(D_{50}=0.21 mm, D_{90}=0.32 mm)
	wider	(D_{50}=0.21 mm, D_{90}=0.51 mm)

In order to limit the number of tests, a choice had to be made between varying the mean diameter of the mixture, like in test A2, or the gradation of the mixture, like in A3. It depends on the result of part A which parameter is chosen. This is described in Section 6.3.

The input values for all tests are given in appendix F1.

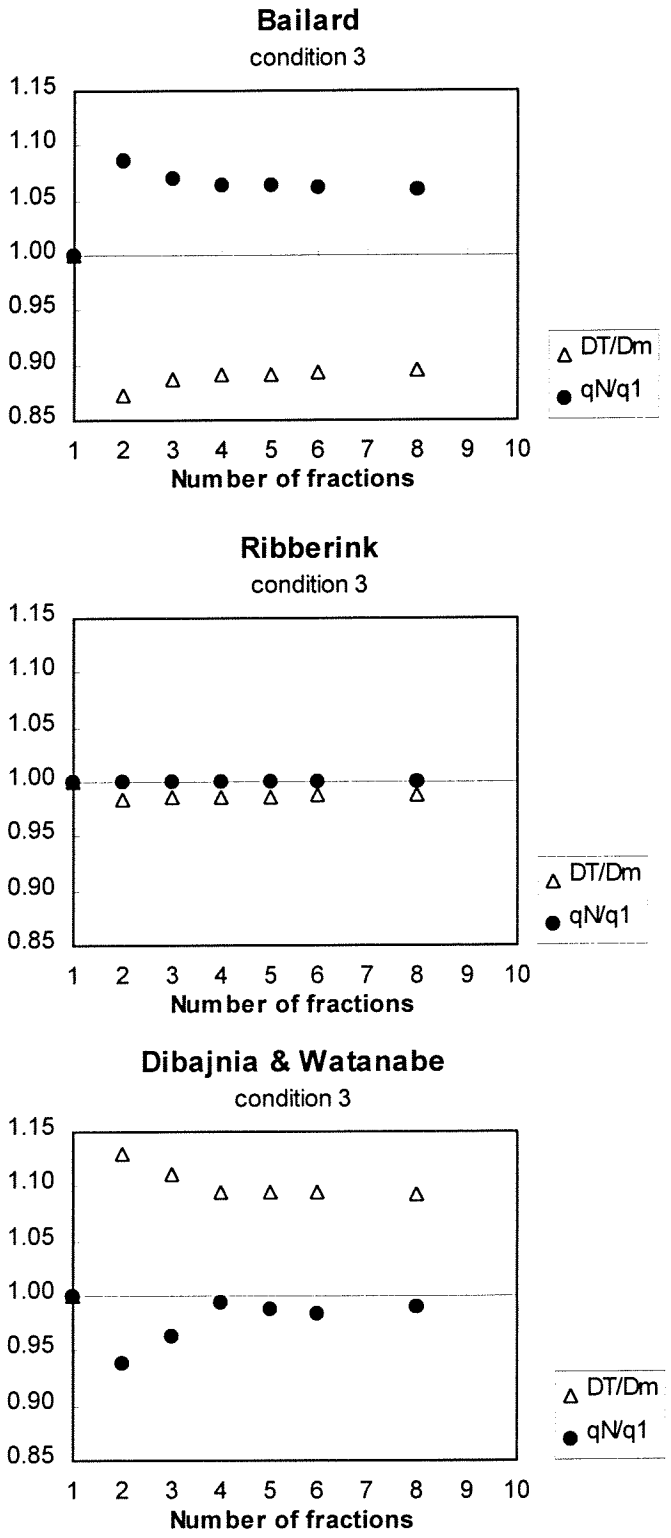

Figure 6-4 Variation in number of fractions for condition 3

6.3 Results of sensitivity analysis

Experimental results about transport of non-uniform sediment are not available. In this section, the results of the sensitivity analysis are given. Most attention is paid to the parameters q_N/q_1, which is the ratio of the calculated transport rate as sum of different fractions and the predicted transport rate of the same sediment, but characterised D_{50}, D_T/D_m, which is the ratio of the average diameter of the transported material and the mean diameter of the original bed material. The parameter p_i gives volume percentage of each fraction of the bed material; $p_{T,i}$ gives the contributions of each fraction to the predicted transport rate in volume percentages.

6.3.1 Test A1: Number of fractions

The results for test A1 for all tests are given in Figure A6 in Appendix F2. In Figure 6.4, the results for condition 3 are given.

For an increasing number of fractions the parameters q_N/q_1 and D_T/D_m converge to a specific value. This can be seen in the figure. A large number of size-fractions requires a long computing time. The best number of fractions is the minimum number were the parameters q_N/q_1 and D_T/D_m are on a constant value. In case of the model of Ribberink the parameters q_N/q_1 and D_T/D_m are very close to 1 for all cases, so an optimum number of fractions can not be determined. From the results for the model of Bailard can be concluded that the optimum number of fractions is 4. However, the differences in results for the different numbers of fractions are very small. For the model of Dibajnia and Watanabe the results for the parameter q_N/q_1 do converge in a very smooth line. This can be due to the occurrence of unsteady effects. The unsteady effects have a strong relation to the grain diameter. The transport rates for small fractions can be strongly reduced, while the transport rate for coarser fractions is not affected at all. This can result in larger differences in total transport rates for small number of fractions. Also from the results of the model of Dibajnia and Watanabe can be concluded that the optimum number of fractions is 4.

The different transport models show very different results for q_N/q_1 and D_T/D_m. The model of Bailard gives for q_N/q_1 a values between 1 and 1.1, with the highest values for condition 3. This means that using the size-fraction method results in a small increase in predicted transport rate. The parameter D_T/D_m lies around 0.9 for all conditions. The transported material has a smaller diameter than the bed material.

Figure 6.5, gives the volume percentages of the size-fractions in the total transport rate, if the bed material is split up in 8 size-fractions, for condition 3. All conditions show the same effects, but these effects are the strongest in case of condition 3. Figure 6.5 shows that in case of Bailard the smallest fractions form a larger part of the total sediment load than originally in the bed material. In this model smaller grains result in higher transport rates. This can be verified by Figure 5.14, which gives the relation between the diameter and transport rate for different models.

The model of Ribberink is not very sensitive for grain-size influences, which was already shown in Figure 5.15. The value of q_N/q_1 and D_T/D_m lies close to 1 in al cases. Figure 6-5 shows that the transported material contains more fine fractions compared to the bed material contains. The differences are very small.

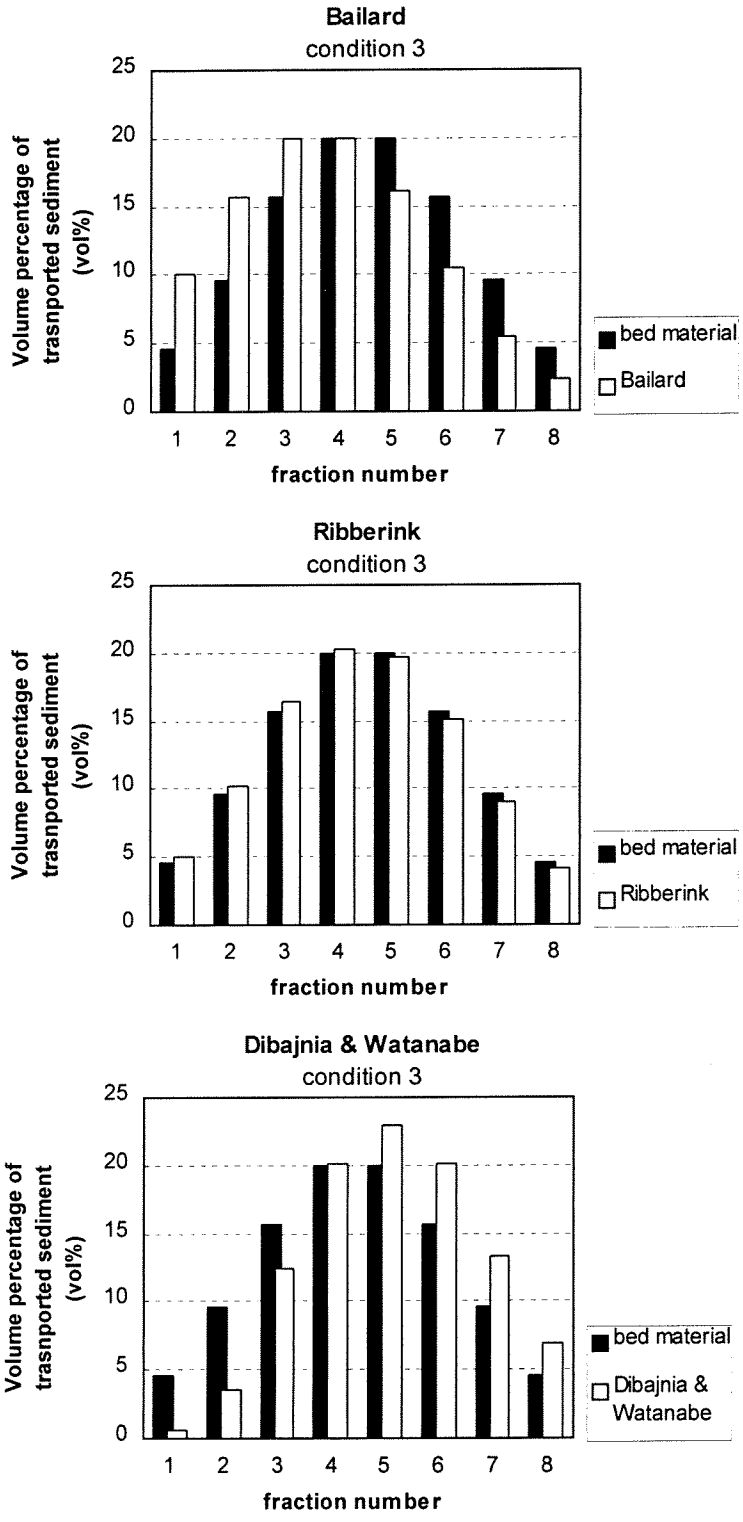

Figure 6-5 Volume percentages for transported material for condition 3, in case of 8 size fractions

The critical value of Shields parameter, which is used in the model of Ribberink, is derived by using D_i. This results in a different critical Shields parameter for the different fractions.

The model of Dibajnia and Watanabe gives for q_N/q_1 a value around 1.05 in case of condition 1 and 2. For condition 3 this value is smaller than 1 for a small number of fractions, and for more fractions it lies around 1, which is shown in figure 6.4. This can be explained by the occurrence of unsteady effects. For condition 1 and 2, the unsteady effects only slightly reduce the contribution of the smallest size-fractions to the total transport rate, and increase the contribution of the coarser fractions, leading to D_T/D_m =1.07. In case of condition 3, the unsteady effects are stronger, due to the higher oscillating velocity. The net transport rate of the small fractions is reduced so much, that the total transport rate q_N is smaller than q_1. Because mainly the transport rates for small fractions are reduced by the unsteady effects, the transported material will have a larger diameter than the bed material. This is shown in Figure 6.4, where the values of D_T/D_m lies around 1.1. The unsteady effects are strongest if the mixture is split into a small number of fractions. The reduced contribution of the small fractions to the net transport rate can clearly be seen in Figure 6.5.

Conclusions:

- The optimum number of fractions for the studied conditions is 4. In most cases for four fractions the parameters q_N/q_1 and D_T/D_m have already reached a constant value. The results of model of Dibajnia and Watanabe for condition 3 are influenced by the unsteady effects.
- The results of the model of Ribberink change only a little bit when the size-fraction method is used; q_N/q_1 and D_T/D_m are close to 1.
- The model of Bailard always gives an increased transport rate if more the sediment is characterised by more than one size-fraction. The transported material has a diameter which is a slightly smaller than the mean diameter of the bed material, because smaller fractions have a larger contribution to the total transport rate than coarser fractions. The imposed condition does not influence these effects.
- For the model of Dibajnia and Watanabe are results are strongly influenced by the imposed hydraulic condition. The transport of the finest fractions is reduced by unsteady effects. Still, for the relatively mild conditions 1 and 2, the predicted transport for N fractions is larger than the predicted transport rate for uniform sediment, because of the larger net transport rates for the larger fractions. Only when the unsteady effect become very strong, as under the most severe condition 3, the total net transport rate calculated from the size-fraction method is smaller than the net transport rate uniform sediment. In this case, the reduction is stronger influenced by the number of size fractions.
- The three transport models show a very different selective behaviour:
  in case of Bailard, mainly fine fractions are transported
  in case of Dibajnia and Watanabe, mainly coarse fractions are transported
  in case of Ribberink, the transported sediment has almost the same composition as the original bed material

6.3.2 Test A2: Mean diameter of the mixture

In figure A7 in appendix F2, the influence of the mean diameter D_m of the mixture on the differences in predicted transport rates for sediment characterised by several fractions or D_{50} only, is shown. The model of Dibajnia and Watanabe is also given in Figure 6.6.

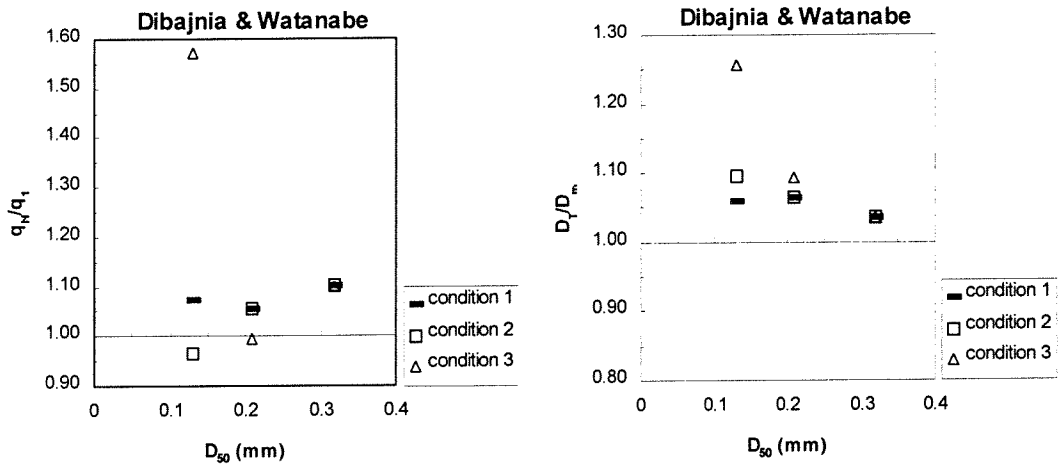

Figure 6-6 q_N/q_1 and D_T/D_m for different mean diameters in case of Dibajnia and Watanabe

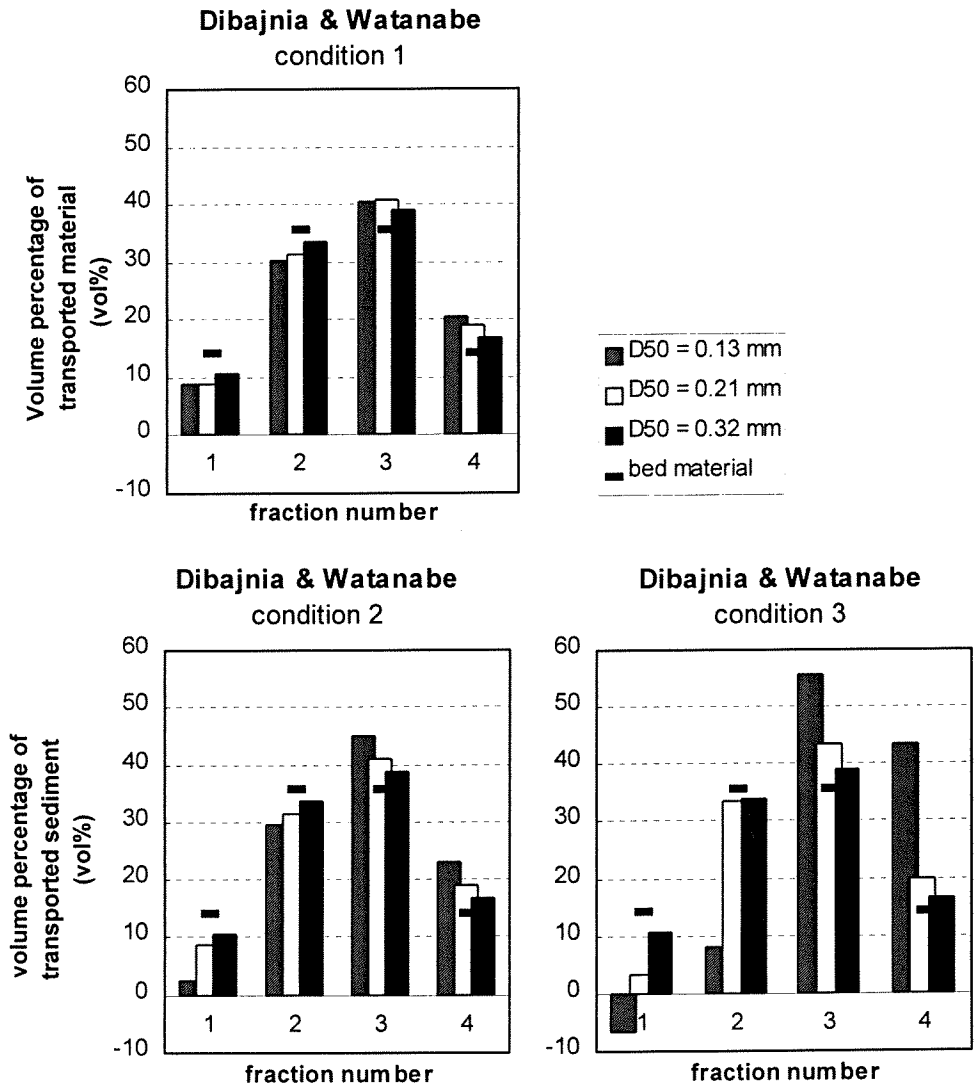

Figure 6-7 Volume percentage for transported material for different values of D_m

For the model of Bailard, q_N/q_1 is higher than 1 for 0.13 and 0.21 mm, and just below 1 for the coarsest sand. D_T/D_m is around 0.9 for all sizes. The condition has no influence on q_N/q_1, and only slightly influences D_T/D_m. Figure A8 shows the volume percentage of every size-fraction in the transported material. This makes clear that the finer fractions are transported more and the coarser fractions are transported less, which results in a slightly higher transport rate, because under the same conditions smaller particles are transported easier than coarser material. These effects are not so strong for the mixture with the largest D_{50}.

For the method of Ribberink, the average diameter of the mixture has no influence on q_N/q_1 or D_T/D_m. Figure A8 shows that also the different values of $p_{T,i}$ do not differ very much from the volume percentages in the original bed material p_i.

For the method of Dibajnia and Watanabe, the condition plays an important role, especially in case of a fine sediment. The occurrence of unsteady effects is clearly shown in Figure 6.7, which gives the contribution of every size-fraction to the total net transport rates.
In case of condition 1, the unsteady effects are small. All mixtures show a small reduction in transport rate for the finest fraction and an increase for the larger fractions (the values of $p_{T,i}$ are almost the same for all three mixtures), resulting in $q_N/q_1 \approx 1.08$ and $D_T/D_m \approx 1.1$.
For condition 2, strong unsteady effects occur for the finest fraction of the fine mixture, resulting in a decrease in transport rate. The unsteady effects are not as strong if the mixture is characterised by 1 fraction. Therefore in both q_N/q_1 and D_T/D_m are larger than 1. For the mixture with D_{50}=0.21 and 0.32 mm there is only a small reduction for the finest fraction and some increase for the coarser fractions, which is not present if the mixtures are characterised by one fraction only. Therefore q_N/q_1 and D_T/D_m are slightly larger than 1.
For condition 3 the predicted transport rate of the uniform sediment with D_{50} = 0.13 mm is strongly reduced by unsteady effects. Although the unsteady effects also influence the finest fraction when this mixture is characterised by several size fractions, still the predicted transport rate for uniform sediment is much smaller than the net transport rate as sum of size fractions, due to the increase in transport rates for the coarser fractions. This results in a surprisingly large value of $q_N/q_1 \approx 1.5$ and $D_T/D_m \approx 1.3$. For the D_{50} = 0.21 mm the unsteady effects in the case of uniform sediment are relatively small; $q_N/q_1 < 1$ and $D_T/D_m > 1$. Finally, for the 0.32 mm sand the situation is the same as in condition 1 and 2: a small reduction of the fine fractions is compensated by an increase of the larger fractions, resulting in q_N/q_1 slightly larger than one and $D_T/D_m > 1$.

Conclusions:

The differences between the predicted transport rates for sediment characterised by several size-fractions and sediment characterised by D_{50} (q_N/q_1) and the diameter of the transported material compared to the bed material (D_T/D_m) are studied for different mean diameters of the sediment mixture.

- For the model of Bailard, these differences are not very sensitive to changes in D_m.
- For the model of Ribberink, these differences are not at all influenced by changes in D_m.
- For the model of Dibajnia and Watanabe, the influence of D_{50} depends on the hydraulic condition. For fine sediment in combination with condition 3 (largest velocities) the transport rate for uniform sediment (q_1) is strongly reduced, which results in $q_N/q_1 = 1.5$. In other cases, q_N/q_1 is close to 1. The transported sediment has in all cases a larger diameter than the bed material, due to an increase of the transport rates of the coarse fractions, and a reduction of the transport rates for the fines fractions, due to unsteady effects.

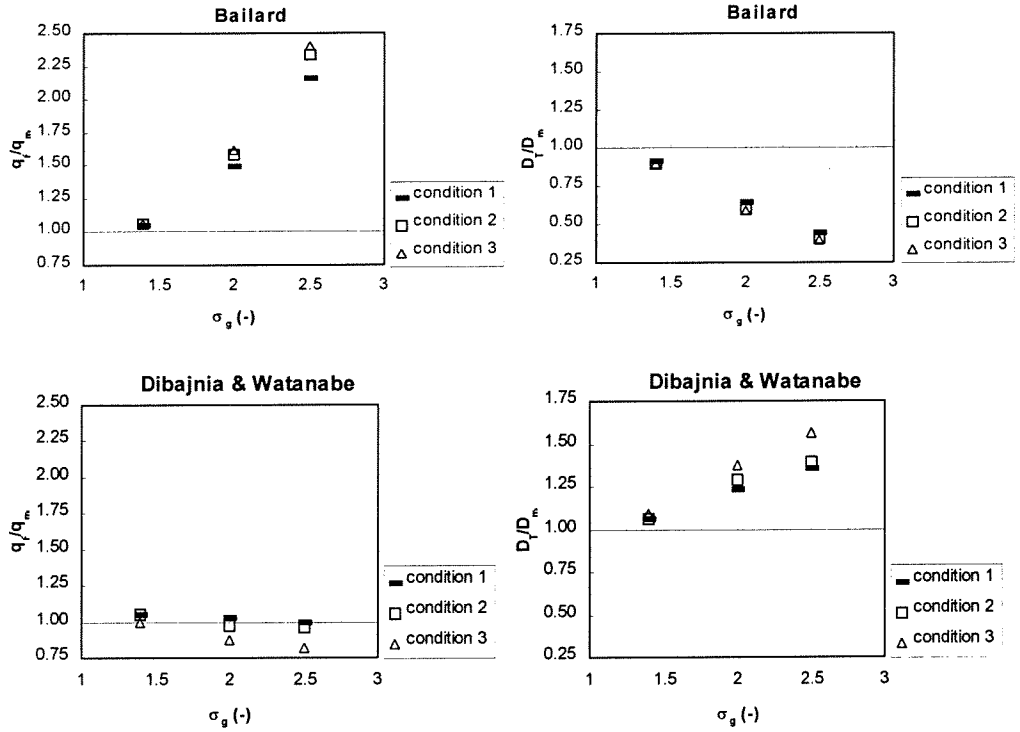

Figure 6-8 Influence of grain-size distribution on gradation effects

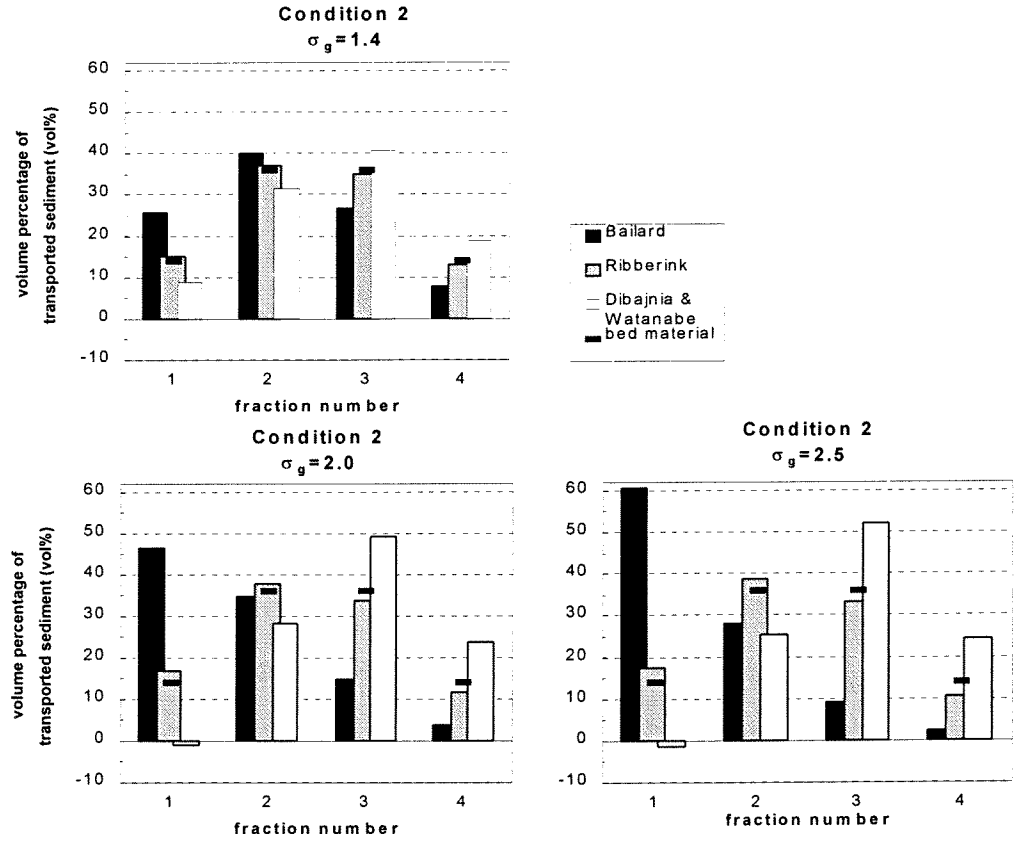

Figure 6-9 Volume percentage of every size-fraction in transported material

6.3.3 Test A3: Grain-size distribution of the mixture

The width of the grain-size distribution is indicated by the geometric standard deviation σ_g. A wider gradation means that the differences between the smallest and the largest diameter increases, while the mean diameter remains the same. In figure A9, for all models q_N/q_1 and D_T/D_m are plotted for all models. The results for Bailard and Dibajnia and Watanabe are also plotted in Figure 6.8.

For the model of Bailard, the ratio q_N/q_1 increases rapidly with increasing σ_g. For condition 3, these effects are the strongest, for condition 1 the weakest. An increase of q_N/q_1 implies in this model an decrease of D_T/D_m. Figure 6.9 gives the values for $p_{T,i}$ for condition 2. It is clear what happens: mainly fine fractions are transported, while the coarse fractions remain on the bed. Figure A10 in Appendix F2 shows the absolute values of the transport rates for q_1 and q_N for all models. The transport rate q_1, represented by the lines, is not influenced by the gradation. The transport rate resulting from the size-fraction method increases with increasing σ_g.

For the model of Ribberink the parameter q_N/q_1 is not at all influenced by the change in σ_g. This is shown in figure A9, and also in A10. The values of k_{sc} and k_{sw} are in this model related to D_{50} and D_{90} (see p.5-21, Section 5.4). The transport rate for uniform sediment increases slightly with increasing σ_g in Figure A10. This figure also shows that the total transport rate q_N is exactly the same as transport rate q_1.
Figure 6.9 shows that for condition 3 the contribution of the fine fractions to the total transport rate increases, and the contribution of the coarsest fractions decreases. This implies that the transported material is finer than the bed material and D_T/D_m is smaller than 1, like shown in Figure A9.

The model of Dibajnia and Watanabe shows the same effects as in the previous test. The transport rates for fine fractions are strongly reduced or even become negative, due to unsteady effects. For the coarse fractions the transport rate increases. These grain-size influences are stronger due to the larger width of the grain-size distribution. This is shown in Figure 6-9 and A11. The parameter D_T/D_m increases strongly with increasing σ_g. The parameter q_N/q_1 decreases for a wider gradation. Figure A10 shows that the difference between q_N and q_1 is not large, especially in case of condition 2.

Conclusions:

- Bailard is very sensitive for the gradation of the mixture: q_N/q_1 increases strongly for increasing σ_g, while D_T/D_m decreases.
- In the model of Ribberink q_N/q_1 does not change at all when σ_g increases.
- The model of Dibajnia and Watanabe implies that for graded sediments the transport rate q_N does not change much compared to q_1 The composition of the transported sediment is very different from the bed material; D_T/D_m lies between 1.1 and 2.2.

To verify the choice of N=4, test A1 is also carried out for a mixture with a wider grain-distribution. The results are given in figure A11. Also in this case a choice of N=4 seems reasonable.

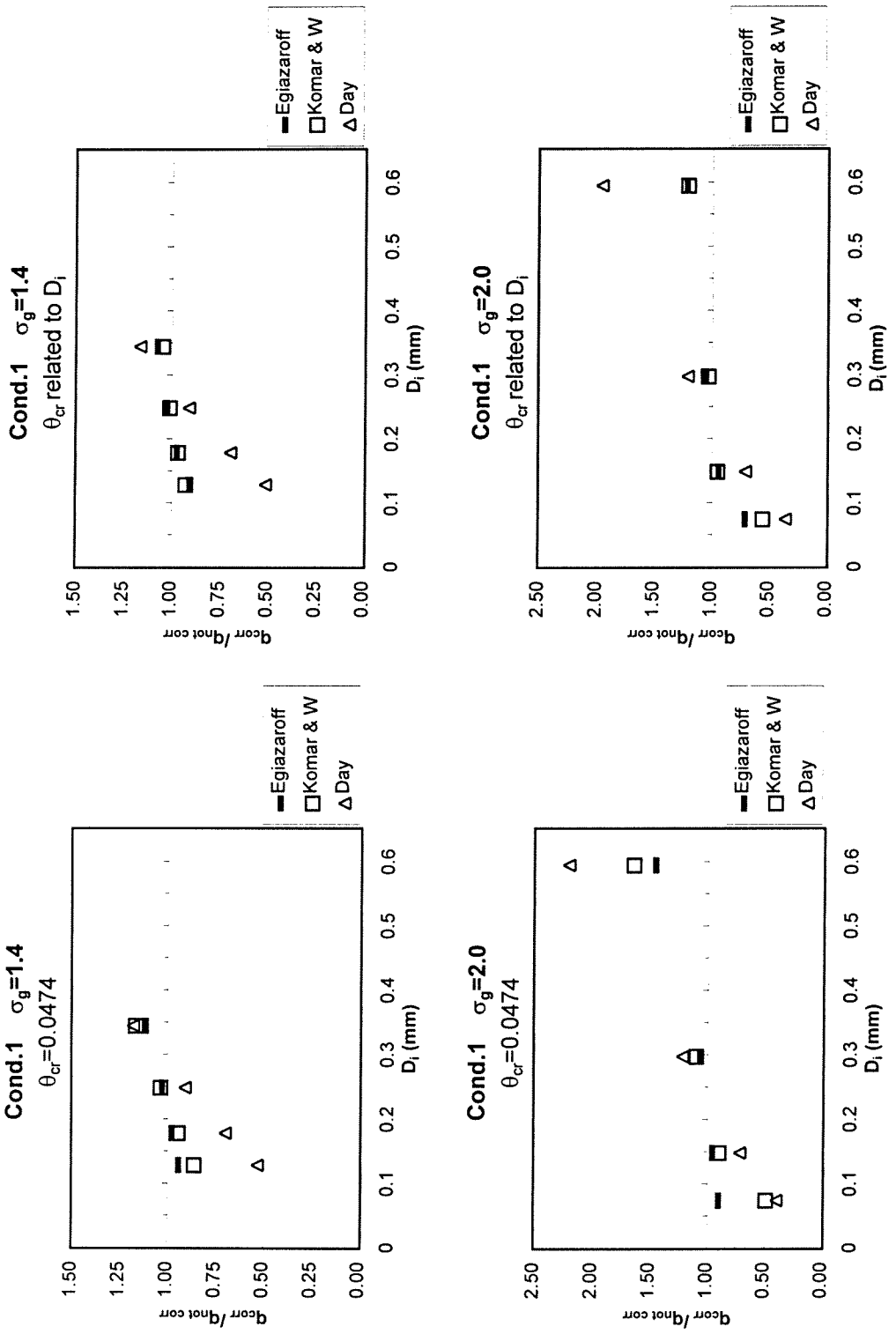

Figure 6-10 Ratio of corrected and uncorrected transport rates for condition 1

6.3.4 Test B: Correction coefficients in the model of Ribberink

This part of the sensitivity analysis is about the model of Ribberink. In this model a hiding and exposure correction can be applied. Four methods are implemented in the computer program to calculate these correction factors. It must be noted that also for these calculations no experimental results are available.

In this test the following parameters are varied:
- hydraulic condition
- method to calculate θ_{cr}
- method to calculate the correction coefficient
- the application of the correction coefficient; for all size fraction or only fine fractions
- the gradation of the bed material σ_g

From part A of the sensitivity analysis can be concluded that the gradation of the mixture σ_g has more effect on the results expressed by the parameters q_N/q_1 and D_T/D_m than changes in the mean diameter of the bed material D_{50}. Therefore, σ_g is varied in this test.

In Appendix F2, Figure A12 shows the values of the correction coefficients for the different diameters of each fraction. The method of Ashida and Michiue, which is a correction on Egiazaroff's method (see section 2.4) only differs for the largest grain diameter in the figure, where it gives a somewhat higher value (2.404 instead of 2.390). The differences between Egiazaroff and Ashida and Michiue are negligible and the last method is not further worked out in this sensitivity analysis. The coefficient ξ_{cr} resulting from the theory of Komar and Wang is influenced by the method of calculating the critical Shields parameter. This is due to the fact that Komar and Wang actually do not use the Shields curve at all, but in this program their expression for the critical shear stress is transformed into the coefficient ξ_{cr} by dividing by θ_{cr} (see eq. 2.).

The ratio of the corrected and uncorrected values of the transport rates for the different fractions are given in figure 6.10 for condition 1 and A13 in Appendix F2 for condition 3. The corrections coefficients are applied on all fractions. The critical value of the Shields parameter is either constant (right hand-sided plots) or based on D_i (left hand-sided plots). From these figures it is clear that all correction methods work in the same way: the transport rates for fine fractions are reduced and for the coarser fraction increased. The strongest correction is given by the method of Day. The magnitude of this correction value depends on the gradation (see eq. 2.45). In case of σ_g=1.4 the third fraction is reduced, but for σ_g=2.0 the third fraction has an increased transport rate. The method of Egiazaroff gives only a small change in transport rates. These effects are a little bit bigger for a wider gradation. The method of Komar and Wang gives a reduced transport for the two finest fractions and an increase in transport for the fractions 3 and 4. For σ_g=1.4 the effects are very small, but for σ_g=2.0 the reduction for the finest fraction is significant larger.

For condition 1 in Figure 6-10 small differences occur between the results calculated with different values of θ_{cr}. These differences do not occur for condition 3 in Figure A14. Due to a larger flow velocity in condition 3 the effective shear stress dominates over the critical shear stress. Correcting the critical Shields parameter does not make many differences. This also explains that for condition 3 the values for the methods of Egiazaroff and Komar & Wang, which both correct the critical Shields parameter, are close to 1. The value of the

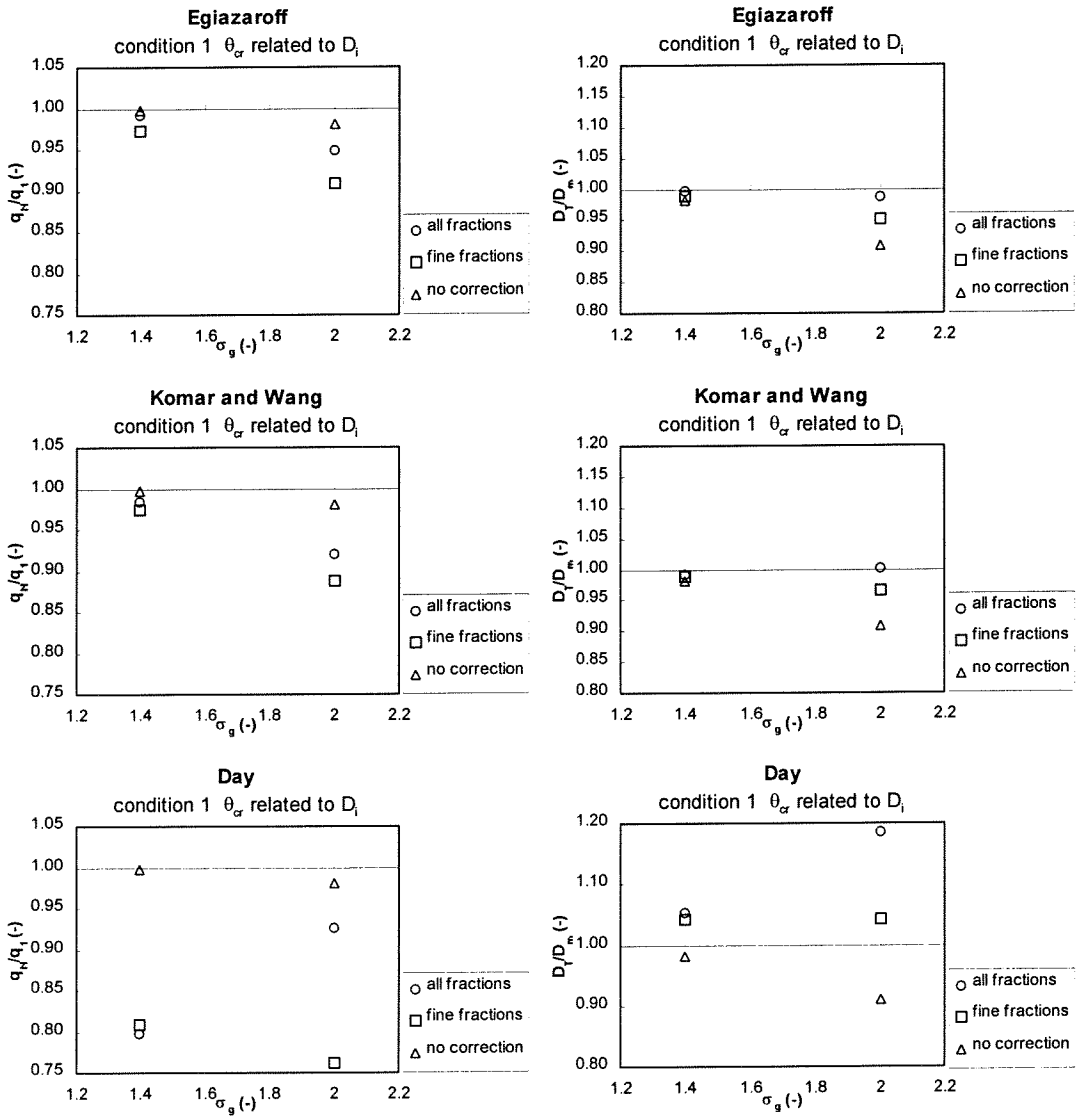

Figure 6-11 q_N/q_1 and D_T/D_m for different correction methods

correction coefficients itself is not influenced by the condition; therefore both figures show the same pattern. No differences between the two conditions can be seen for the method of Day.

Figure 6.11 gives the values of q_N/q_1 and D_T/D_m for the three correction methods under condition 1. A division is made between a correction for all fractions and for fine fractions only. For Egiazaroff and Komar & Wang, the transport rate of the smallest fraction is reduced. When all fractions are corrected, this effect is compensated by the increased transport rate for the coarsest fraction, which result in a q_N/q_1 very close to 1. When only the fine fractions are corrected, there is no compensation which means q_N/q_1 is smaller than 1. This explains that for correction of all fractions the value of D_T/D_m is higher than when only fine fractions are corrected. The method of Day gives a strong decreased transport rate for σ_g=1.4, with no differences between correction for small fraction only or for all fractions, because the transport rate for the coarsest fraction is almost not changed. For σ_g=2.0 the transport for the coarsest fractions increase, which gives a higher total transport rate and therefore a q_N/q_1 closer to 1, and also a high value for D_T/D_m. When only fine fractions are corrected, the total transport rate further decreases and also the diameter of the transported material increases less than for correction of all fractions.

Figure 6.12 gives the volume percentages for the different fractions of the transported material, for condition 1 and σ_g = 2.0. Not many changes are realised by the methods of Egiazaroff and Komar and Wang, but Day shows some significant changes.

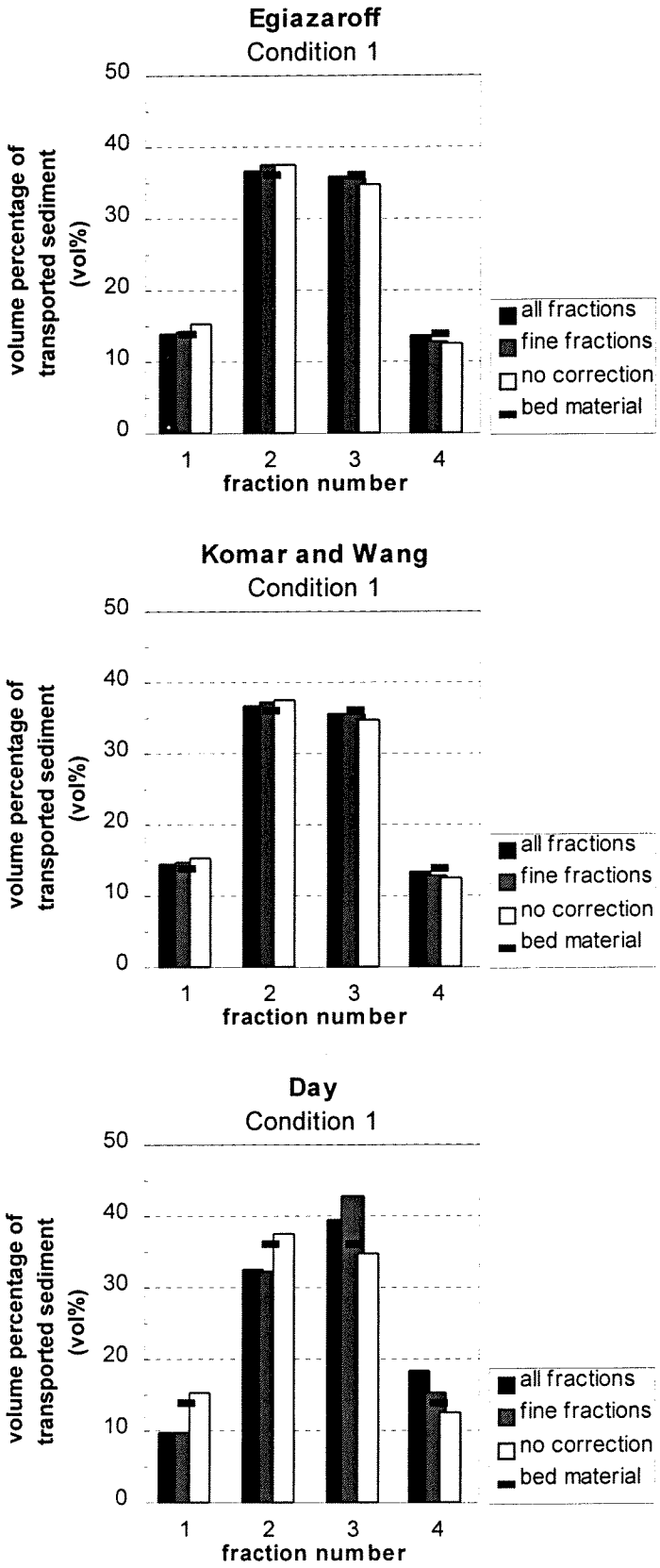

Figure 6-12 Volume percentages for size-fractions of transported material; θ_{cr} related to D_i

Conclusions:

- For all methods, the transport rates of the smallest fractions are reduced, while for the coarser fractions the transport slightly increases. The diameter of the transported material is larger than the diameter of the original bed material.
- The different methods for hiding and exposure correction give similar changes in q_N/q_1 and D_T/D_m. The effects are the weakest for Egiazaroff, while the method of Day gives the strongest influences. Only for $\sigma_g = 1.4$, the method of Day gives different results. It shows a large decrease of q_N/q_1 , while Egiazaroff and Komar and Wang predict $q_N/q_1 = 1$. The correction of Day also affects the predicted transport rate for the size-fraction method for small values of σ_g.
- The gradation is has much impact on the results of the size-fraction method. A wider gradation result in smaller values of q_N/q_1 and more differences between the diameters of the transported material and the bed material.
- Applying the correction for only fine fractions gives a lower q_N/q_1, because the reduction of the small fractions is not compensated by the increase of coarse fractions. D_T/D_m is smaller than 1 when only fine fractions are corrected, and close to 1 when all fractions are corrected.
- The correction of θ_{cr} by both Egiazaroff and Komar and Wang is not effective under condition 3. The effective Shields parameter is much higher than the critical Shields parameter in this case, due to the high flow velocity. The method of Day shows no differences in the correction between condition 1 and 3. The absolute values of the correction coefficients are not influenced by the hydraulic condition.
- The method of Ashida and Michiue gives the same results as the method of Egiazaroff in this sensitivity analysis.

7 Conclusions and recommendations

The main goals of this study were:

- to complete a data-set for sediment transport under waves in combination with currents in sheet-flow conditions
- to verify different existing transport models for uniform sediment using the experimental results
- to determine which parameters play an important role in modelling of transport rates of non-uniform sediments

For this purpose, oscillating water tunnel experiments were carried out. The complete data set consist of net transport rates for three different grain-sizes (D_{50}=0.13, 0.21 and 0.32 mm). The data-set is used to investigate the influence of the grain-diameter. Attention is paid to both time-dependent measurements and net transport rates.

In order to do numerical research on sand transport rates of non-uniform sediments, an existing computer program which contains three transport models, developed by Bailard, Ribberink and Dibajnia & Watanabe, was extended by the implementation of a size-fraction method. Because no experimental data are available yet, a sensitivity analysis was done in order to determine which parameters play an important role in predicting transport rates of non-uniform sediments.

7.1 Conclusions

7.1.1 Experimental research

Time-dependent measurements

- In the sheet-flow layer there is a significant difference in the slope of the concentration profile for the different grain diameters. For the coarse sand (0.32 mm) the concentration decreases very fast with increasing height; the fine sediment (0.13 mm) shows a much smaller gradient, while the results for the dune sand (0.21 mm) lies in between. For the different grain-sizes the sheet-flow layer has a thickness (using 1 vol% as boundary value) of:

  $\delta_s \cong 22$ mm D_{50}=0.13 mm
  $\delta_s \cong 11$ mm D_{50}=0.21 mm
  $\delta_s \cong 7$ mm D_{50}=0.32 mm

  The thickness of the sheet-flow layer is inversely proportional to D_{50}, according to:
  $\delta_s = N*1/D_{50}$ N= 2.2 - 2.9

- The time-averaged velocity profile shows a logarithmic distribution in the suspension layer. The velocity gradient is higher for the fine sand (0.13 mm) than for 0.21 and 0.32 mm sand, which is probably caused by a higher bed roughness due to a thicker sheet-flow layer.

- The value of the concentration decay parameter α for the suspended coarse sand lies around 2.05. This is close to the values found for the 0.21 mm sand (2.29) and the fine sand (1.68). The turbulence intensity for fine sand is reduced due to increasing sheet-flow layer thickness, compared to the dune-sand (0.21 mm). For the coarse sand (0.32 mm), the turbulence intensity is stronger, due to the thinner sheet-flow layer (see Section 5.2).

- The differences in concentration profiles between the dune sand (0.21 mm) and the coarse sand are less significant than between the dune sand and the fine sand. The sharp, little peaks in the suspension layer around flow reversal play a dominant role in case of the 0.13 mm sand, but they do not occur for the coarse sand. For the 0.21 mm sand they do occur at levels close to the bottom. These suspension ejection effects, together with time-lag effects play an important role in the transport process of fine sediment. Just before the end of a positive or negative part of the wave cycle lot of particles are brought into suspension. These particles have not enough to settle before the flow reversal. They remain suspended and in the successive half of the wave cycle they are transported in the opposite direction. These unsteady processes essentially influence the net transport rate.

- For all grain-sizes three different concentration layers can clearly be distinghuised: the pick-up layer, the upper sheet-flow layer (together they form the sheet-flow layer) and the suspension layer. The transition between pick-up layer and upper sheet-flow layer lies in all cases around 500 g/l. The thickness of these layers is strongly related to the grain-size.

- The ADV-measurements close to the bottom are overestimated, due to the high sediment concentration. It was therefore not useful to calculate the sediment fluxes.

Net transport rates

- Unsteady effects play an important role in the grain-size effects on net transport rates. The occurrence of unsteady effects depends on the combination of grain-size, flow velocity and wave period. This can be indicated by the parameter ω_c, which gives the relation between the fall time of a particle and the concerning part of the wave period. For $\omega_c > 1$ it is likely that many unsteady effects occur, for $\omega_c < 1$ not many unsteady effects occur.

- As long as the condition can be considered as quasi-steady, which means that the phase lag between flow velocity and sediment concentration is small, a smaller grain-size results in an increased transport rate. This increase is larger for higher oscillating velocities. When unsteady effects occur, the transport rate decreases for smaller grains. Without a steady current, this can result in large transports in the direction opposite to the propagation direction of the waves. A larger net current velocity diminishes the unsteady effects.

- An increase in wave period implies a smaller transport rate, also for high periods where unsteady effect are not expected to occur. The wave period has a large effect on unsteady effects: a shorter wave period gives the grains less time to settle, so they remain in suspension until the successive half wave cycle. This results in a decreased transport rate for small grains under short wave periods.

- In the quasi-steady situation, the net transport rate depends on the magnitude of the flow velocity. Both an increase in oscillating velocity û and net current velocity <u> result in more sediment transport. When unsteady effects occur, an increased net current velocity diminishes the transport in negative direction, thus increasing the net transport rate. An increased oscillating velocity gives stronger unsteady effects and therefore a smaller transport rate. The grains are brought into suspension to a higher level and it takes more time before they have settled.

7.1.2 Verification of transport models for uniform sediment

- The model of Bailard gives good results for the 0.32 mm sand; the transport rates are overpredicted around 1.5 times. For the 0.21 mm sand the overprediction has factor between 2 and 4, and for the fine sand this goes up to factor 20. A decrease in grain-size results for this model in a large increase of predicted transport rates. The most overpredicted results occur for tests where unsteady effects played an important role. For the range of grain-sizes which were studied here, this model gives unsatisfying results.

- The model of Ribberink gives no systematic over- or underprediction for the 0.13 and 0.21 mm grains, and a overprediction for the 0.32 mm sand with a factor around 1.5. Very large overpredictions occur only for conditions where unsteady effects are dominant. Grain-size influences are taken into account in a satisfying way. Overall, the model of Ribberink gives the best results.

- The model of Dibajnia and Watanabe gives good results for the fine sediment, but overpredicts for the 0.21 mm with a factor around 2, and for the 0.32 mm around 2.5. A decrease of the grain diameter results in this model in a decrease of the predicted transport rate. The delayed behaviour of the suspended sediment is taken into account in this model. This model is very useful in situations were unsteady effects play an important role.

7.1.3 Modelling of non-uniform sediment transport processes

The effect of using the size-fraction method on the predicted net transport rate is indicated by the parameter q_N/q_1. This parameter is the ratio of the predicted transport rate for a mixture characterised by N fractions, and the predicted transport rate for a mixture characterised by D_{50} only. Three parameters were studied which could influence this effect:

the mean diameter of the mixture D_{50}
the gradation of the mixture σ_g
the hydraulic condition, which is a combination of flow velocity and wave period

- For the model of Bailard the gradation of the mixture is the parameter which results in the largest differences between the predicted transport rate of a mixture characterised by N fractions, and the predicted transport rate of a mixture characterised by D_{50} only. For the model of Ribberink (without hiding and exposure correction) none of the three parameters has much influence q_N/q_1. For the model of Dibajnia and Watanabe the effects of the size-fraction method (thus q_N/q_1) *can* be influenced by a change in mean diameter of the mixture, but this depends on the imposed hydraulic condition. A larger gradation (σ_g) results in a larger $q_N/q1$.

- For the tests which were carried out in this sensitivity analysis, the ratio between the predicted total net transport rates as sum of several size-fractions and the predicted transport rate for uniform sediment characterised by D_{50} (the magnitude of parameter q_N/q_1) lies around:

Bailard:	0.9	for small grain-size variations (σ_g=1.4)
	2 - 2.5	for large grain-size variations (σ_g=2.5)
Ribberink:	1	without hiding and exposure correction
	0.95	correction factors according to Egiazaroff
	0.95-0.8	correction factors acc. to Komar & Wang
	0.9-0.75	correction factors according to Day
Dibajnia and Watanabe:	1.05, no unsteady effects; small grain-size variations	
	0.9, no unsteady effects, large grain-size variations	
	1.5, for fine sand under severe conditions	

  Using the size fraction method for the model of Ribberink *without* hiding and exposure correction results in very small changes in predicted transport rates compared to the traditional method where the sediment mixture was characterised by D_{50} only.

- The three models show a very different selective process:

Bailard:	mainly fine fractions are transported ($D_T/D_m<1$)
Ribberink:	the composition of the transported sediment is the same as for the bed material ($D_T/D_m=1$, $p_i=p_{T,i}$)
Dibajnia and Watanabe:	mainly the coarse fractions are transported ($D_T/D_m>1$)

  This agrees with the conclusions from the verifications of the models for uniform transport (Section 7.1.2).

- In the second part of the sensitivity analysis, in the model of Ribberink correction factors for hiding and exposure are applied. Four different methods were used to calculate these factors. For all methods, the transport rates of the smallest fractions are reduced, while for the coarser fractions the transport rate slightly increases. The effects are the weakest for Egiazaroff, while the method of Day gives the strongest influences. For a wider gradation the correction of the transport rates always leads to more changes in predicted transport rates (q_N/q_1) and transported diameter (D_T/D_m). The method of Ashida and Michiue gives the same results as the method of Egiazaroff.

- The correction of the critical value of the Shields parameter is not effective for conditions with a high flow velocity, which often occur under sheet-flow conditions. In that case the effective Shields parameter is much higher than the critical Shields parameter. Correcting this parameter does not make many differences. Correction of the effective Shields parameter, which is done in the method of Day, gives a reduced transport rate for fine fractions and an increased transport rate for coarse fractions for conditions outside and within the sheet-flow regime.

- Applying the correction on fine fractions only, results in a smaller mean diameter of the transported material. The transport rates for the coarsest fractions are not increased.

7.2 Recommendations for future research

- The method of measuring flow velocities close to the bottom must be improved. The desired measuring device should be able to measure velocities in conditions with very high sediment concentrations, without disturbing the flow. Accurate time-dependent fluxes can be determined then which could provide a better insight in the transport processes.

- The shape of the particles could play an important role in the transport process under sheet-flow conditions. Attention should also be paid to this sediment parameter, instead of the grain-size and gradation only.

- The results from this and previous analysis of the complete data set should be used to improve the existing transport models or to develop a new model. The best option seems to be a combination of the model of Dibajnia and Watanabe and the model of Ribberink. In conditions which can be considered as quasi-steady, the model of Ribberink is able to predict grain-size influences in a promising way. For conditions where unsteady effects become important, the model of Dibajnia and Watanabe can be used. The parameter ω_c could be used to indicate the occurrence of unsteady effects.

- The model of Ribberink, whether or not in combination with the size-fraction method, must be verified with measurements under conditions outside the sheet-flow regime. The occurrence of bed forms and ripples then, which leads to more suspended material, could reduce the usefulness of this model. The critical value of the Shields parameter plays a more important role for conditions outside the sheet-flow regime, and correction of this parameter by different methods will lead to more changes in the predicted transport rates.

- In order to find out which selecting processes are dominant and which model gives the best results, the calculated results of the different transport models after the implementation of the size-fraction method must be verified with measured transport rates of non-uniform sediment. Oscillating water tunnel experiments with various non-uniform sediments can provide the necessary data.

- The transport models in combination with the size-fraction method are tested in the sensitivity analysis for bed material which consists of one type of sand. Also other compositions of bed-material should be tested and verified, e.g. grain-size distributions which are not log-normal or a mixture of sands with different densities. The influence of the relation between D_{16}, D_{50} and D_{84}, which indicates the number of fine and coarse fractions, could also be important. More hydraulic conditions should be applied than only the three used in this sensitivity analysis, to investigate the effects of both wave and current velocity and the wave period influence.

- In the last years, an extensive experimental program is carried out in the LOWT, providing several data-sets on sediment transport. Field observations should be carried out in order to verify the reliability of these experiments as simulation of natural conditions. Time-dependent velocities and concentrations close to the sea bed must be measured under similar conditions as in the tunnel experiments. For example, measuring time-dependent concentrations can be used to determine whether unsteady effects really play an important role in cross-shore transport under natural conditions.

References

ABRAMOWITZ, M. AND STEGUN, I.A. (ED) (1964) *Handbook of mathematical functions; with formulas, graphs and mathematical tables.* USGPO, Washington

AL SALEM, A.A. (1993) *Sediment transport in oscillatory boundary layers under sheet-flow conditions.* Ph.D. Thesis, Delft University of Technology

BAILARD, J.A. (1981) *An energetics total load sediment transport model for a plane sloping beach.* J. Geophysic Res., Vol. 86, No. C11, pp. 10,938-10,954

BAGNOLD, R.A. (1954) *Mechanics of marine sedimentation.* The sea, Vol. 3, ed. M.N. Hill, Interscience, New York

DIBAJNIA, M. (1991) *Study on non-lineair effects in beach processes.* University of Tokyo, Japan

DIBAJNIA, M. AND WATANABE, W. (1992) *Sheet-flow under non-lineair waves and currents.* Proc. of the 23rd Int. Conf. on coastal Eng., Venice, pp. 2015-2028

EGIAZAROFF, J.V. (1965) *Calculation of non-uniform sediment concentrations.* Proc. ASCE, J. Hydr. Div, 91, HY4, July

EINSTEIN, H.A. (1950) *The bed load function for sediment transportation in open channel flows.* US Soil Conservation Service, Techn. Bulletin No. 1025, Sept.

HASSAN, W.N. (1996) *Grain-size influence on the sediment-transport process under waves and currents in the sheet-flow regime.* M.Sc Thesis, International Institue for Infrastructural, Hydraulic and Environmental Eng. (IHE), Delft, The Netherlands

JANSSEN, C.M. AND HOUT, G. VAN DER (1997) *Sediment transport for two sands with different grain diameters under combined wave-current sheet-flow conditions.* Data report Z2137, Part I, April 1997, DELFT HYDRAULICS, The Netherlands

JANSSEN, C.M., HASSAN, W.N., RIBBERINK, J.S. AND WAL, R.J. VAN DER (1996) *Net transport rates and transport mechanisms of fine sand in combined wave-current flow conditions.* Data report H2462, Part IV, DELFT HYDRAULICS, The Netherlands

JANSSEN, C.M. (1995) *Sand transport in oscillatory sheet-flow; a literature review.* Comm. on Hydr. and Geotechn. Eng., Delft University of Technology, The Netherlands

JONSSON, I.G., (1966) *Wave boundary layers and friction factors.* Proc. 10th Int. Conf. on Coast. Eng., pp. 127-148

KATOPODI, I. ET. AL.(1994) *Intra-wave sediment transport in an oscillatory flow superimposed on a mean current.* Data report H1684, Part III, August 1994, DELFT HYDRAULICS, The Netherlands

KOELEWIJN, H. (1994) *Sediment transport under sheet-flow conditions.* M.Sc. Thesis, Delft University of Technology

KOMAR, P.D. AND WANG, C. (1984) *Processes of selective grain transport and the formation of placers on beaches.* Journ. of Geology, Vol. 92, pp. 637-655

MADSEN, O.S. AND GRANT, W.D. (1976) *Sediment transport in the coastal environment.* Rep. 209, Ralph M. Parsons Lab., Massachusetts Inst. of Tech., Cambridge, Massachusetts

MILLER, R.L. AND BYRNE, R.J. (1966) *The angle of repose for a single grain on a fixed rough bed.* Sedimentology, Vol.6, pp. 303-314

RAMADAN, K.A.H. (1994) *Time-averaged sediment transport phenomena in combined wave-current flows.* Report H1889.11, Part I, January 1994, DELFT HYDRAULICS, The Netherlands

RIBBERINK, J.S. (1987) *Mathematical modelling of one-dimensional morphological changes in rivers with non-uniform sediment.* Comm. on Hydr. and Geotechn. Eng., Delft University of Technology

RIBBERINK, J.S. (1989) *The large oscillating water tunnel. Technical specifications and performances.* Report H840, Part I, DELFT HYDRAULICS, The Netherlands

RIBBERINK, J.S. (1994) *Time-averaged sediment transport phenomena in combined wave-current flows.* Delft Hydraulics report H1899.11, Part II

RIBBERINK, J.S. (1997) *Bed load for steady flows and unsteady oscillating flows.* Submitted for publication in Coastal Engineering

RIBBERINK, J.S. AND CHEN, Z. (1993) *Sediment transport of fine sand under asymmetric oscillatory flow.* Report H840, Part VII, January 1993, DELFT HYDRAULICS, The Netherlands

RIBBERINK, J.S. AND AL-SALEM, A.A. (1994) *Sediment transport in oscillatory boundary layers in cases of rippled bed and sheet-flow.* Journal of Geoph. Res., Vol. 99, No. C6, pp.12707-12727

RIBBERINK, J.S. AND AL SALEM, A.A. (1995) *Sheet-flow and suspension of sand in oscillatory boundary layers.* Coastal Engineering, Vol. 25, pp 205-225

RIJN, L.C. VAN, RIBBERINK, J.S., RENIERS, A. AND ZITMAN, T. (1995) *Yearly-averaged sand transport at the -20 and -8 m NAP depth contours of JARKUS profiles 14, 20, 76 and 103.* Report 1887, DELFT HYDRAULICS, The Netherlands

SLEATH, J.F.A. (1978) *Measurements of bed load in oscillatory flow.* J. Waterway, Port, Coastal and Ocean Eng., ASCE, Vol. 104, No. WW4, pp. 291-307

SWART, D.H. (1974) *Offshore sediment transport and equilibrium beach profiles.* Delft. Hydr. Lab. pub., No. 131, DELFT HYDRAULICS, The Netherlands

WAL, R.J. VAN DER (1996) *Grain-size influence on sediment transport in sheet-flow conditions for combined wave-current flow.* M.Sc. Thesis, Delft University of Technology

A Calculation methods and techniques

A.1 Splitting a mixture into size-fractions

This appendix derives a method to divide a sand mixture with a given D_α and D_β, into different size-fractions. D_α and D_β indicate that α or β % (by weight) of the mixture has a diameter smaller than D_α or D_β. The method is only briefly described, but more details are given by Ribberink [Ribberink, 1987, Appendix I].

In the computer program TRSP, a sand mixture is characterised by D_{50} and D_{90}. To divide this mixture into a number of size-fractions, more information about the grain-size distribution is needed. The sand used in the experiments in the LOWT in series E, H and I and J show that a log-normal distribution would be a good estimation of the real gradation. This log-normal probability distribution of diameter D is given by:

$$f(D) = \frac{1}{\sigma_y D\sqrt{2\pi}} \exp\left\{-\tfrac{1}{2}\left(\ln D - \mu_y\right)^2 \sigma_y^{\,2}\right\} \tag{A.1}$$

in which μ_y and σ_y are resp. the mean value and the standard deviation of $y = \ln D$ (y has a normal distribution). The parameters μ_y and σ_y are given by:

$$\mu_y = \ln(D_{50}) \tag{A.2}$$

$$\sigma_y = \frac{\ln D_\alpha / D_\beta}{-z_\alpha - z_\beta} \tag{A.3}$$

Equation A1 can be transformed to a standard normal distribution (which is a normal distribution with mean value = 0 and standard deviation = 1) of the stochastic variable z ($z=(y-\mu_y)/\sigma_y$), by:

$$f(z) = \frac{1}{\sqrt{2\pi}} \exp\left(-\tfrac{1}{2}z^2\right) \tag{A.4}$$

For a standard normal distribution, the following equation counts:

$$\int_{-\infty}^{z_\alpha} \frac{1}{\sqrt{2\pi}} \exp\left(-\tfrac{1}{2}z^2\right)^2 dz = \frac{\alpha}{100} \tag{A.5}$$

The values of z_α are tabled. It can be found that $z_{50}=0$ and $z_{90}=+1.28$ [Abramovitch & Stegun, 1964]. This gives for σ_y:

$$\sigma_y = \frac{\ln D_{50}/D_{90}}{-1.28} \tag{A.6}$$

In a log-normal grain-size distribution D_m is not equal to D_{50}, but is given by:

$$D_m = D_{50} \exp(0.5 \cdot \sigma_y^2) \tag{A.7}$$

Ribberink chose as upper and lower boundary for the grain-size distribution:

$$P(D>D_u)=P(D<D_l)=2.28\ \%$$

which is equal to: $z_u=2$ and $z_l=-2$

To divide the mixture into N size fractions, the region between these boundaries must divided into N equal parts Δz:

$$\Delta z = \frac{z_u - z_l}{N} = \frac{4}{N} \tag{A.8}$$

Every fraction i, where i is the number of the size-fraction which lies between 1 and N, has a z-value z, given by:

$$z_i = -2 + \frac{2(2i-1)}{N} \tag{A.9}$$

and an upper and lower boundary:

$$\begin{aligned} &upper: \quad z_{u,i} = z_i + \tfrac{1}{2}\Delta z \\ &lower: \quad z_{l,i} = z_i - \tfrac{1}{2}\Delta z \end{aligned} \tag{A.10}$$

The mean diameter of fraction i is given by its z-value, according to:

$$D_i = \exp\left(z_i * \sigma_y + \mu_y\right) \tag{A.11}$$

The probability p_i, which gives the share of fraction i in the total transport, is related to the boundaries:

$$p_i = 0.5\left\{erf\left(0.5\sqrt{2 * z_{u,i}}\right) - erf\left(0.5\sqrt{2 * z_{l,i}}\right)\right\} \tag{A.12}$$

in which erf implies a standard error function, which is also tabled [Abramowitz & Stegun, 1964].

Because of the choice for the boundaries for the grain-size distribution was $P(D>D_u)=P(D<D_l)=0.0228$, the sum of all probabilities is:

$$\sum_{i=1}^{N} p_i = 0.9545 \tag{A.13}$$

Therefore, for each fraction the calculated probability must be divided by a factor 0.9545.

A log-normal grain-size distribution (D_{50} = 0.21 mm, σ_g = 1.4)divided into 8 equal parts of Δz is shown in figure A1.

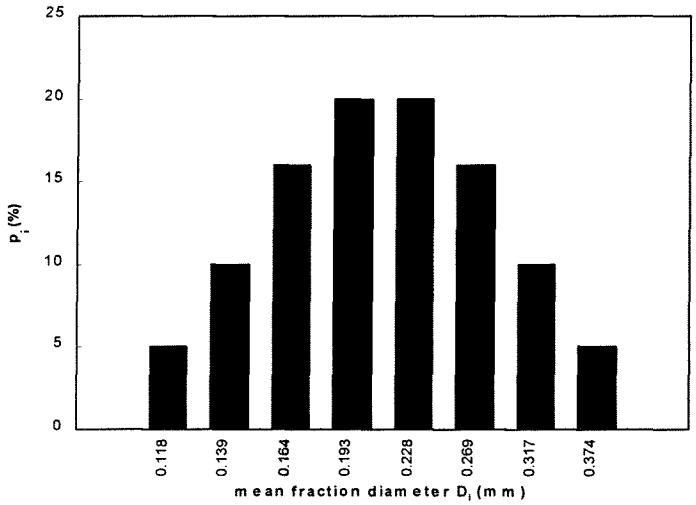

Figure A1 Log-normal grain-size distribution divided in 8 equal parts

A.2 Mass conservation technique

To calculate the net transport rate, a mass conservation technique was used.
At the bottom of both cylindrical risers and in the recalculation pipe sand traps are constructed. After a tunnel run the trapped sand, which is eroded from the test section, can be removed and weighted.

Because the amount of trapped sand is measured at both ends of the test section, the sediment continuity equation can be integrated from the left-hand-side and also from the right-hand-side. This results in two estimations for the transport rate at the measurement location, under the condition that the porosity of the sand bed in the test section is known. The porosity of the sand bed can be determined from the weights of the sand collected in the traps (volume without pores) and the volume change (including pores) in the test section.

The following equations are used in the analysis:

Measured porosity:

$$1-\varepsilon_0 = \frac{G}{\rho_s}\frac{1}{\Delta V_{ip}} \tag{A.14}$$

Transport rate at the measurement location:

$$\begin{aligned} &\textit{left trap estimate:}\quad q_{s,l} = \frac{\Delta V_{l,ip}(1-\varepsilon_0)}{\Delta t W} - \frac{G_l}{\rho_s}\frac{1}{\Delta t W} \\ &\textit{right trap estimate:}\quad q_{s,r} = \frac{\Delta V_{r,ip}(1-\varepsilon_0)}{\Delta t W} + \frac{G_r}{\rho_s}\frac{1}{\Delta t W} \end{aligned} \tag{A.15}$$

in which:

$\Delta V_{l,ip}$ = total eroded volume including pores, from the part of the tunnel test section to the left of the measurement location during one test [m^3]
$\Delta V_{r,ip}$ = total eroded volume including pores, from the part of the tunnel test section to the left of the measurement location during one test [m^3]
ΔV_{ip} = $\Delta V_{l,ip}+\Delta V_{r,ip}$ = total eroded volume, including pores, from the tunnel test section during one test [m^3]
G = $G_l + G_r$ = total (dry) weight of the sand collected in both traps [kg]
G_l = total (dry) weight of the sand collected in the left trap [kg]
G_r = total (dry) weight of the sand collected in the right traps (piston and recirculating system) [kg]
ρ_s = density of sand [kg/m^3]
ε_0 = porosity of sand bed [-]
W = width of the tunnel test section [m]
q_s = net transport rate without pores per unit width and time for one test at the measurement location [m^2/s]
Δt = test duration [s]

Both equations should give the same answer for the measured transport rate for a certain test as long as the measured porosity is substituted. However, the porosity found during the test varied between 0.54 and 0.67. This measured variation may be due to errors in the bed level measurement (see app. B4) The average value, 0.38 for series J and 0.37 for the series I, is used to calculated the transport rates. Previous experiments with dune sand like used in series J showed also a porosity of 0.38 [Ribberink and Al Salem, 1992], and in series H with 0.13 mm sand the average porosity was 0.39 [Janssen et al., 1996].

In the plots in Appendix B2 and C2, the results from the equations are given. The left part is the result from the left trap estimate; the right part is the result form the right trap estimate. At x = 2 both equations should give the same results.

B Experimental results series J

B.1 Results per test

test	duration	condition			sand traps (weight under water)				volume change	loss of sand	calc. porosity	transport rate at x=2 m	
	(sec)	period (sec)	<U> (m/s)	û (m/s)	piston (kg)	open leg (kg)	recirc. (kg)	total (10^{-3} m3)	total (10^{-3} m3) (without pores)	(10^{-3} m3)		q_l (10^{-6} m/s)	q_r (10^{-6} m/s)
J1-t1	910	7.2	0.236	1.04	2.0	12.9	6.8	13.15	12.61	-0.54	0.38	37.9	39.9
J1-t2	777	7.2	0.247	1.12	2.5	14.4	5.7	13.70	14.39	0.70	0.31	48.8	45.8
J1-t3	731	7.2	0.246	1.07	0.9	11.9	6.7	11.82	11.19	-0.63	0.38	41.3	44.2
J1-t4	1212	7.2	0.246	1.07	3.1	16	7.3	16.00	15.76	-0.24	0.38	35.3	37.0
J2-t1	611	7.2	0.252	1.29	4.3	11.4	7.4	14.00	21.64	7.64	0.39	95.5	53.9
J2-t2	598	7.2	0.245	1.26	4.1	10.8	7.1	13.33	15.63	2.30	0.42	67.3	54.5
J2-t3	590	7.2	0.249	1.29	5.1	11.7	6.5	14.12	16.39	2.27	0.40	72.1	59.3
J2-t4	597	7.2	0.250	1.29	4.0	10.5	6.8	12.91	15.24	2.33	0.38	70.6	57.6
J3-t1	1934	7.2	0.414	0.46	0.1	8.2	3.5	7.15	6.54	-0.61	0.41	9.4	10.4
J3-t2	1835	7.2	0.419	0.46	0.0	5.6	2.4	4.85	4.34	-0.51	0.33	7.0	7.9
J3-t3	2550	7.2	0.412	0.46	0.0	6.3	3.1	5.70	5.32	-0.38	0.34	6.6	7.1
J3-t4	2190	7.2	0.413	0.47	0.0	5.6	2.9	5.15	5.06	-0.09	0.37	7.3	7.4
J4-t1	1290	7.2	0.415	0.72	0.0	10.0	8.9	11.45	11.07	-0.39	0.35	27.9	29.0
J4-t2	1692	7.2	0.408	0.65	0.0	9.2	7.6	10.18	10.83	0.65	0.39	21.2	19.9
J4-t3	1454	7.2	0.416	0.65	0.0	8.3	7.1	9.33	9.41	0.08	0.36	21.2	21.0
J4-t4	1377	7.2	0.404	0.65	0.0	7.5	6.1	8.24	8.57	0.32	0.41	20.4	19.7
J5-t1	958	4.0	0.252	1.04	0.1	4.7	10.1	9.03	10.96	1.93	0.33	29.0	22.3
J5-t2	946	4.0	0.241	1.05	0.0	5.1	10.4	9.39	10.13	0.73	0.42	26.0	23.4
J5-t3	1241	4.0	0.240	1.04	0.0	6.6	13.1	11.94	13.20	1.26	0.37	25.9	22.8
J5-t4	932	4.0	0.240	1.04	0.0	5.3	11.0	9.88	10.85	0.97	0.37	26.9	23.4
J6-t1	1091	12.0	0.221	1.09	1.2	9.2	4.4	8.97	11.76	2.79	0.47	44.9	36.6
J6-t2	996	12.0	0.231	1.09	1.8	10.1	4.6	10.00	11.19	1.19	0.46	43.3	39.3
J6-t3	1200	12.0	0.229	1.09	1.8	12.9	6.0	12.55	13.15	0.61	0.37	43.4	41.7
J6-t4	978	12.0	0.228	1.08	1.0	10.3	4.9	9.82	10.61	0.79	-----	43.4	40.7

Table A1 Results per test series J

B.2 Net transport rates along the tunnel

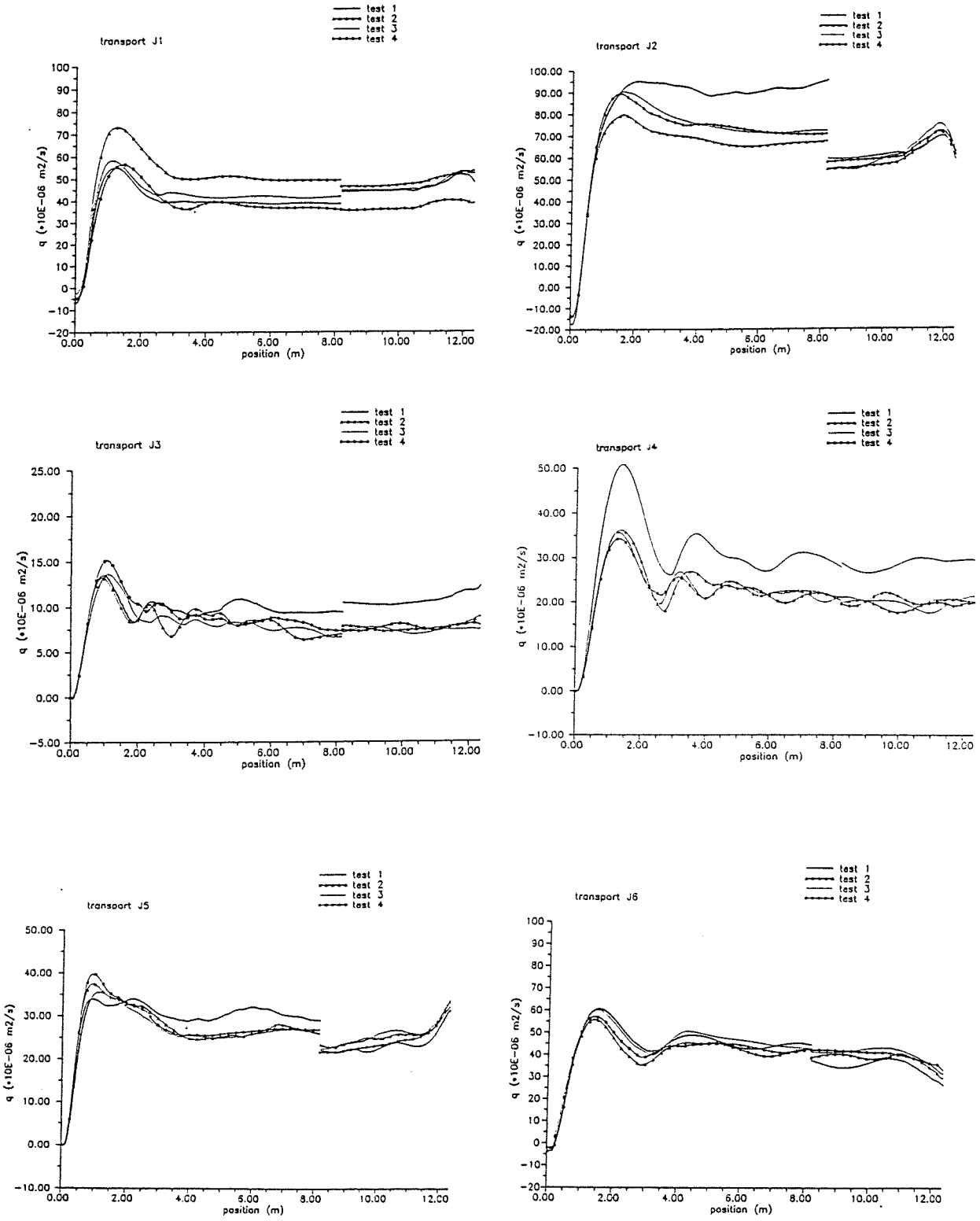

Figure A2 Net transport rates along the tunnel

B.3 Calculated correction volume

test	z_b x=12.34 m (mm)	z_e x=12.34 m (mm)	Correction volume incl. pores ($10^{-3}m^3$)	Correction volume excl. pores ($10^{-3}m^3$)	loss of sand ($10^{-3}m^3$)	Corr. vol/ loss of sand (%)
J1-t1	-20.57	10.03	1.57	0.97	-0.54	-178.7
J1-t2	-17.45	-15.88	0.071	0.04	0.69	6.3
J1-t3	-19.53	-19.66	-0.006	-0.00	-0.63	0.6
J1-t4	-4.56	-14.06	-0.47	-0.29	-0.24	119.4
J2-t1	-5.08	14.78	1.12	0.70	7.64	9.1
J2-t2	-17.84	20.38	2.09	1.30	2.30	56.2
J2-t3	-10.29	19.01	1.65	1.02	2.27	45.1
J2-t4	-13.41	10.68	1.28	0.80	2.33	34.1
J3-t1	-3.12	-13.09	-0.49	-0.31	-0.61	50.4
J3-t2	-12.76	-12.70	0.003	0.00	-0.51	-0.3
J3-t3	-11.26	-17.58	-0.29	-0.18	-0.38	47.9
J3-t4	-18.10	-10.81	0.34	0.21	-0.09	-241.1
J4-t1	-15.63	-12.05	0.17	0.10	-0.38	-27.0
J4-t2	-16.08	-15.30	0.04	0.02	0.65	3.4
J4-t3	-14.52	-14.00	0.02	0.01	0.08	17.9
J4-t4	-15.42	-24.55	-0.39	-0.24	0.33	-75.0
J5-t1	-24.51	-32.69	-0.32	-0.20	1.93	-10.1
J5-t2	-25.33	-29.56	-0.17	-0.10	0.74	-14.0
J5-t3	-19.86	-32.94	-0.52	-0.32	1.26	-25.7
J5-t4	-8.34	-25.39	-0.77	-0.47	0.97	-49.0
J6-t1	-11.59	4.10	0.82	0.51	2.79	18.1
J6-t2	-8.14	-8.72	-0.03	-0.02	1.19	-1.5
J6-t3	-14.84	-14.26	0.03	0.02	0.60	2.7
J6-t4	-12.04	5.34	0.91	0.56	0.80	70.1

Table A2 Calculated correction volumes, series J

Notes:

- Column 2 and 3 give the bed level height at the utmost end of the tunnel (z=12.34 m) before (z_b) and after (z_e) the tunnel run.
- The correction volume is an estimation of the volume missed by the BLSS. It depends on the differences between z_e and z_b.
- The loss of sand in column 6 comes from Table A1. This loss of sand is equal to the differences between the volume of sand transported out of the tunnel and the amount of sand found in the sand traps.
- In the last column the correction volume is divided by the loss of sand, to indicate the order of magnitude of the correction volume.

B.4 Accuracy of BLSS results

Measurements

At every test, the bed level was measured before and after the tunnel run, using the BLSS. For one bed level sounding two measurements were done; one starting at the left end of the tunnel and moving the instrument to the right, and one measurement moving back to the beginning point. Only one of these is needed to calculate the net transport rates, but comparing two measurements of exactly the same bed can give an indication of the reliability of the results.

A very small over estimation of the bed level height can give a relatively big positive or negative loss of sand; for example: 0.5 mm difference in height over the whole tunnel means (0.5/100)*3*123.4 =1.85 l loss of sand.

Calculated differences

For series J, the differences between two soundings of the same bed are given in Table A3.

test	difference in volume begin tests (10^{-3} m^{3})	difference in volume end tests (10^{-3} m^{3})	loss of sand during test (10^{-3} m^{3})
J1	-0.127	0.390	7.64
J1	-0.405	-2.510	2.30
J1	-0.259	1.630	2.27
J1	-0.060	0.961	2.33
J2	-0.076	------	-0.54
J2	0.003	0.973	0.69
J2	-0.098	0.938	-0.63
J2	-0.089	0.122	-0.24
J3	-0.388	-0.056	-0.61
J3	-0.247	0.622	-0.51
J3	0.179	0.170	-0.38
J3	0.064	1.820	-0.09
J4	0.090	0.536	-0.38
J4	0.314	0.888	0.65
J4	0.092	0.151	0.08
J4	0.171	0.937	0.33
J5	-0.077	0.550	1.93
J5	0.592	2.440	0.74
J5	0.114	0.835	1.26
J5	0.391	1.690	0.97
J6	0.436	1.590	2.79
J6	0.198	1.280	1.19
J6	0.198	0.807	0.60
J6	0.079	1.870	0.80

Table A3 Measured inaccuracies in bed level soundings

The begin tests in Table A3 is a bed level sounding of the sand bed *before* a tunnel run. An end tests in Table A3 is a bed level sounding of the sand bed *after* a tunnel run. For test J2-t1 the difference in the begin test could not be calculated, because these bed level soundings were not recorded during this test. Test J2 was carried out first. The difference is calculated by subtracting the second sounding from the first one. A positive amount of sand means that the first bed level was higher than the second one; a negative difference means that the second bed level is higher. The table shows that the differences are between -2.51 and 2.44 l (around 0.8 mm). The average value of these measured differences is 0.42 l, with a standard deviation σ = 0.79 l. It is remarkable that the averaged value is not zero. It can imply a systematic error. To indicate the influence of these inaccuracies, in the last column the losses of sand are given for each test. In many cases the calculated differences have the same order of magnitude as the sand losses, which indicates the results are not very reliable.
In Figure A3 the values given in Table A3 are plotted in a successive order.

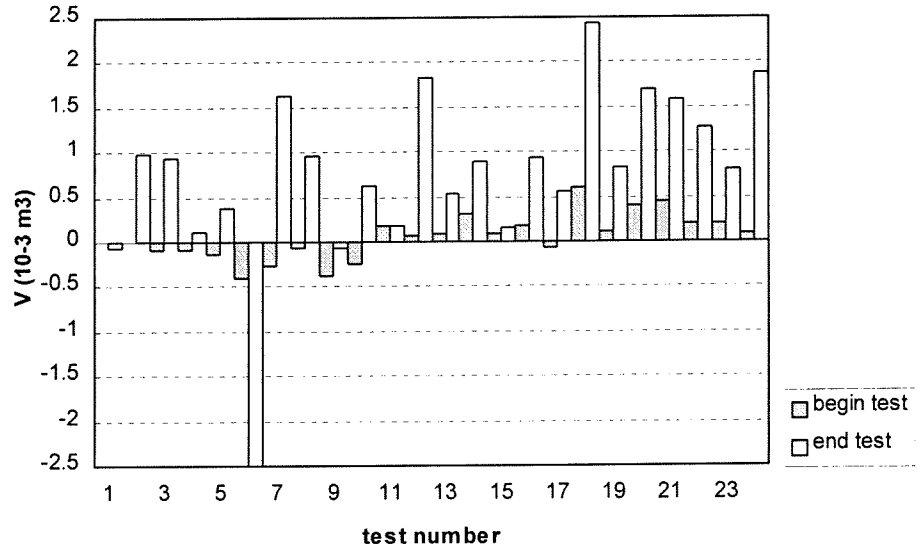

Figure A3 Inaccuracies in bed level soundings during series J

From this figure can be concluded:
- The error occurring after a test is remarkably higher than before a test.
- The errors are larger in magnitude for tests which are carried out later in time.

Before carrying out the measurements, the profilers were set on a fixed plate at the left end of the tunnel, as a reference level. Afterwards, controlling of the zero setting of the profilers sometimes showed a little change, varying from 0 to 15 mV for one or more sticks. The calibration factor for this instrument is 0.04 m/V; 1 mm corresponds with 25 mV. When two profilers gave more than 15 mV change, new measurements were carried out. During the experiments of series J, the change in zero level was small at the start of this series, but later on in this series, for some tests the change in zero-setting was larger, and sometimes the bed level sounding was done again because of these changes.

Figure A4 shows the two bed level soundings pj1-t2e and pj1-t2f, (two data-files resulting from the bed level sounding of the sand bed after test 2 for condition J1) which are carried out after test j1-t2. For all three profiles the differences are given. This figure shows that:
- When comparing the two soundings, errors occur only in pj1-t2f
- Errors occur only for all three profilers at the same point along the tunnel.

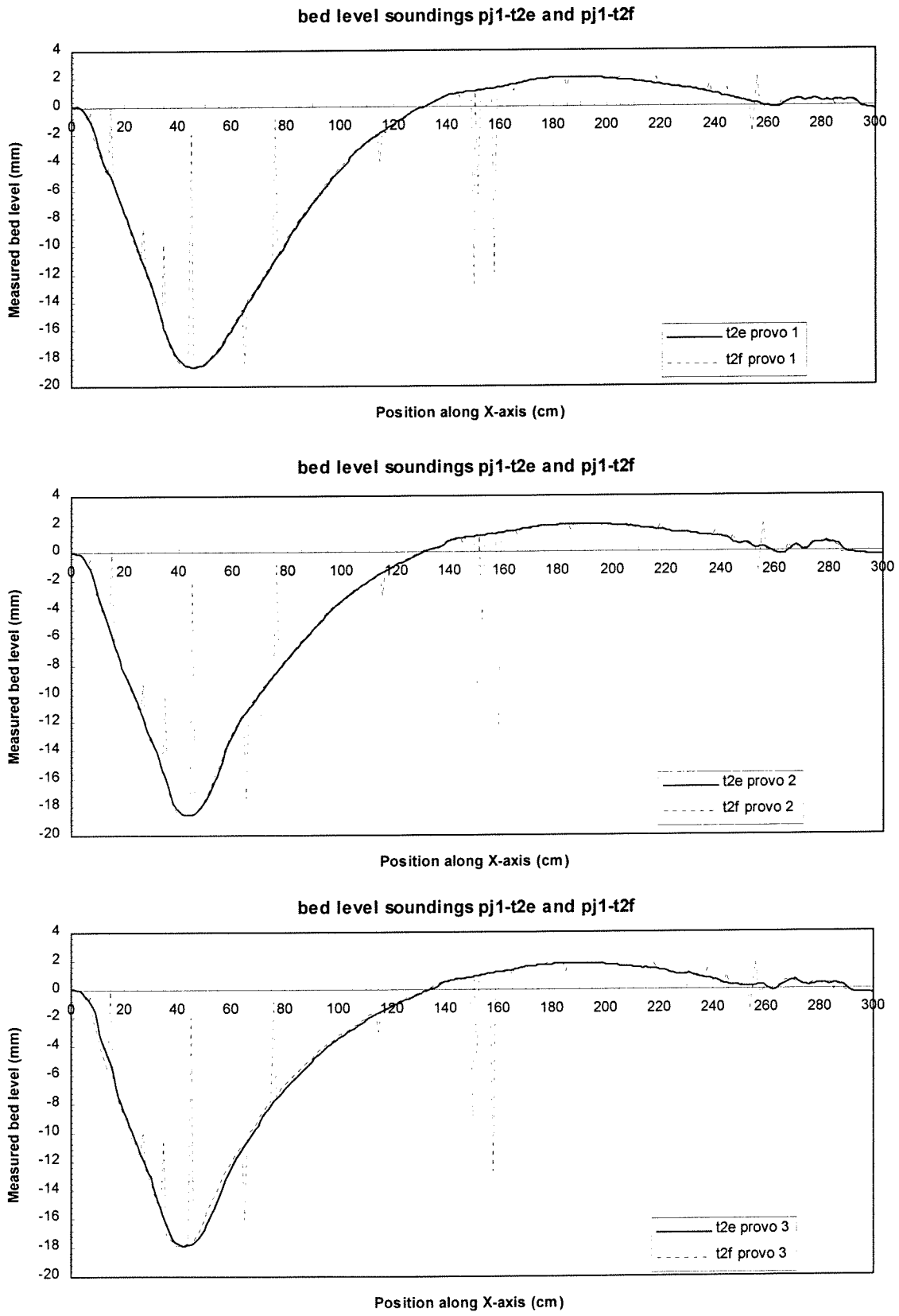

Figure A4 Differences between bed level soundings pj1-t2e and pj1-t2f for the first 3 m in the tunnel

Causes of inaccuracies

In January, after the experiments, the BLSS was inspected by the instrumentation division of the laboratory. They found out that the profilers were somewhat porous. When they were put into the water for a while, a very little amount of water could penetrate in the profilers which resulted in changes in the measured values and a change in the zero-setting. This explains that the errors occurred in the second bed-level sounding only, because by then the profilers where in the water for some time, so water could penetrate in them which resulted in a change in the zero-setting and differences between two bed level soundings of the same bed. It can be assumed that during the experimental series the instrument became more and more inaccurate, because perhaps the process of penetration of water in the profilers took place quicker. This explains why the differences between two soundings became larger, and also the change in zero-setting increased for tests which were carried out later in time.

Before a test, the sand bed is almost horizontal, because it just has been flattened. After a test there is a big erosion hole at the left end of the tunnel and some bed form might occur. Possibly the profilers can not follow these changes while moving along the tunnel, which might be caused by the speed of the measurement carriage. This problem could be solved by moving the carriage much slower over the bed.

Recommendations

Some recommendations to improve the accuracy of the measurements:

- Always make two measurements of a sand bed, it will be possible to make a comparison and get at least an indication about the accuracy.
- The carriage must be moved slowly through the tunnel. Moving too fast can cause errors in measuring only a few points, but this can make a lot of difference.
- If it is possible, a fixed plate at the right end should be made, comparable to the one at the left. The zero-setting can be fixed then. There would also be no uncertainty whether the changes in the last tunnel section are measured or not.

B.5 Flow velocity distribution over cross-section

The transport in the middle of the tunnel can be calculated using the following formula:

$$\langle q_s \rangle_{\max} = \frac{\langle u^3 \rangle_{\max}}{\overline{\langle u^3 \rangle}} \cdot \overline{\langle q_{s,meas} \rangle} = C \cdot \overline{\langle q_{s,meas} \rangle} \qquad \text{(B.1)}$$

in which:

$\overline{\ldots}$	= averaged over cross-section
$\langle \ldots \rangle$	= averaged over wave-cycle
$\langle q_s \rangle_{max}$	= calculated transport in the middle of the cross-section
$\langle u^3 \rangle_{max}$	= third order velocity moment in the middle of the cross-section
$\overline{\langle u^3 \rangle}$	= third order velocity moment averaged over the cross-section
$\overline{\langle q_{s,meas} \rangle}$	= measured transport
C	= correction factor

In case of sinusoidal waves in combination with a net current, the third order velocity moment is calculated by:

$$\langle u^3 \rangle_{max} = \langle u \rangle_{max}^{\ 3} + 3\langle u \rangle_{max} \cdot u_{rms}^{\ 2} \qquad \text{(B.2)}$$

in which: <u>= time averaged velocity
u_{rms} = root mean square of the oscillating velocity

This is averaged over the cross-section:

$$\overline{\langle u^3 \rangle} = \overline{\langle u \rangle^3} + 3\overline{\langle u \rangle \cdot u_{rms}^{\ 2}} \qquad \text{(B.3)}$$

Because the oscillatory component is more or less constant over the width of the cross-section this can be approximated by:

$$\overline{\langle u^3 \rangle} = \overline{\langle u \rangle^3} + 3\overline{u_0^{\ 3}} \cdot u_{rms}^{\ 2} \qquad \text{(B.4)}$$

Koelewijn found that the distribution of time averaged velocity <u> over the cross-section can be approximated by (see Figure 4.2):

$$\begin{aligned} \langle u \rangle &= \left[0.147 \cdot \ln(0.15 + x) + 1.19\right]\langle u \rangle_{max} && -0.15 < y < -0.10 \\ \langle u \rangle &= \left[1 - 16.136 \cdot y^2\right]\langle u \rangle_{max} && -0.10 < y < 0.10 \\ \langle u \rangle &= \left[0.147 \cdot \ln(0.15 - x) + 1.19\right]\langle u \rangle_{max} && 0.10 < y < 0.15 \end{aligned} \qquad \text{(B.5)}$$

She found that this formula can be written as:

$$\overline{\langle u^3 \rangle_{max}} = C_1 \langle u \rangle_{max}^{\ 3} + 3C_2 \langle u \rangle_{max} \cdot u_{rms}^{\ 2} \qquad \text{(B.6)}$$

with: $C_1 = 0.698$
$C_2 = 0.865$

Using this last formula for the results of series J gives the following results for the correction factor C from eq. B1: (B.7)

test	$\langle u \rangle_{max}$ (m/s)	$\hat{u}$ (m/s)	u_{rms} (m/s)	$\langle u^3 \rangle_{max}$ (m^3/s^3)	$\overline{\langle u^3 \rangle}_{log}$ (m^3/s^3)	C -
J1	0.24	1.06	0.75	0.425	0.366	1.16
J2	0.25	1.28	0.91	0.625	0.538	1.16
J3	0.41	0.46	0.33	0.205	0.165	1.24
J4	0.41	0.65	0.46	0.328	0.272	1.20
J5	0.24	1.04	0.74	0.406	0.349	1.16
J6	0.23	1.09	0.77	0.415	0.357	1.16

Table A4 Correction factor C

A more accurate way to calculate the correction factor, is to use the formulas which give the logarithmic velocity distribution (see Figure 4.2) in a spreadsheet in order to calculate $\langle u \rangle$ at every half centimetre along the cross-section. The average of this value is $\overline{\langle u \rangle}$, which can be used to get $\overline{\langle u^3_{avg} \rangle}$. An even better way is to calculate u^3 at every half-centimetre, of which the average is $\overline{\langle u^3 \rangle}$. The results for the new correction factor C_{new} are given in Table A5.

test	$\langle u \rangle_{max}$ (m/s)	$\overline{\langle u \rangle}$ (m/s)	$\overline{\langle u^3 \rangle}$ (m^3/s^3)	C_{new} (-)	$\overline{\langle u^3_{avg} \rangle}$ (m^3/s^3)
J1	0.244	0.207	0.359	1.18	0.358
J2	0.248	0.210	0.533	1.17	0.531
J3	0.415	0.352	0.164	1.25	0.159
J4	0.409	0.347	0.267	1.23	0.262
J5	0.240	0.203	0.344	1.18	0.342
J6	0.227	0.193	0.351	1.18	0.350

$\overline{\langle u \rangle}$ = time averaged horizontal velocity averaged over cross-section
$\overline{\langle u^3 \rangle}$ = third order velocity moment calculated by averaging $\langle u^3 \rangle$ over cross-section
$\overline{\langle u^3_{avg} \rangle}$ = third order velocity moment calculated with $\overline{\langle u \rangle}$

Table A5 Accurate correction factor, using spread-sheet

There are some differences with the results of the simplified formula. The values $\overline{\langle u^3_{avg} \rangle}$ and $\overline{\langle u^3 \rangle}$ show only very small differences. The correction factor C_n from Table A5 is used to calculate the corrected transport rates, which are used in comparing the results with previous experiments and models.

Using this method means that the assumption is made that there is a direct relationship between the net transport rate $\langle q_s \rangle$ and the third order velocity moment u^3. However, the values of C_n are quite similar to what Van der Wal (1996) found in his study, when he used the model of Dibajnia and Watanabe instead of u^3 to calculate the correction for the velocity distribution over the cross-section.

C Experimental results series I, part 1

C.1 Results per test

Table A6 Results per test series I

test	duration	condition			sand traps (weight under water)				volume change	loss of sand	calc. porosity	transport rate at x=2 m	
	(sec)	period (sec)	<U> (m/s)	û (m/s)	piston (kg)	open leg (kg)	recirc. (kg)	total (10^{-3} m3)	total (10^{-3} m3) (without pores)	(10^{-3} m3)		q_l (10^{-6} m/s)	q_r (10^{-6} m/s)
I1-t1	576	7.2	0.248	1.47	6.6	10.5	2.5	11.88	12.80	0.92	0.344	81.9	76.5
I1-t2	643	7.2	0.264	1.48	8.2	10.4	2.6	12.85	13.12	0.27	0.413	78.6	77.2
I1-t3	475	7.2	0.258	1.48	5.9	8.9	2.2	10.30	10.36	0.06	0.402	84.0	83.6
I1-t4	490	7.2	0.265	1.46	4.9	9.9	2.1	10.24	11.37	1.13	0.428	81.7	74.1
I2-t1	470	7.2	0.258	1.72	19.0	12.8	4.6	22.06	24.13	2.07	0.397	141.8	127.2
I2-t2	445	7.2	---	---	11.8	14.1	4.5	18.42	21.11	2.69	0.411	146.1	126.2
I2-t3	461	7.2	0.262	1.68	12.7	14.5	5.5	19.81	21.37	1.56	0.425	129.5	118.3
I2-t4	390	7.2	0.242	1.70	9.3	12.8	4.3	16.00	18.52	2.52	0.389	139.7	118.1
I3-t1	878	7.2	0.417	0.74	0.0	6.3	2.8	5.52	4.46	-1.06	0.289	17.2	21.2
I3-t2	769	7.2	0.422	0.65	0.0	4.5	2.0	3.91	3.70	-0.24	0.292	18.2	19.0
I3-t3	886	7.2	0.424	0.67	0.0	6.5	2.6	5.52	4.72	-0.80	0.351	20.0	23.0
I3-t4	814	7.2	0.410	0.64	0.0	5.7	2.6	5.03	5.07	0.04	---	17.4	17.4
I4-t1	756	7.2	0.422	0.92	0.0	12.7	6.6	11.70	10.45	-1.25	0.356	42.1	49.6
I4-t2	742	7.2	0.415	0.92	0.0	10.2	6.0	9.82	10.07	0.24	0.385	47.9	46.8
I4-t3	771	7.2	0.416	0.91	0.0	11.2	7.0	11.03	10.82	-0.21	0.385	42.4	43.3
I4-t4	812	7.2	0.415	0.92	0.0	10.2	6.1	9.88	9.21	-0.67	0.255	41.0	43.1
I5-t1	320	7.2	0.438	1.49	5.2	17.2	10.7	20.06	19.03	-1.03	0.391	167.0	177.7
I5-t2	360	7.2	0.471	1.52	6.5	17.8	10.2	20.91	21.41	0.50	0.384	164.2	159.5
I5-t3	360	7.2	0.457	1.51	7.2	18.1	11.0	22.00	21.94	-0.06	0.381	165.9	166.4
I5-t4	328	7.2	0.427	1.48	6.5	17.4	10.1	20.61	21.20	0.59	0.392	163.3	157.3

C.2 Net transport rates along the tunnel

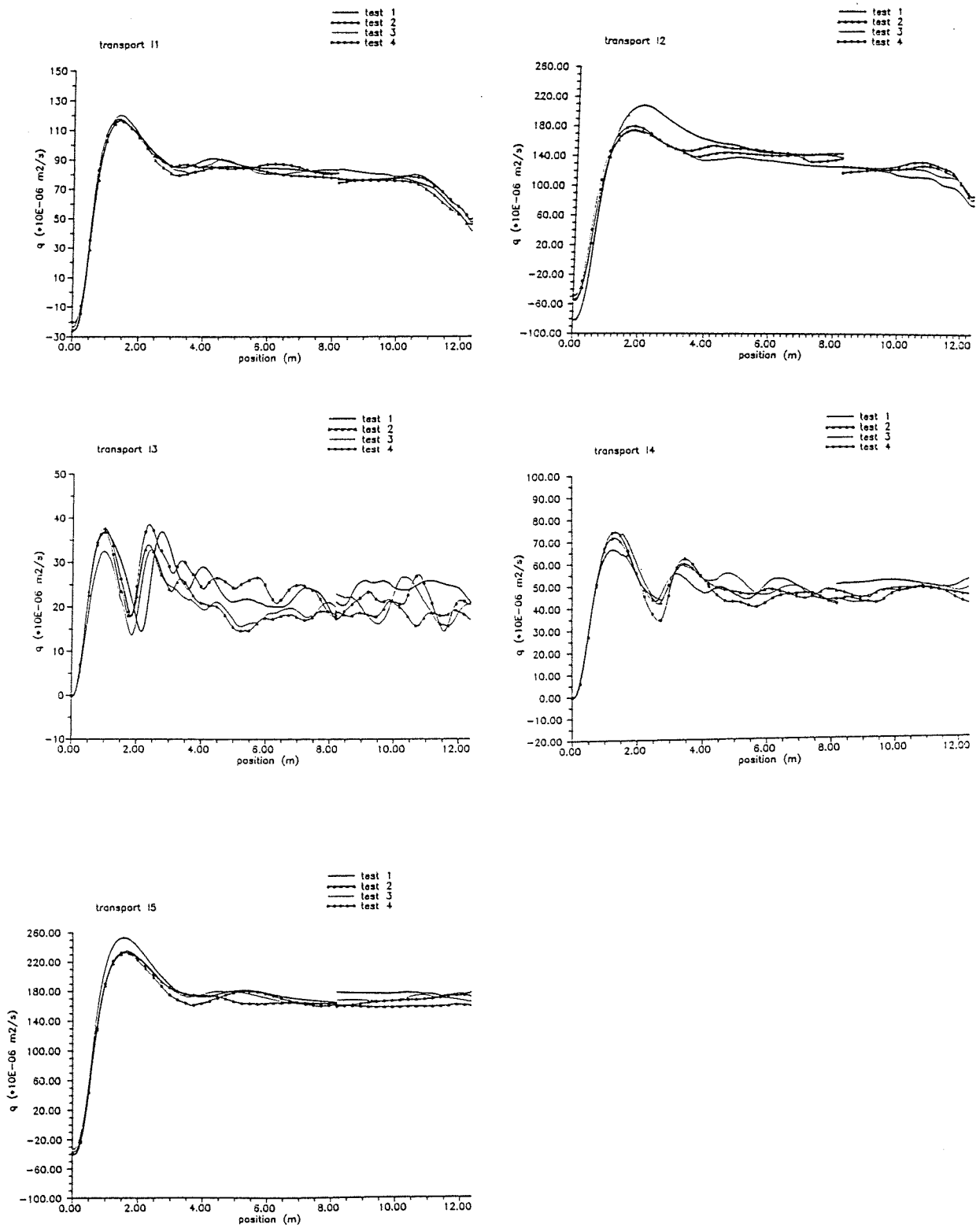

Figure A5 Net transport rates along the tunnel, series I

C.3 Calculated correction volumes

test	z_b x=12.34 m (mm)	z_e x=12.34 m (mm)	Correction volume incl. pores ($10^{-3}m^3$)	Correction volume excl. pores ($10^{-3}m^3$)	loss of sand ($10^{-3}m^3$)	Corr. vol/ loss of sand (%)
I1-t1	1.69	-1.95	-0.20	-0.12	0.92	-13.0
I1-t2	9.05	16.60	0.46	0.28	0.27	105.8
I1-t3	13.61	3.45	-0.60	-0.36	0.06	-606.9
I1-t4	-3.19	-18.03	-0.72	-0.44	1.13	-38.8
I2-t1	-4.62	-7.29	-0.14	-0.08	2.07	-4.0
I2-t2	-1.76	-31.97	-1.36	-0.83	2.69	-30.8
I2-t3	3.19	-10.48	-0.71	-0.43	1.56	-27.8
I2-t4	7.36	-24.22	-1.56	-0.95	2.52	-37.8
I3-t1	-12.50	-2.93	0.48	0.29	-1.06	-27.5
I3-t2	-4.30	-3.45	0.04	0.03	-0.24	-11.2
I3-t3	-8.92	-8.33	0.03	0.02	-0.80	-2.2
I3-t4	-8.27	-14.32	-0.29	-0.18	0.04	-442.2
I4-t1	5.47	-13.48	-0.98	-0.60	-1.25	48.0
I4-t2	-16.61	-6.58	0.48	0.29	0.24	119.3
I4-t3	-5.92	-14.91	-0.44	-0.27	-0.21	124.8
I4-t4	-15.37	-10.32	0.24	0.15	-0.67	-21.7
I5-t1	-0.52	-20.44	-0.96	-0.59	-1.03	57.2
I5-t2	-11.13	-4.49	0.33	0.20	0.50	40.3
I5-t3	-8.85	-12.70	-0.19	-0.11	-0.06	187.6
I5-t4	-13.41	0.78	0.72	0.44	0.59	74.6

Table A7 Calculated correction volumes series I

For notes see Table A2.

D Experimental results series I, part 2

D.1 Results LDFM

Test	height (mm)	low (s)	high (s)	⟨u⟩ (m/s)	û (m/s)	Number of waves for ensemble-averaging	remarks
I1-L11	95	408.4	552.4	0.233	1.48	20	
I1-L12	64	638.8	782.8	0.216	1.51	20	
I1-L21	48	194.4	338.4	0.191	1.54	20	
I1-L22	24	543.8	687.8	0.170	1.55	20	some peaks in laser signal
I1-L23	18	730.8	795.6	0.152	1.52	20	some peaks in laser signal
I1-L31	36	544.8	688.8	0.170	1.56	20	
I1-L32	25	717.5	861.5	0.162	1.55	20	
I1-L33	18	879.4	987.4	0.133	1.47	15	
I1-L41	101	432.1	576.1	0.249	1.47	20	
I1-L42	70	597.7	705.7	0.222	1.49	20	
I1-L43	47	734.5	878.5	0.194	1.55	20	

Table A8 Results LDFM

Notes:

- See also data-report page 11 and Table 3.3. (Janssen and Van der Hout (1997))
- 'Low' refers to the starting point (in seconds) of the measurement; 'high' refers to the end point of the measurement. The time in between corresponds with the number of waves used for ensemble averaging. The tunnel run started at t = 0 s.
- A limited number of waves is used for ensemble averaging, so more than one average value could be calculated from one tunnel run. For example, during tunnel run I1-L1, two times 20 waves were used for ensemble-averaging. This resulted in measurement I1-L11 and I1-L12.

D.2 Results ADV

Test	height (mm)	low (s)	high (s)	⟨u⟩ (m/s)	û (m/s)	LDFM 100 mm <u> (m/s)	LDFM 100 mm û (m/s)	Number of waves for ensemble-averaging
I1-A21	38	185.04	257.04	0.172	1.50	0.222	1.48	10
I1A-22	39	257.04	329.04	0.186	1.44	0.226	1.49	10
I1-A23	15	350.6	422.6	0.147	1.52	0.225	1.47	10
I1-A24	16	479.56	551.56	0.139	1.52	0.224	1.45	10
I1-A41	27	142.2	178.2	0.172	1.50	0.226	1.48	5
I1-A42	29	293.32	365.32	0.189	1.47	0.234	1.48	10
I1-A43	10	379.76	415.76	0.129	1.40	0.236	1.48	5
I1-A44	11	494.76	566.76	0.142	1.40	0.233	1.48	10
I1-A51	30	120.76	192.76	0.178	1.51	0.223	1.48	10
I1-A52	32	257.6	329.6	0.168	1.50	0.227	1.47	10
I1-A53	17	380	452	0.153	1.43	0.233	1.49	10
I1-A54	17	501.72	573.72	0.149	1.45	0.222	1.49	10
I1-A61	14	127.68	163.68	0.147	1.54	0.222	1.49	5
I1-A62	19	279.0	351.0	0.155	1.55	0.227	1.48	10
I1-A63	8	379.76	487.76	0.133	1.44	0.232	1.46	15
I1-A64	9	487.52	552.32	0.150	1.46	0.235	1.47	9
I1-A71	10	194.32	266.32	0.155	1.49	0.224	1.49	10
I1-A72	2	367.4	439.4	0.132	1.41	0.231	1.48	10
I1-A73	8	504.4	576.4	0.147	1.46	0.231	1.49	10
I1-A74	0	597.84	669.84	0.114	1.33	0.234	1.49	10
I1-A75	2	705.2	777.2	0.119	1.38	0.218	1.49	10
I1-A81	0	236.48	308.48	0.125	1.36	0.226	1.48	10
I1-A82	3	366.16	438.16	0.130	1.43	0.233	1.49	10
I1-A83	5	546.16	618.16	0.151	1.53	0.235	1.50	10
I1-A84	6	647.04	719.04	0.157	1.495	0.240	1.50	10

Table A9 Results ADV

Notes:

- See also data-report page 11 and Table 3.4. (Janssen and Van der Hout (1997))
- A limited number of waves is used for ensemble-averaging, because during the tunnel run the bed level varied due to local erosion caused by the instrument.
- 'Low' refers to the starting point (in seconds) of the measurement; 'high' refers to the end point of the measurement. The time in between corresponds with the number of waves used for ensemble averaging. The sand bed was considered to be at a constant level during the period between 'low' and 'high'.
- The flow velocity was also measured using LDFM during these tests at 10 cm above the sand bed.

D.3 Results OPCON

Test	height (mm)	low (s)	high (s)	⟨c⟩ (g/l)	LDFM 100 mm <u> (m/s)	LDFM 100 mm û (m/s)	amplification factor	zero level (Volts)	change in zero level (Volts)	No. of waves for ens-averg.
I1-O11	111	504.48	554.88	-0.25	0.219	1.46	10x	0	0.08	7
I1-O12	78	713.28	785.28	0.25	0.228	1.47				10
I1-O13	57	828.48	900.48	0.75	0.227	1.49				10
I1-O14	58	950.88	1022.88	0.74	0.224	1.50				10
I1-O15	48	1181.28	1253.28	0.81	0.220	1.50				10
I1-O21	53	356.88	428.88	0.99	0.257	1.48	10x	6.95	0.08	10
I1-O31	12	272.52	308.52	8.64	0.227	1.50	1x	1.00	0.08	5
I1-O32	15	380.52	438.12	6.32	0.236	1.48				8
I1-O33	10	466.92	538.92	14.09	0.238	1.49				10
I1-O34	14	632.52	704.52	7.66	0.241	1.51				10
I1-O35	15	718.92	754.92	6.78	0.238	1.52				5
I1-O36	34	790.92	862.92	4.76	0.237	1.52				10
I1-O37	36	942.12	978.12	4.48	0.236	1.52				5
I1-O41	30	217.68	289.68	2.17	0.247	1.50	1x	1.00	0.002	10
I1-O42	22	404.88	476.88	3.42	0.255	1.51				10
I1-O43	18	505.8	577.8	4.67	0.256	1.52				10
I1-O44	18	577.8	613.68	3.94	0.253	1.54				5
I1-O45	31	865.68	937.68	1.93	0.249	1.52				10
I1-O51	28	596.64	668.64	3.52	0.226	1.47	1x	1.00	0.004	10
I1-O52	42	798.36	870.36	1.25	0.234	1.48				10
I1-O53	41	1043.04	1115.04	1.18	0.230	1.49				10
I1-O61	99	311.4	347.4	0.11	0.225	1.46	10x	0.00	0.165	5
I1-O62	102	412.2	484.2	0.11	0.225	1.46				10
I1-O63	50	556.2	628.2	1.15	0.234	1.47				10
I1-O64	55	707.4	779.4	0.78	0.230	1.49				10
I1-O65	40	916.2	988.2	1.77	0.226	1.50				10
I1-O66	42	1024.2	1096.2	1.48	0.227	1.49				10

Table A10 Results OPCON

Notes:

- See also data-report page 11 and Table 3.5. (Janssen and Van der Hout (1997))
- The amplification factor, the zero level and the change in zero level are parameters related to the measuring instrument.
- For more notes see Table A9.

D.4 Results CCM

Test	height (mm)	low (s)	high (s)	⟨c⟩ (g/l)	LDFM 100 mm <u> (m/s)	LDFM 100 mm û (m/s)	zero-level U_0 (Volts)	Number of waves for ensemble-averaging
I1-C11	-1	348.96	492.96	886.0	0.214	1.48	2.3816	20
I1-C12	-3	543.36	687.36	1154.3	0.233	1.49		20
I1-C13	1	701.84	831.44	282.0	0.228	1.50		18
I1-C14	4	888.96	1032.96	38.6	0.229	1.50		
I1-C21	-7	118.88	262.88	1335.1	0.227	1.49	2.3597	20
I1-C22	-4	306.08	450.08	1408.1	0.235	1.49		20
I1-C23	-3	471.6	615.6	1178.7	0.239	1.49		20
I1-C24	-2	702.08	846.08	1065.8	0.238	1.51		20
I1-C25	3	899.84	1043.84	66.4	0.234	1.51		20
I1-C26	7	1105.28	1249.28	36.1	0.239	1.50		20
I1-C31	3	75.2	147.2	103.5	0.247	1.45	2.3379	10
I1-C32	2	211.76	283.76	169.5	0.257	1.44		10
I1-C33	2	456.56	564.56	163.1	0.259	1.46		10
I1-C34	4	607.76	751.76	62.8	0.262	1.44		15
I1-C35	6	773.36	917.36	48.7	0.256	1.47		20
I1-C36	10	989.36	1097.36	33.5	0.253	1.47		15
I1-C37	8	1198.16	1270.16	43.8	0.252	1.47		10
I1-C41	-2	269.6	413.6	965.3	0.226	1.46	2.3512	20
I1-C42	0	456.8	536.0	496.9	0.232	1.47		11
I1-C43	-1	597.76	705.76	944.9	0.238	1.48		15
I1-C44	0	828.16	936.16	602.1	0.239	1.51		15
I1-C45	3	953.6	1025.6	85.6	0.229	1.53		10
I1-C46	4	1061.6	1133.3	63.4	0.226	1.53		20
I1-C47	7	1248.8	1392.8	27.5	0.232	1.50		20
I1-C48	8	1432.8	1576.8	20.6	0.231	1.47		20

Table A11 Results CCM

Notes:

- See also data-report page 12 and Table 3.6. (Janssen and Van der Hout (1997))
- The zero level is a parameter related to the measuring instrument.
- For more notes see Table A9.

E Previous experimental series

series	test	D_{50} (mm)	T (sec)	<u> (m/s)	u_1 (m/s)	u_2 (m/s)	u_{rms} (m/s)	R	<q_s> ($10^{-6}m^2/s$)
B	B7	0.21	6.5	0.048	0.725	0.250	0.50	0.66	12.4
	B8	0.21	6.5	0.038	1.005	0.305	0.70	0.65	38.9
	B9	0.21	6.5	0.030	1.290	0.430	0.92	0.67	69.8
	B19	0.21	9.1	0.002	0.745	0.215	0.54	0.64	18.6
	B11	0.21	9.1	0.022	0.970	0.280	0.70	0.64	44.8
	B12	0.21	9.1	0.029	1.370	0.380	0.97	0.64	120.9
	B13	0.21	6.5	0.010	1.050	0.150	0.71	0.57	21.0
	B14	0.21	9.1	-0.064	1.055	0.135	0.70	0.56	22.0
	B15	0.21	5.0	0.030	0.760	0.220	0.51	0.64	15.2
	B16	0.21	12.0	0.005	0.830	0.200	0.56	0.62	19.8
C-I	C1	0.21	6.5	0.015	0.819	0.239	0.55	0.65	18.7
	C2	0.21	6.5	0.055	0.824	0.227	0.55	0.65	25.5
	C3	0.21	6.5	0.357	0.828	0.217	0.65	0.64	51.2
	C4	0.21	6.5	0.203	0.813	0.220	0.58	0.64	35.5
	C5	0.21	6.5	0.470	0.840	0.200	0.73	0.65	78.1
C-II	C9	0.21	6.5	0.021	0.855	0.176	0.56	0.62	20.5
	C10	0.21	6.5	-0.460	1.200	0.250	0.89	0.39	47.6
	C11	0.21	6.5	0.029	1.138	0.277	0.83	0.63	51.5
	C12	0.21	6.5	-0.105	1.120	0.235	0.79	0.39	-29.7
	C13	0.21	6.5	0.556	1.270	0.184	0.92	0.63	162.6
D	D11	0.13	6.5	0.019	0.795	0.205	0.56	0.63	9.0
	D12	0.13	6.5	0.062	1.227	0.330	0.91	0.63	-228.3
	D13	0.13	6.5	0.041	1.030	0.270	0.73	0.63	-30.2
	D14	0.13	6.5	0.017	0.635	0.155	0.45	0.62	7.6

Table A12 Previous experimental series, a-symmetric waves

Notes:

- The transport rates are corrected for the variations in velocity over the cross-section.
- These asymmetric waves are second order Stokes waves. They can be described by:

$$u = u_1 \cos(\omega t) + u_2 \cos(2\omega t) \tag{E.1}$$

- For these waves, the parameter u_{rms} is given by:

$$u_{rms} = \sqrt{\tfrac{1}{2}\left(u_1^{\,2} + u_2^{\,2}\right)} \tag{E.2}$$

- The parameter R indicates the degree of asymmetry and is given by:

$$R = \frac{u_1 + u_2}{2 \cdot u_1} = \frac{1}{2}\left(1 + \frac{u_2}{u_1}\right) \tag{E.3}$$

Symmetric waves

series	test	D_{50} (mm)	T (sec)	<u> (m/s)	û (m/s)	u_{rms} (m/s)	R	<q_s> ($10^{-6}m^2/s$)
E	E1	0.21	7.25	0.176	1.69	1.18	0.55	107.2
	E2	0.21	7.25	0.239	1.47	1.03	0.57	111.7
	E3	0.21	7.25	0.311	1.14	0.84	0.64	80.8
	E4	0.21	7.25	0.443	0.95	0.64	0.72	84.9
H	H2	0.13	7.2	0.227	0.68	0.48	0.67	19
	H3	0.13	7.2	0.244	0.93	0.65	0.63	35
	H4	0.13	7.2	0.248	1.09	0.77	0.61	40
	H5	0.13	7.2	0.241	1.30	0.90	0.59	52
	H6	0.13	7.2	0.234	1.47	1.04	0.58	56
	H7	0.13	7.2	0.419	0.49	0.35	0.93	16
	H8	0.13	7.2	0.429	0.67	0.47	0.82	47
	H9	0.13	7.2	0.437	0.94	0.66	0.73	86
	H4s	0.13	4.0	0.250	1.06	0.75	0.62	9
	H12s	0.13	12.0	0.243	1.08	0.76	0.61	99
	H24	0.13	4.0	0.242	0.70	0.50	0.67	13
	H12	0.13	12.0	0.234	0.68	0.48	0.67	20
J	J1	0.21	7.2	0.244	1.06	0.75	0.62	46.3
	J2	0.21	7.2	0.248	1.28	0.91	0.60	74.4
	J3	0.21	7.2	0.415	0.46	0.33	0.95	9.0
	J4	0.21	7.2	0.409	0.65	0.46	0.81	25.3
	J5	0.21	4.0	0.240	1.04	0.74	0.62	29.2
	J6	0.21	12.0	0.227	1.09	0.77	0.60	49.2
I	I1	0.32	7.2	0.259	1.47	0.86	1.04	94.0
	I2	0.32	7.2	0.254	1.70	1.12	1.20	152.3
	I3	0.32	7.2	0.419	0.65	0.46	0.46	23.6
	I4	0.32	7.2	0.417	0.92	0.65	0.65	53.3
	I5	0.32	7.2	0.452	1.50	1.06	1.06	193.7

Table A13 Previous experimental series, sinusoidal waves

Notes:

- The transport rates are corrected for the variations in velocity over the cross-section.
- The parameter R indicates the degree of asymmetry and is given by:

$$R = \frac{\hat{u} + \langle u \rangle}{2 \cdot \hat{u}} \qquad \text{(E.4)}$$

F Implementation of size-fraction method

F.1 Input for sensitivity analysis

Standard settings:
Bailard $k_{sc}=k_{sw}=D_{50}$
Ribberink k_{sc}=max of $3*\theta*D_{90}$ and $D_{50}(1+6(\theta-1))$
$k_{sw}=D_{50}(1+6(\theta-1))$
critical Shields related to D_i or D_{50}
no hiding and exposure correction
Dibajnia & Watanabe (no choices are made here)

For all cases:
$\tan\varphi$ = angle of internal friction = 0.625
ρ_s = density of sediment = 2650 kg/m^3

1. Number of fractions

Standard mixture D_{50}=0.21 mm D_{90}=0.32 mm W_s=26 mm/s

N=2	*D_i (mm)*	*W_s (mm/s)*	*p_i (%)*
fraction 1	0.151	16	50
fraction 2	0.292	43	50
N=3			
fraction 1	0.135	14	24
fraction 2	0.210	28	52
fraction 3	0.326	48	24
N=4			
fraction 1	0.128	12	14
fraction 2	0.178	22	36
fraction 3	0.248	35	36
fraction 4	0.344	51	14
N=5			
fraction 1	0.124	12	10
fraction 2	0.161	18	24
fraction 3	0.210	28	33
fraction 4	0.273	39	24
fraction 5	0.356	53	10
N=6			
fraction 1	0.121	11	7
fraction 2	0.151	16	17
fraction 3	0.188	24	26
fraction 4	0.234	32	26
fraction 5	0.292	43	17
fraction 6	0.363	54	7

N=8			
fraction 1	0.118	11	5
fraction 2	0.139	14	10
fraction 3	0.164	19	16
fraction 4	0.193	25	20
fraction 5	0.228	31	20
fraction 6	0.269	39	16
fraction 7	0.317	47	10
fraction 8	0.374	56	5

2. Mean diameter of the mixture

Finer sediment:	D_{50}=0.13 mm	D_{90}=0.18 mm	W_s=12 mm/s
	D_i (mm)	*W_s (mm/s)*	*p_i (%)*
fraction 1	0.089	6	14
fraction 2	0.114	10	36
fraction 3	0.148	16	36
fraction 4	0.190	24	14

Coarser sediment:	D_{50}=0.32 mm	D_{90}=0.48 mm	W_s=42 mm/s
	D_i (mm)	*W_s (mm/s)*	*p_i (%)*
fraction 1	0.199	26	14
fraction 2	0.273	40	36
fraction 3	0.375	56	36
fraction 4	0.515	74	14

3. Grain-size distribution

Standard:	D_{50}=0.21 mm	D_{90}=0.32 mm	W_s=26 mm/s	σ_g=1.4
Wider gradation:	D_{50}=0.21 mm	D_{90}=0.51 mm	W_s=26 mm/s	σ_g=2.0
	D_i (mm)	*W_s (mm/s)*	*p_i (%)*	
fraction 1	0.074	4	14	
fraction 2	0.148	16	36	
fraction 3	0.297	43	36	
fraction 4	0.594	83	14	
Widest gradation:	D_{50}=0.21 mm	D_{90}=0.68 mm	W_s=26 mm/s	σ_g=2.5
	D_i (mm)	*W_s (mm/s)*	*p_i (%)*	
fraction 1	0.053	2	14	
fraction 2	0.133	13	36	
fraction 3	0.332	49	36	
fraction 4	0.832	105	14	

4. Wave conditions	<u> (m/s)	û (m/s)	u_{rms} (m/s)	T (s)	
Condition 1	0.08	0.5	0.35	6	
Condition 2	0.16	1.0	0.71	7	
Condition 3	0.24	1.5	1.06	8.5	= H6/E2/I1

F.2 Results of sensitivity analysis

F.2.1 Test A1: Number of fractions

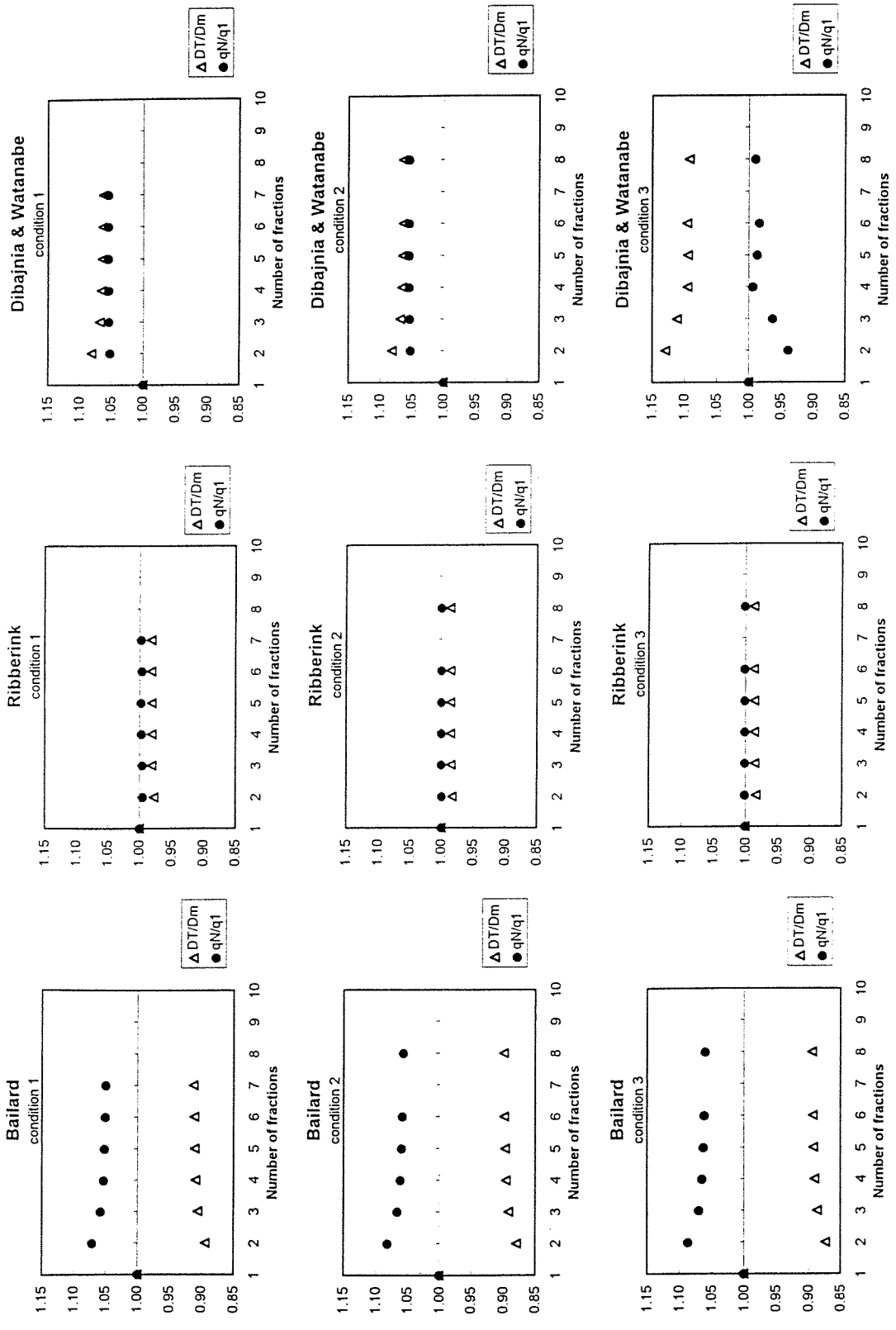

Figure A6 q_N/q_1 and D_T/D_m for different numbers of fractions; $\sigma_g = 1.4$

F.2.2 Test A2 Mean diameter of the mixture

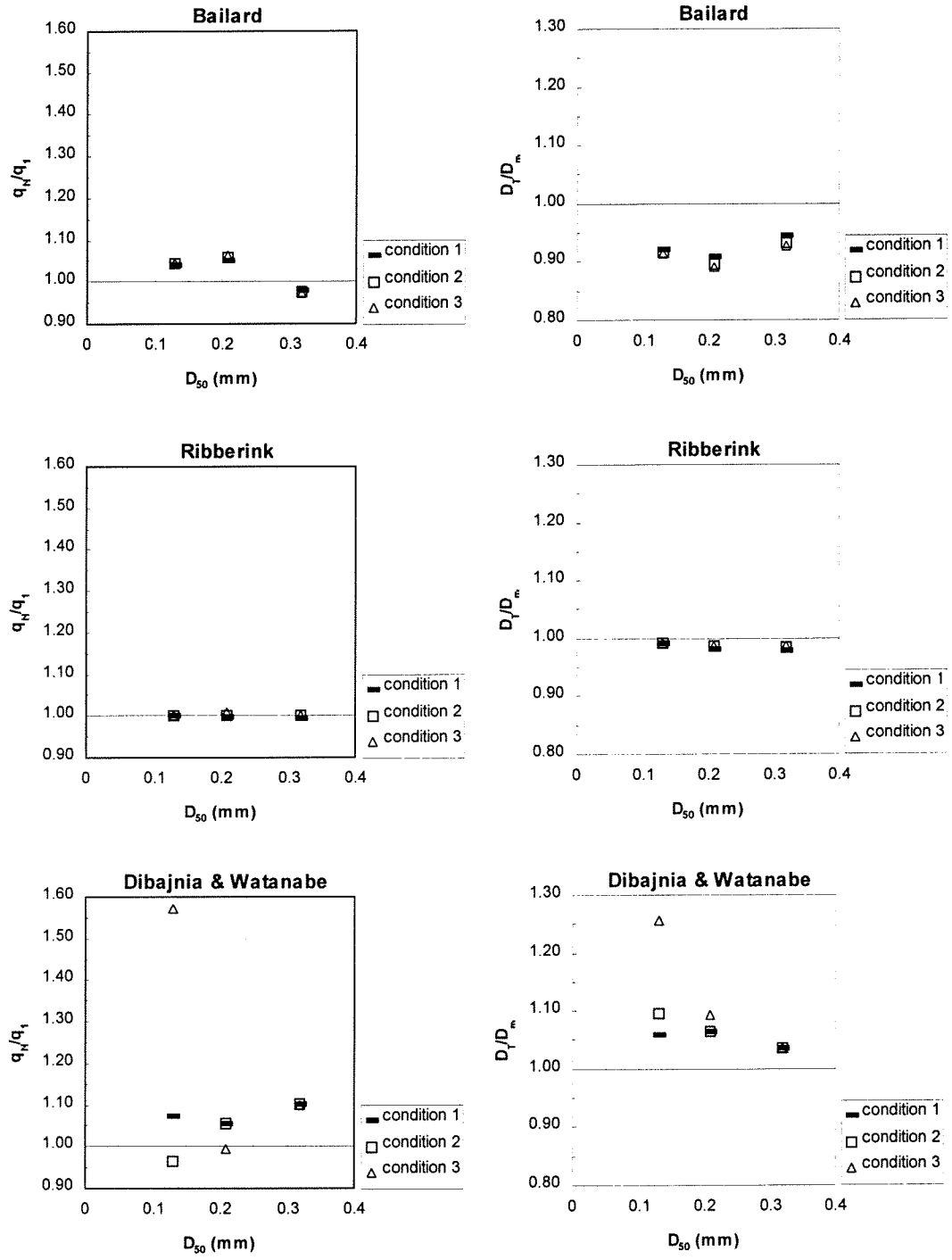

Figure A7 q_N/q_1 and D_T/D_m for different mean diameters of the mixture

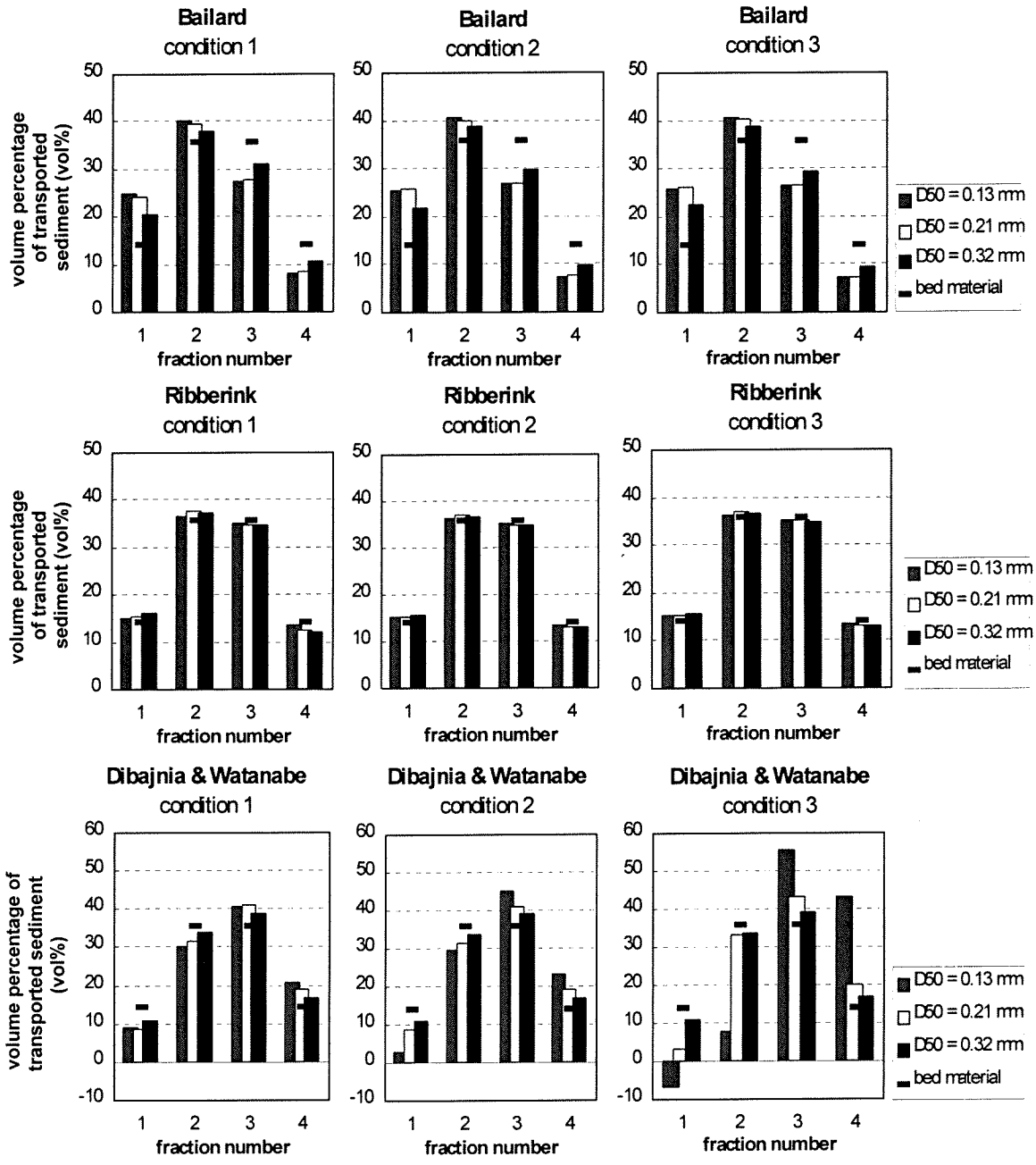

Figure A8 Volume percentages of fractions of transported material for different mean diameters

F.2.3 Test A3 Gradation of the mixture

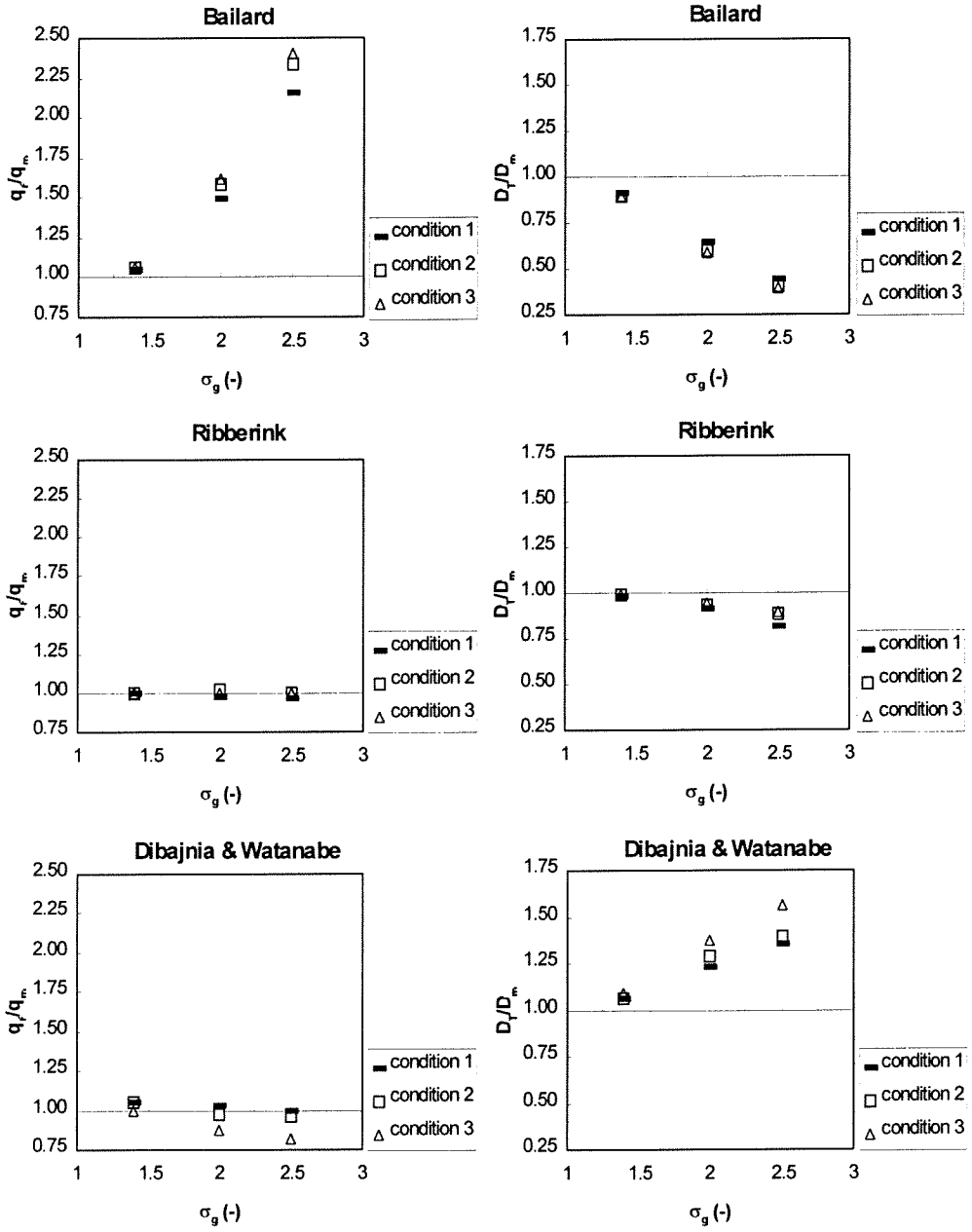

Figure A9 q_N/q_1 and D_T/D_m for different gradations of the mixture

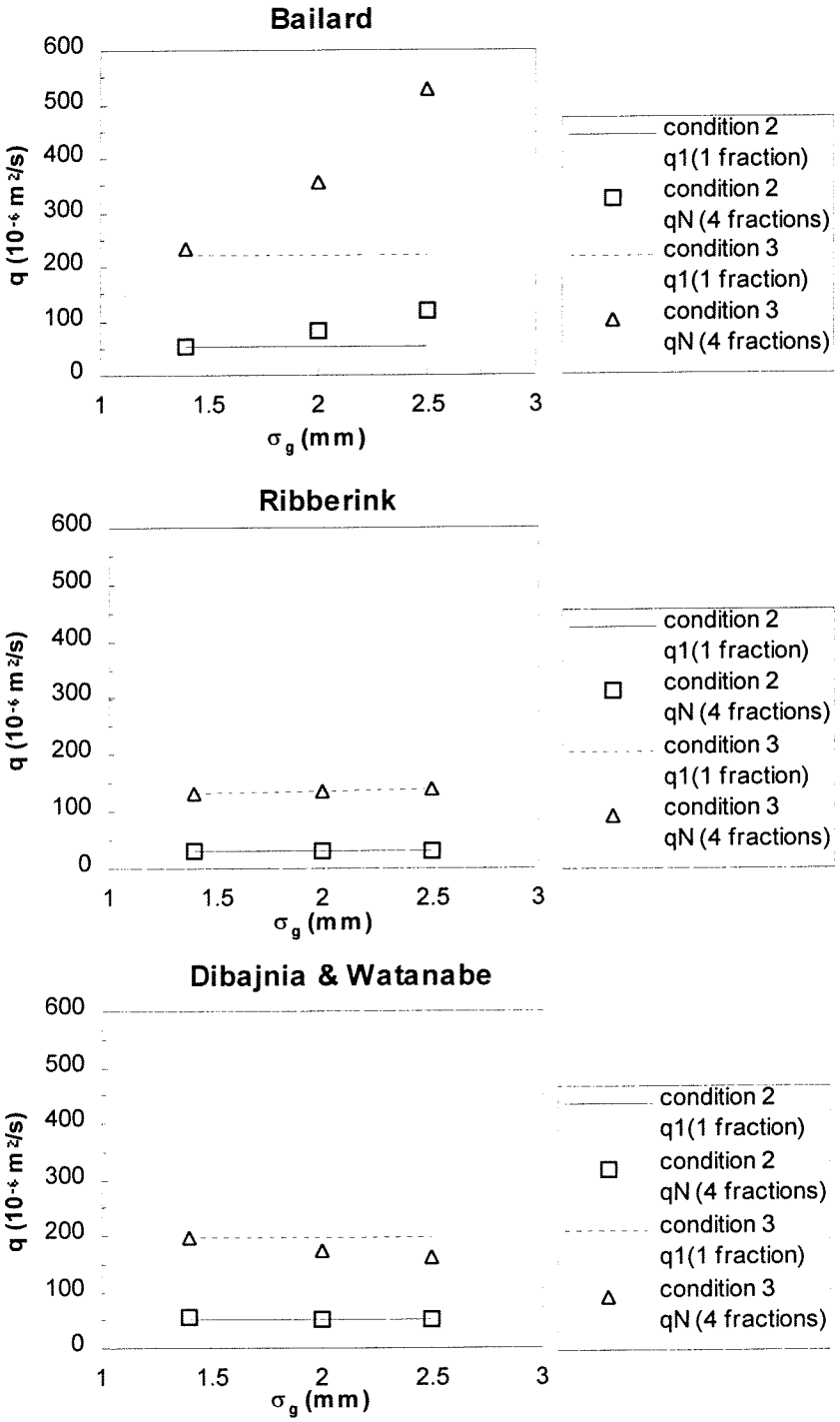

Figure A10 Absolute transport rates for different gradations

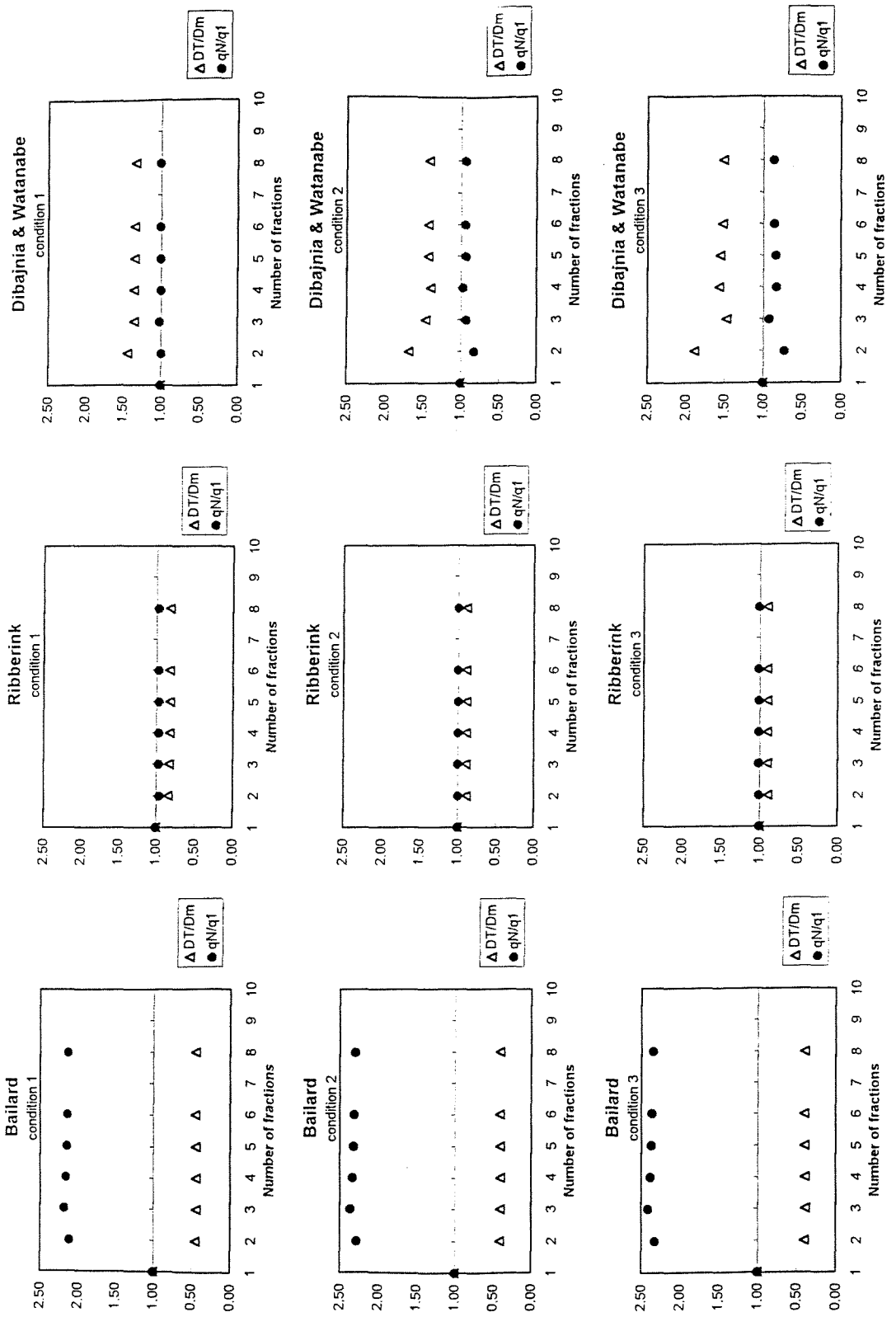

Figure A11 q_N/q_1 and D_T/D_m for different numbers of fractions; $\sigma_g = 2.5$

F.2.4 Correction coefficients in the model of Ribberink

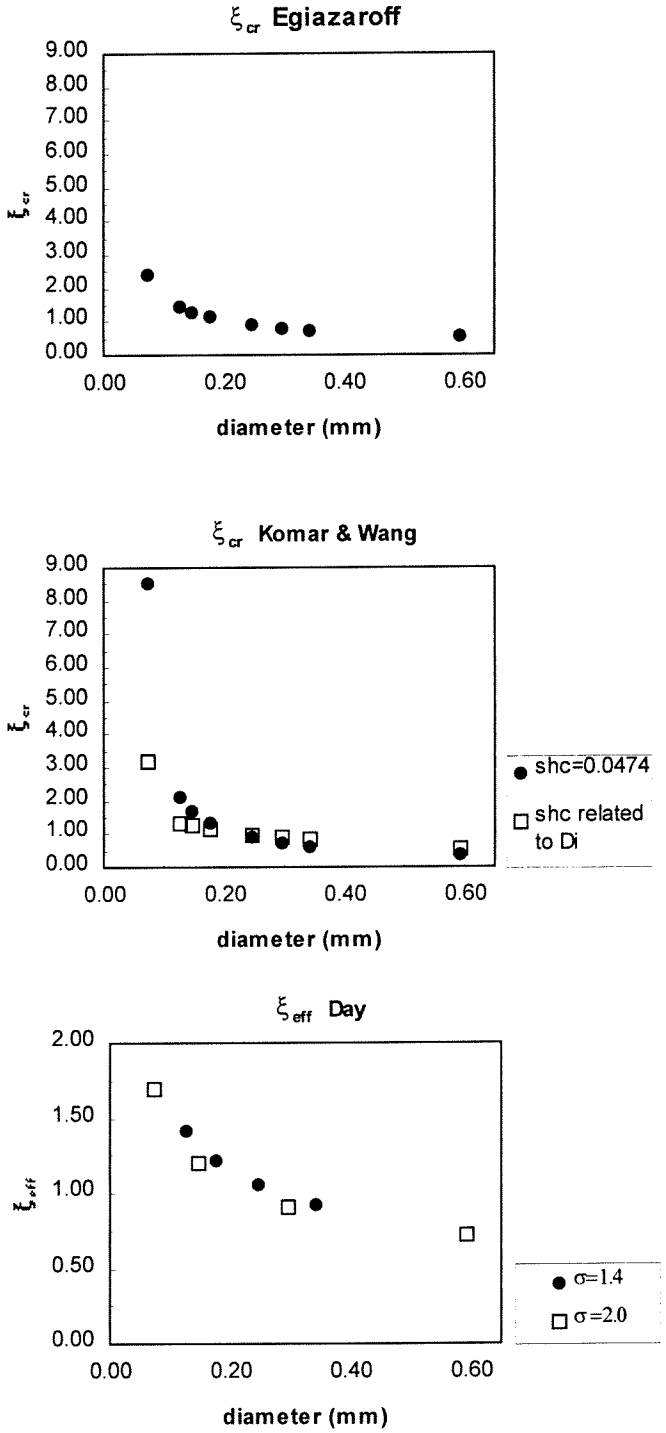

Figure A12 Values of different correction coefficients, valid for all conditions

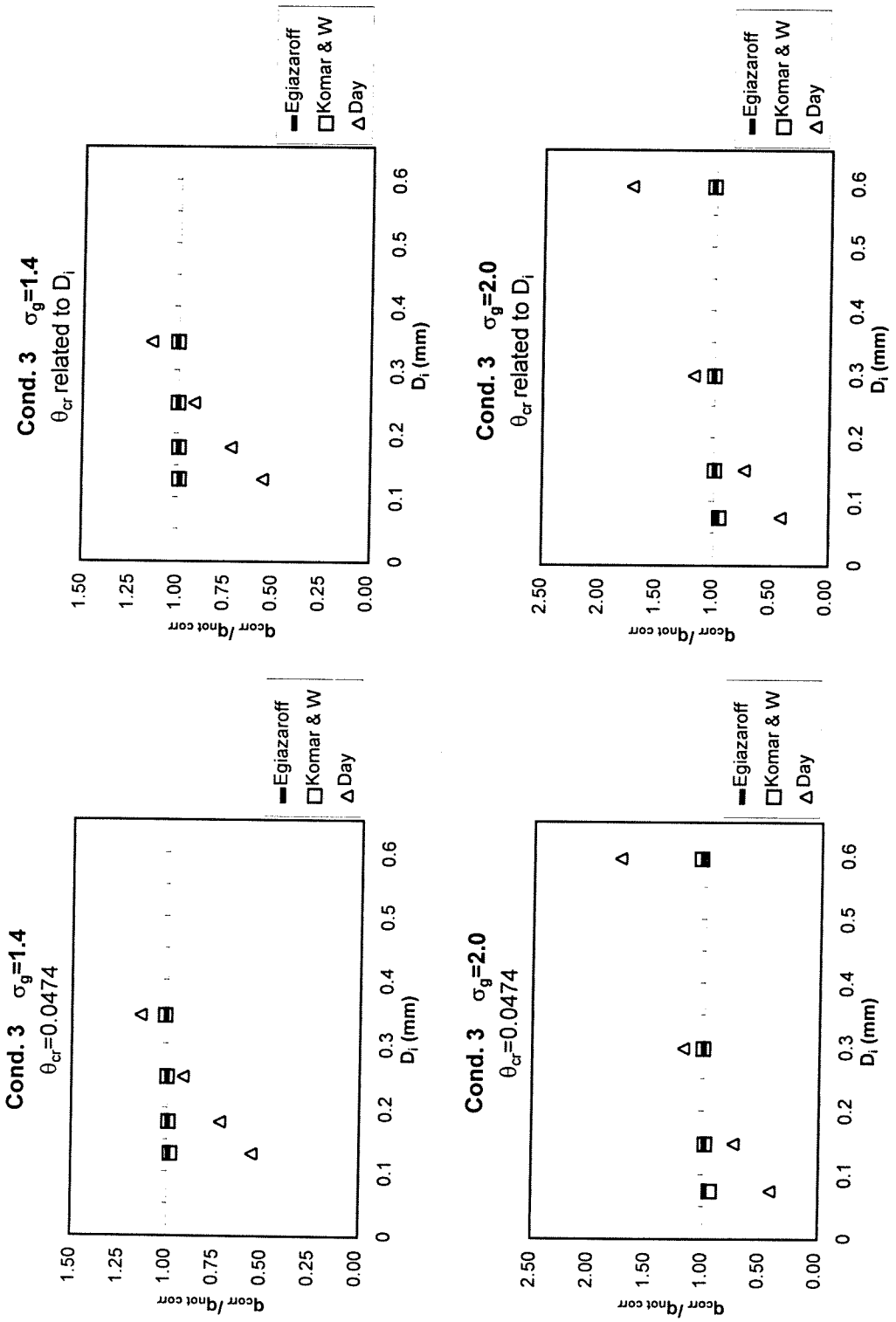

Figure A13 Ratio of corrected and uncorrected transport rates for condition 3

F.3 Program listing

F.3.1 Procedure TOTAAL from unit Reken

```
PROCEDURE TOTAAL        (var qN,phisN:  real;
                         var q_f,pT_f:    ftype);

VAR i:   integer;

BEGIN
  i := 1;
  qN := 0;
  phisN := 0;
  D_T := 0;
  D_m := 0;
  FOR i := 1 to Ni DO BEGIN
    q_f[i] := qc_f[i] * 0.01 * p_f[i];
    qN := qN + q_f[i];
  END;
  writeln(f,'Het totale transport is ',qN:12,' m2/s');

  if keuze = '7' then begin
    if (keuzemeth = '1') or (keuzemeth = '4') then begin
      phisN := qN/(Ws_m*D50_m);
      writeln(f,'en het totale transport dimensieloos is ',phisN:12);
    end;
    if (keuzemeth = '3') then begin
      phisN := qN/(sqrt( ((rhos_m-rho)/rho)*g*macht(D50_m,3)));
      writeln(f,'en het totale transport dimensieloos is ',phisN:12);
    end;
  end;

  i := 1;
  FOR i := 1 to Ni DO BEGIN
    pT_f[i] := (q_f[i]/qN) * 100;
    D_m := D_m + ((p_f[i]*D_f[i])/100);
    D_T := D_T + (q_f[i]/qN)*D_f[i];
    writeln(f,'  transport van fractie ',i,' is ',q_f[i]:12,' m2/s, dat is ',pT_f[i]:4:1,' %');
    writeln(dat,q_f[i]:12,'  ',pT_f[i]:4:1);
  END;
  writeln(f);
  writeln(f,'D_T = ',D_T:7:6,' en D_m = ',D_m:7:6, 'm');
  writeln(f,'D_T/D_m = ',(D_T/D_m):5:4);
  writeln(f,'=============================================================================');
  writeln(dat);
  writeln(dat,qN:12,'  ',(D_T/D_m):5:4);
  writeln(dat);
  writeln(dat);
END;
```

F.3.2 Procedure Fracties from unit Inout

```
PROCEDURE Fracties;

VAR    sigmay,muy,deltaz,delta,pister,help1,help2:        real;
       i:                                  integer;
       z_f,zu_f,zl_f:                          ftype;

BEGIN
    FOR i:= 1 to 20 DO z_f[i] := 0;
    FOR i:= 1 to 20 DO zu_f[i] := 0;
```

```
    FOR i:= 1 to 20 DO zl_f[i] := 0;
    sigmay := (ln(D50_m/D90_m)/-1.28);
    muy := ln(D50_m);
    deltaz := 4/Ni;
    delta := (rhos_m-rho)/rho;
    for i := 1 to Ni do begin
      z_f[i]  := -2 + (2*(2*i-1)/Ni);
      zl_f[i] := z_f[i] - 0.5*deltaz;
      zu_f[i] := z_f[i] + 0.5*deltaz;
      D_f[i]  := macht(2.7182818,(z_f[i]*sigmay + muy));
      Ws_f[i] := 10*visco/D_f[i]*(sqrt(1+(0.01*delta*g*macht(D_f[i],3))/sqr(visco))-1);
      pister := 0.5*(erf(0.7071068*zu_f[i])-erf(0.7071068*zl_f[i]));
      p_f[i] := (pister/0.95425)*100;
      rhos_f[i] := rhos_m;
      tanfi_f[i] := tanfi_m;
      writeln;
      textcolor(white);
      writeln('  Voor fractie ',i,' geldt:');
      writeln;
      normvideo;
      writeln('    D_',i,'  = ',D_f[i]:9:6,' m');
      writeln('    Ws_',i,' = ',Ws_f[i]:9:6,' m/s');
      writeln('    p_',i,'  = ',p_f[i]:6:3,' %');
      writeln;
      writeln('    rho_',i,'  = rho_m = ',rhos_m:6:0,' kg/m3');
      write  ('    tan f_',i,' = tan f_m = ',tanfi_m:7:4);
      writeln;
      textcolor(14);
      writeln('                                    <enter> om door te gaan');
      readln;
      normvideo;
      clrscr;
    end;

END;
```

F.3.3 Unit uCorrect

```
INTERFACE USES uTools,uCentral,crt;

VAR  sigy,sigg,D16_m,D84_m,D50_s,rhos_s:        real;
   keuzes,keuzec,keuzec1,keuzeday:     char;


PROCEDURE Correctie;

IMPLEMENTATION

PROCEDURE SHCKR(var dster,shc: real);

VAR  ds:  real;

begin
   ds:= g*(rhos_s-rho)/(rho*sqr(visco));
   ds:= macht(ds,1/3);
   dster := d50_s*ds;
   WRITELN(f);
   WRITE(f,'D*  = ',dster:7:4);
   if (dster > 1) and (dster <=4) then shc := 0.24/dster;
   if (dster > 4) and (dster <=10) then shc := 0.14*macht(dster,-0.64);
   if (dster > 10) and (dster <=20) then shc := 0.04*macht(dster,-0.1);
   if (dster > 20) and (dster <=150) then shc := 0.013*macht(dster,0.29);
   if dster > 150 then shc := 0.055;
   WRITELN(f,'  Shields kritiek = ',shc:12);
   writeln(f);
end;


PROCEDURE C1(var psicr,psieff: real);        {Egiazaroff}
```

```
BEGIN
  psicr :=  sqr(log(19)/(log(19 * (D_f[i] / D50_m))));
  psieff := 1;
  WRITELN(f,'Correctie volgens Egiazaroff:');
  WRITELN(f,'  psicr = ',psicr:8:6,' psieff = ',psieff:8:6);
  if Ni > 1 then writeln (dat,' ',psicr:8:6,'  ',psieff:8:6,' [',i,']  Egi');
END;


PROCEDURE C2(var psicr,psieff: real);        {Ashida & Michuie}

BEGIN
  IF (D_f[i]/D50_m) < 0.4 THEN BEGIN
    psicr := 0.85 * (D50_m/D_f[i]);
    psieff := 1;
    WRITELN(f,'Correctie volgens Ashida & Michuie');
    WRITELN(f,'  psicr = ',psicr:8:6,' psieff = ',psieff:8:6);
    if Ni > 1 then writeln (dat,' ',psicr:8:6,'  ',psieff:8:6,' [',i,']  A&M');
  END
  ELSE BEGIN
    psicr :=  sqr(log(19)/(log(19 * (D_f[i] / D50_m))));
    psieff := 1;
    WRITELN(f,'Correctie volgens Ashida & Michuie (in dit geval gelijk aan Egiazaroff)');
    WRITELN(f,'  psicr = ',psicr:8:6,' psieff = ',psieff:8:6);
    if Ni > 1 then writeln (dat,' ',psicr:8:6,'  ',psieff:8:6,' [',i,']  A&M');
  END;
END;


PROCEDURE C3(var psicr,psieff: real);        {Komar & Wang}

VAR alfakom,alfarad,shckom:     real;

BEGIN
  alfakom := 61.5 * macht((D_f[i]/D50_m),-0.3),
  alfarad := (alfakom * 3.14159265)/180;
  shckom := 0.00071 * macht(D_f[i],-0.43) * (sin(alfarad)/cos(alfarad));
  psicr := (shckom/shc);
  psieff:= 1;
  WRITELN(f,'Correctie volgens Komar & Wang');
  WRITELN(f,'  alfa  = ',alfakom:8,'  Shields kritiek volgens Komar en Wang = ',shckom:12);
  WRITELN(f,'  psicr = ',psicr:8:6,'  psieff = ',psieff:8:6);
  if Ni > 1 then writeln(dat,' ',psicr:8:6,'  ',psieff:8:6,' [',i,']  K&W');
END;


PROCEDURE C4(var psicr,psieff: real);        {Day}

VAR Da:   real;

BEGIN
  psicr := 1;
  begin
     Da := D50_m * 1.6 * macht((D84_m/D16_m),-0.28);
     psieff := sqr((0.4/(sqrt(D_f[i]/Da))) + 0.6);
  end;
  WRITELN(f,'Correctie volgens Day:');
  WRITELN(f,'  D16_m = ',D16_m:7:6,'   D84_m = ',D84_m:7:6);
  WRITELN(f,'  Da    = ',Da:7:6);
  WRITELN(f,'  psicr = ',psicr:8:6,'  psieff = ',psieff:8:6);
  if Ni > 1 then writeln(dat,' ',psicr:8:6,'  ',psieff:8:6,' [',i,']  Day');
END;


PROCEDURE C5(var psicr,psieff: real);

BEGIN
   psicr := 1;
   psieff := 1;
   WRITELN(f,'Geen correctie:');
```

```
   WRITELN(f,'  psicr = ',psicr:8:6,'  psieff = ',psieff:8:6);
   if Ni > 1 then writeln(dat,' ',psicr:8:6,'  ',psieff:8:6,' [',i,']  geen');
END;


Procedure Correctie

BEGIN

 if keuze <> '7' then begin
  repeat
     clrscr;
     writeln;
     textcolor(12);
     writeln('Wilt u voor de kritieke Shieldsparameter:');
     writeln;
     textcolor(14);
     writeln('Een vaste waarde, nl.:');
     textcolor(white);
     writeln('  1) 0.0474 (Mayer-Peter & M ller)');
     writeln('  2) 0.035');
     writeln('  3) eigen keuze');
     textcolor(14);
     writeln('of:');
     textcolor(white);
     writeln('  4) een waarde gerelateerd aan de D50 van het mengsel');
     IF Ni > 1 then writeln('  5) een waarde gerelateerd aan de D van de betreffende fractie');
     gotoxy(65,2);
     readln(keuzes);
  until (keuzes = '1') or (keuzes = '2') or (keuzes = '3') or
       (keuzes = '4') or (keuzes = '5');

  IF keuzes = '3' THEN BEGIN
    gotoxy(3,12);
    textcolor(10);
    write('  Uw eigen keuze voor Shields kritiek = ');
    readln(shc);
  END;
  IF keuzes = '1' THEN shc := 0.0474;
  IF keuzes = '2' THEN shc := 0.035;

  IF (keuzes = '1') or (keuzes = '2') or (keuzes = '3') THEN BEGIN
    writeln(f);
    writeln(f,'Shields kritiek = ',shc:12);
    writeln(f);
  END;
 end;

  IF (keuzes = '4') or (keuzes = '5') THEN BEGIN
    IF (keuzes = '4') THEN BEGIN
        D50_s := D50_m;
        rhos_s := rhos_m;
    END
    ELSE BEGIN
        D50_s := D_f[i];
        rhos_s := rhos_f[i];
    END;
    SHCKR(dster,shc);
  END;


if keuze <> '7' then begin
  IF Ni > 1 THEN BEGIN

    repeat
      Clrscr;
      Writeln;
      Textcolor(12);
      Writeln('Welke methode wilt u gebruiken voor het berekenen van de hiding-' );
      Writeln('en exposure coefficient ?');
      Writeln;
```

```
      textcolor(white);
      Writeln('  1) Egiazaroff          (corrigeert shieldscr)  ');
      Writeln('  2) Ashida & Michuie    (corrigeert shieldscr)  ');
      Writeln('  3) Komar & Wang        (geeft nieuwe shieldscr) ');
      Writeln('  4) Day                 (corrigeert shieldseff)  ');
      Writeln('  5) Geen correctie ');
      gotoxy(30,3);
      readln(keuzec);
    until (keuzec = '1') or (keuzec = '2') or (keuzec = '3')
      or (keuzec = '4') or (keuzec = '5')
  END
  ELSE keuzec := '5';

  Gotoxy(3,10);
  IF keuzec = '4' THEN BEGIN
   repeat
    Writeln;
    textcolor(12);
    Writeln('Voor het gebruik van de formule van Day moeten de D16 en D84 van het mengsel');
    Writeln('bekend zijn. Wilt u deze waarden:');
    Writeln;
    textcolor(white);
    Writeln('1) hier opgeven omdat ze bekend zijn ?');
    Writeln('2) schatten met behulp van D50_m en D90_m ?');
    Writeln('  (hierbij wordt uitgegaan van een log-normale korrelgrootte verdeling)');
    gotoxy(40,12);
    readln(keuzeday);
   until (keuzeday = '1') or (keuzeday = '2');

    IF keuzeday = '1' THEN BEGIN
      Gotoxy(1,18);
      textcolor(10);
      Write('  D16_m [m] = '); Readln(D16_m);
      Write('  D84_m [m] = '); Readln(D84_m);
      normvideo;
    END
    ELSE BEGIN
      sigy:= ln(D50_m/D90_m)/-1.28;
      sigg:= exp(0.995*sigy);
      D16_m := D50_m/sigg;
      D84_m := D50_m*sigg;
      Gotoxy(1,18);
      Writeln('D16_m = ',D16_m:7:6,' m   D84_m = ',D84_m:7:6,' m');
      Writeln;
      Writeln;
      textcolor(14);
      Writeln('                              <enter> om door te gaan');
      readln;
      normvideo;
    END;

  END;
end;

  IF (Ni > 1) and (keuzec <> '5') THEN BEGIN
   if keuze <> '7' then begin
    clrscr;
    repeat
      Textcolor(12);
      Writeln;
      Writeln('Voor welke fracties wilt u corrigeren ?');
      Writeln;
      textcolor(white);
      Writeln('  1) Voor alle fracties');
      Writeln('  2) Alleen voor fijne fracties, die waarvoor geldt dat D_f < D50_m ');
      Gotoxy(45,2);
      readln(keuzec1);
    until (keuzec1 = '1') or (keuzec1 = '2');
   end;

    IF keuzec1 = '2' THEN BEGIN
```

```
      IF D_f[i] > D50_m THEN keuzec := '5';
    END;
  END;


  CASE keuzec of
    '1': C1(psicr,psieff);
    '2': C2(psicr,psieff);
    '3': C3(psicr,psieff);
    '4': C4(psicr,psieff);
    '5': C5(psicr,psieff);
  END; {einde case}
END;

end.
```